2015

BIOMOLECULE LOCALIZATION AND SURFACE ENGINEERING WITHIN SIZE TUNABLE NANOPOROUS SILICA PARTICLES

Daniel M. Schlipf
University of Kentucky, dschlipf@gmail.com

BIOMOLECULE LOCALIZATION AND SURFACE ENGINEERING WITHIN SIZE
TUNABLE NANOPOROUS SILICA PARTICLES

_____

Dissertation

_____

A dissertation submitted in partial fulfillment of the

requirements for the degree of Doctor of Philosophy in the

College of Engineering

at the University of Kentucky

By

Daniel Michael Schlipf

Lexington, Kentucky

Director: Dr. Barbara L. Knutson, Professor of Chemical Engineering

Lexington, Kentucky

2015

ABSTRACT OF DISSERTATION

BIOMOLECULE LOCALIZATION AND SURFACE ENGINEERING WITHIN SIZE
TUNABLE NANOPOROUS SILICA PARTICLES

Mesoporous silica materials are versatile platforms for biological catalysis, isolation of small molecules for detection and separation applications. The design of mesoporous silica supports for tailored protein and biomolecule interactions has been limited by the techniques to demonstrate biomolecule location and functionality as a function of pore size. This work examines the interaction of proteins and lipid bilayers with engineered porous silica surfaces using spherical silica particles with tunable pore diameters (3 – 12 nm) in the range relevant to biomolecule uptake in the pores, and large particle sizes (5 - 15 µm) amenable to microscopy imaging

The differentiation of protein location between the external surface and within the pore, important to applications requiring protein protection or catalytic activity in pores, is demonstrated. A protease / fluorescent protein system is used to investigate protein location and protection as a function of pore size, indicating a narrow pore size range capable of protein protection, slightly larger than the protein of interest and approaching the protease dimensions. Selective functionalization, in this case exterior-only surface functionalization of mesoporous particles with amines, is extended to larger pore silica materials. A reaction time dependent functionalization approach is demonstrated as the first visually confirmed, selective amine functionalization method in protein accessible supports.

Mesoporous silica nanoparticles are effective supports for lipid bilayer membranes and membrane associated proteins for separations and therapeutic delivery, although the role of support porosity on membrane fluidity is unknown. Transport properties of bilayers in lipid filled nanoparticles as a function of pore diameter and location in the particle are measured for the first time. Bilayer diffusivity increases with increasing pore size and is independent of bilayer location within the core, mid or cap of the particle, suggesting uniform long range bilayer mobility in lipid filled pores. Application of lipid bilayers on mesoporous silica was examined for membrane

associated proteins A unique method to adhere functional proteins in lipid bilayers on mesoporous silica particles is established using vesicles derived from cell plasma membranes and their associated proteins. This method of membrane protein investigation retains proteins within native lipid membranes, stabilizing proteins for investigation on supports.

Daniel M. Schlipf

February 18th, 2015

BIOMOLECULE LOCALIZATION AND SURFACE ENGINEERING WITHIN SIZE

TUNABLE NANOPOROUS SILICA PARTICLES

By

Daniel Michael Schlipf

Dr. Barbara L. Knutson

Director of Dissertation

Dr. Thomas D. Dziubla

Director of Graduate Studies

February 18th, 2015

DEDICATION

This work is dedicated to the family and friends I've lost

while completing this dissertation.

My Mother,

Adelaide Virginia McManus

My Friend and Professor,

A.K. Ray

ACKNOWLEDGEMENTS

TABLE OF CONTENTS

LIST OF TABLES

LIST OF FIGURES

CHAPTER 1
Introduction

1.1 Introduction

Mesoporous silica materials are a versatile class of inorganic materials that can be synthesized in a variety morphologies such as thin films, membranes and particles of controlled size. In addition to their morphological versatility, these materials are chemically and physically robust with pore diameters and surface chemistries that can be tuned through a variety of synthetic procedures for application specific properties. These materials have been successfully employed in the fields of separations, catalysis, isolation of small molecules for detection and drug delivery while continually evolving for greater applications.   In regards to the development of these materials, there remain some unanswered fundamental questions such as biomacromolecular accessibility to pore spaces, control and location of surface functionalities and porosity roles on supported membranes. Santa Barbara Amorphous Batch 15, or SBA-15, materials revolutionized the mesoporous silica field due to their highly ordered, large particles sizes and large pore diameters (up to 30 nm).[3] Tuning of particle shape and sizing using surfactant combinations, such as P123 and CTAB, lead to micron diameter spherical, porous particles.[4] With their large particles sizes, capable of microscopic imaging, these large, spherical particles make an ideal platform for the direct visual investigation of biomacromolecule, functional group and membrane location on particles..

Protein adsorption and interactions with mesoporous silica are of interest for a broad range of applications including drug delivery, chemical synthesis, biosensors and bioseparations. A major challenge in designing mesoporous silica supports for tailored protein interaction is the differentiation of protein interactions at the surface of the particle from interactions within the pore, important features when considering mesoporous silica as a protective support for active proteins. The ability to confirm the accessibility of proteins to pores as a function of pore size or surface functionalization is limited in most mesoporous silica thin films and nanoparticles. Confirmation of protein binding is often performed via bulk solution depletion measurements, with little coupling of protein size and charge to pore diameter and surface charge of the materials.[5, 6] Confocal microscopy has been demonstrated as a tool to investigate protein diffusion into

1

pores, but current systems do not effectively delineate surface bound from pore associated proteins.[7] Work presented in this dissertation develops the use of pore size tunable silica particles for investigation of protein accessibility within porous substrates.

Differentiating the chemical properties of the external and pore surface of sol-gel derived mesoporous materials by selective functionalization is important to advancing their application as platforms for biological catalysis, isolation of small molecules for detection and drug delivery. This need has been identified within the porous nanoparticle community resulting in selectively functionalized, nanoporous (<5.5 nm diameter) nanoparticles. [8-12] However, the extension of these selective external functionalization techniques to large pore of mesoporous silica, appropriate for loading active proteins and biomolecules, is inferred from indirect measurements: direct visual localization is prevented in nanoparticles due to their nanoscale. The effectiveness of methods of selective functionalization of nanomaterials, such as pore blocking, were evaluated for the first time in larger diameter (> 7 nm) pores in this work. Surface functionalization techniques were extended to tethering of lipid membrane to particle surfaces. Lipid bilayer membranes have been demonstrated as effective biomimetic surface functionalization for biological sensing, semi-permeable transport and isolation of small molecules for detection. Lipid bilayers perform these functions using a host of membrane associated and transmembrane proteins. Outside of self-assembled lipid vesicles, lipid bilayers require support on an external substrate. Mesoporous silica is an ideal support for lipid bilayers: the physically robust silica provides support to the fragile self-assembled bilayer and the porosity of the support act as reservoirs for molecular flux through the membrane. Unfortunately, the impact of porous supports on bilayer properties, such as bilayer fluidity, is unknown. Porous nano-particles are often used to support lipid bilayers, where characterization is limited due to the nano-scale of the particle support. In this work, bilayer properties, such as location and fluidity, are investigated as a function of nanopore diameter and a techniques derived from this system are applied to a whole cell membrane with receptor signaling demonstrated.

1.2 Research Objectives

Mesoporous silica materials have become frequently used platforms for isolation of small molecules for detection, catalysis and separations. These applications would be

advanced by controlled protein incorporation, advanced surface functionalization or lipid bilayer membrane incorporation into mesoporous and particle surfaces. Understanding and characterizing the effect of pore size on the interaction of biomolecules is often difficult due to the dimensions of the nanoparticles. Due to their large particle diameters, surface functionalities and tunable pore sizes, SBA-15 mesoporous silica materials are able to be visually characterized and can simulate a variety of porous environments. The objectives of this research are to develop a materials platform for understanding protein accessibility and protection in mesoporous domains as a function of pore size, develop techniques to place surface functional groups in distinct locations in large-pore particles and determine effects of porosity on lipid membrane functionality at the particle surface. These materials will then be evaluated as platforms to investigate whole cell membrane support for investigation of membrane protein binding.

In Chapter 2, a review of mesoporous particle development and applications is provided. A discussion of materials synthesis techniques will emphasize porous silica platforms and methods of tuning pore sizes within particles. Following materials synthesis, the interaction of proteins with mesoporous supports and techniques for locating and confirming protein location and activity within mesoporous supports will be described. In addition, surface functionalization techniques are summarized with specific emphasis on methods to separately functionalize external particle surfaces from pore walls. Finally, the development of porous silica materials as lipid bilayer membrane supports is described along with their applications, setting the stage to understand porous support effects on bilayer membrane fluidity.

Chapter 3 focuses on the development of porous silica materials as protein supports, placing emphasis on both protein activity and localization using the fluorescent protein Enhanced Green Fluorescent Protein (EGFP).Uniquely, both EGFP activity and location can both be obtained from fluorescence emission data during particle imaging. The use of the protease Pepsin A cleaves accessible GFP from the porous support where only GFP diffused within pores and inaccessible to Pepsin A retain their fluorescence after Pepsin treatment. As a function of tunable pore diameter, this platform of pore accessibility and activity is a technique developed to correlate protein size and pore

accessibility along with an effective method to inactivate and remove proteins from external particle surfaces.

The ability to surface functionalize silica materials post synthetically increases their application versatility. A major challenge confronting functionalized nanoparticles is the selective functionalization of external particle surfaces while leaving interior pore spaces unchanged. Chapter 4 presents techniques and evidence to functionalize the outside of porous particle post synthetically. This work is unique in that 1) it is true post-synthetic functionalization, requiring no pore template for blocking pores during functionalization as is seen in literature [7] 2) functional group location is visually localized using confocal microscopy, confirming functional group location and 3) this is the first demonstration of selective functionalization in materials with protein accessible pore diameters.

Chapter 5 examines the interaction of lipid bilayer membranes with porous mesoporous silica supports as a function of pore size. As opposed to wrapping particles with lipid membranes via lipid vesicle fusion, lipids are deposited within the nanopores and on particle surfaces by evaporation deposition. Lipids are rehydrated and sonicated to form bilayers on particles surfaces and within pores where accessibility is confirmed via confocal imaging. Additionally, FRAP measurements of bilayer diffusivity within and on particle surfaces indicates both pore size and surface chemistry effect on diffusivity. This work is the first comprehensive measurement of bilayer fluidity throughout particles, in multiple locations. Additionally, this work provides the same particle system for investigation of a multiple variables, surface chemistry and pore diameter, eliminating the possibility of different support effects on bilayer fluidity.. Chapter 6 expands on imaging and bilayer formation techniques developed in chapter 5, utilizing large diameter particles as supports for cell plasma membrane derive membranes. The versatility in this support system is in both the particle support and cell derived membrane. The surface chemistry of particle supports can be tailored for application specific interactions while the cell derived membranes can be used to incorporate a variety of membrane proteins through cell transfection prior to vesicle formation. Chapter 6 demonstrates this versatility through by demonstrating ligand binding to membranes expressed with receptors, while no membrane association occurs in non receptor expressed membranes.

CHAPTER 2

Background

2.1 Synthesis of Porous Silica Materials

The field of well ordered, mesoporous (2 nm - 50 nm pore diameters) silica materials (MSMs) originated in 1992 with the the synthesis of MCM-41 materials.[13, 14] Porous silica materials are inorganic metal oxides that can be synthesized in a variety of morphologies (thin films, membranes, particles) with mesopores derived from a variety of pore templates.[4, 15] MSMs are inexpensive to produce, chemically and physically robust and employ well known aqueous based synthesis chemistry with existing applications as platforms in separations and catalysis.[16, 17] The structures of MSMs are finely tunable and synthetically versatile, allowing for a broad range of after post-synthesis surface chemistries. Since the original synthesis of MCM-41 materials, greater particle shape and pore size control has been developed leading to the SBA-15 class of materials. [3] SBA-15 materials are synthesized under acidic, rather than basic, synthesis conditions using pluronic copolymer pore templates for increased achievable pore diameters and diameter tunability. These materials can be synthesized with easily tunable particle shapes and sizes as well as tunable pore diameters using different templating systems.[4] Chapters 3,4, 5 and 6 demonstrate the use of spherical SBA-15 class materials for investigating protein localization and protection, selective surface functionalization, lipid membrane coating and membrane protein function in these pore size tunable materials.

2.1.1 Sol Gel Chemistry

Sol-gel, solution-gelation, chemistry is the foundation for the synthesis of both non-porous and porous silica materials. Sol-gel chemistry describes the process of silica alkoxide precursor hydrolysis and condensation to form a tetrahedrally coordinated network of SiO_2.[18] Sols are generally prepared in aqueous alcohol solutions and are catalyzed by either acids or bases, both of which mechanisms are in **Figure 2.1**. Both the acid and base catalyzed reactions use alkoxide silane precursors which undergo hydrolysis and polycondensation to form the silica network.[1, 18] Acid catalysis promotes the protonation of ethoxy groups resulting in the rapid hydrolysis of TEOS and slow condensation, resulting in small particle diameters. In basic conditions, precipitation

occurs rapidly, resulting in the formation of larger diameter particles. On the other hand, base catalyzed synthesis of silica materials requires the nucleophilic attack of TEOS by hydroxide ions, resulting in the formation of an unstable transition product. Solution concentrations of hydrolyzed Si(OH)4 must reach supersaturation levels before particle nucleation begins, resulting in smaller particle diameters. [19, 20]

Acid Hydrolysis
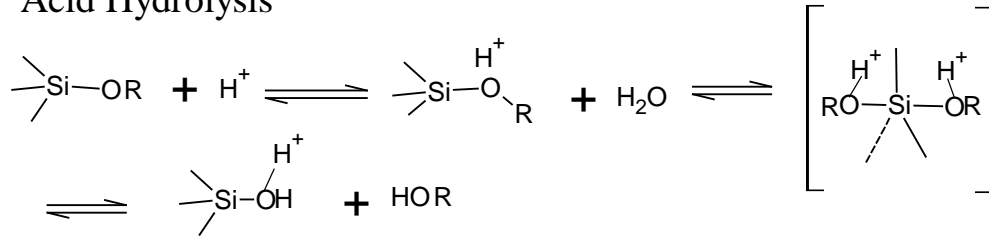
Acid Condensation
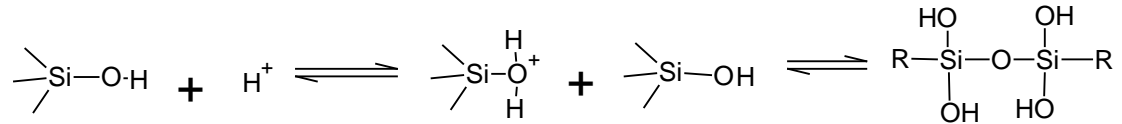
Base Hydrolysis
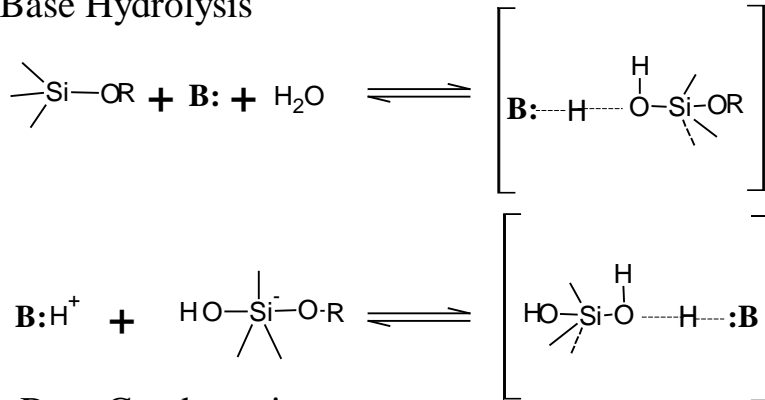
Base Condensation
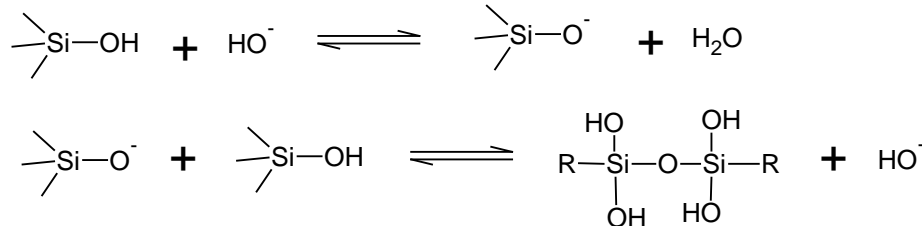
Figure 2.1 Reaction mechanism of alkoxy silane precursor hydrolysis and condensation under acidic and basic conditions. [19, 20]

After the initiation of TEOS condensation, materials are thermally treated to increase the polycondensation of the silica network and particle growth, followed by drying.[18] Drying of the material removes excess water and alcohol, which are part of the initial sol and products of the hydrolysis and condensation reactions. Thermal treatment of the as-formed silica materials promotes silica condensation, increasing the SiO_2 density and robustness of the materials around the surfactant pore templates.

2.1.2 Pore Templates

The porosity within MSMs comes from a variety of surfactants and block copolymers which self-assemble into pore templates. The structure of the ordered porous network, either cubic, hexagonal or lamellar, is dependent upon both template and solution composition.[21] MCM based silica materials, synthesized via base catalysis, are generally characterized by their nanoparticle sizes (50 nm - 500 nm diameter). Pore templates for these materials are most notably cetyltrimethylammonium bromide (CTAB), which self assembles into a micellar pore template structure resulting in rather narrow pore diameters (2.5 nm). Methods of increasing pore diameters in these nanoparticle materials generally involve the expansion of micelles using an organic template swelling agent such as trimethylbenzene (TMB) which insert themselves into the hydrophobic template core, expanding micelle diameters and subsequently pore diameters up to 4.8 nm.[22, 23]Additionally, increasing surfactant chain lengths from 8 to 16 carbons increases the assembled micelle diameter resulting in increased pore diameters from 1.8 nm to 3.8 nm.[23] Other methods such as altering reactant and template concentrations as well as reaction temperature can be used to expand pore diameters upwards of 6.6 nm while retaining pore wall thickness and rigidity of synthesized materials. [24]

Spherical SBAS materials, adapted from P123 templated, acid catalyzed SBA-15 materials, use a dual surfactant templating procedure which results in significantly increased, tunable pore diameters between 3 and 15 nm. The secondary surfactant, cetyltrimethylammonium bromide (CTAB), is used to promote spherical particle formation. Nonionic triblock copolymers, such as P123 and F127, with respective structures of (Ethyleneoxide)$_{20}$-(Propyleneoxide)$_{70}$-(Ethyleneoxide)$_{20}$ (Sigma-Aldrich 435465) and (Ethyleneoxide)$_{101}$-(Propyleneoxide)$_{56}$- (Ethyleneoxide)$_{101}$ (Sigma-Aldrich

P-2443), form significantly larger pore templates than ionic surfactants by themselves, resulting in increased pore diameters.[25, 26] Templates used specifically in this work are comprised of polymeric triblock copolymer (P123) and cationic surfactants (CTAB), and upon formation of micelles assemble into a hexagonal phase, creating hexagonal templated porous materials.[4] Tunability of pore diameters comes from temperature dependent solvation of the ethyleneoxide (EO) end units of the P123 copolymer during template formation. Templates form when PO blocks cross over one another to form a hydrophobic core, which EO blocks protruding into the surrounding solution. At increased synthesis temperatures EO end units are less solvated in the aqueous synthesis sol, resulting in their retraction into the more hydrophobic core of the pore template, increasing pore template diameters (**Figure 2.2**).[25] The process of hydrothermal aging and holding materials during synthesis at elevated synthesis temperatures results in temperature tunable pore diameters during synthesis, between 3 and 15 nm.[27] The hydrothermal aging method of pore diameter tuning in SBAS materials is preferable to methods of MCM materials as there are no changes in synthesis reagents, merely changes in synthesis temperature. After heat treatment and particle formation from the sol-gel condensation around hexagonally oriented pore templates, removal of the pore template is required to create accessible porous systems. Removal of templates can occur by either solvent extraction or calcination. Solvent extract removes template by solubilizing the template and washing it away in an alcohol solution, often ethanol.[28] On the other hand, calcination removes porous template by burning the carbonaceous species from the pores of the materials while simultaneously heat treating the SiO_2 materials, increasing pore wall thickness and materials robustness.[29]
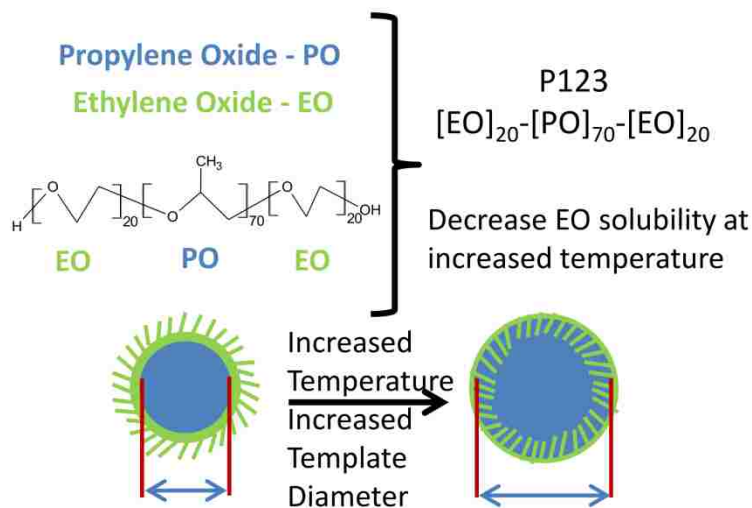
Figure 2.2 With increasing temperature ethylene oxide end units in P123 become less solvated and infiltrate the hydrophobic propylene oxide core, increasing the template and subsequently pore diameters.

2.2 Protein Adsorption in Porous Silica Materials

Proteins and enzymes are natural catalysts capable of creating complex products with high enantiospecificity and selectivity although they suffer from low stability in bulk solution in large scale applications.[30] In addition to having large scale application roles, therapeutic protein delivery is an area of intense research for disease treatment and prevention.[31] Porous MSMs have been identified as materials for stabilization, loading and delivery of proteins and enzymes in solution. Specifically, SBA-15 silica materials have increased the use of MSMs for protein loading with their large pore diameters, accessible to adsorbing and diffusing proteins. These protein accessible materials are frequently used for protein catalysis, protein separations, biological signaling and drug delivery.[32-38] The confining effects of pore walls provide confirmation stability to adsorbed proteins, thus retaining protein activity in environments where the protein may otherwise denature in solution.[39]

2.2.1 Protein loading methods

A variety of methods exist to load active proteins on the surface of mesoporous silica including adsorption, encapsulation, and covalent binding. The most common method of loading proteins on mesoporous supports is electrostatic adsorption. Because of the generally negative charge of silica materials and positive charge of most biological proteins at neutral pH, an inherent attraction is present between the silica surface and proteins in solution. Electrostatic adsorption is pH and protein dependent, which has been demonstrated as an effective protein capture and release tool in solution. Lu et.al. utilized pH shifts to electrostatically release and re-adsorb Lysozyme, where its activity on macrosubstrates was measured whilst free in solution prior to re-adsorption.[40] In cases where proteins do not adsorb to silica surface, post-synthetic functionalization is used to induce adsorption. A variety of charged (amine, carboxylic acids) and hydrophobic (phenyl) groups can be used to induce adsorption.[41] Protein encapsulation during particle synthesis is also used for loading proteins.[42, 43] The byproducts of MCM synthesis, often alcohols and water, in addition to the acid or base catalysts are unfavorable for sustained protein activity, therefore sugars and liposomes are used to stabilize proteins during entrapment. In addition to entrapment and adsorption, covalent immobilization of enzymes on mesoporous supports is common. Frequently an amine to amine linker is used for covalent anchoring, where amine functionalized silica materials are connected to amine groups expressed on protein surfaces via glutaraldehyde.[44] Unfortunately, covalent immobilizations of enzymes on supports leads to deactivation by altering protein conformation. [45] Due to the potential for inactivation, electrostatic adsorption is used as the method of protein attraction and diffusion into mesopores in this work.

2.2.2 Protein localization in mesoporous silica

While porous silica supports are frequently used for protein immobilization, effective evidence of protein accessibility to MSM pore spaces is unclear. Frequently, solution depletion measurements are used to confirm the localization of proteins within mesoporous supports.[5, 6]

Using US-Vis measurements to measure protein uptake, size selective adsorption of bovine serum albumin (BSA), lysozyme (LYS) and myoglobin (MYO) on SBA-15 materials with different pore diameters (3.8 nm, 7.7 nm and 24.0 nm) has been

demonstrated using bulk solution protein measurements.[5] Bulk measurements of protein concentration (at 280 nm) can be used to measure the amount of protein adsorbed materials but cannot identify the location of proteins on supports within the pores or on the external surface of the particle. Additionally, considering a significant majority of all proteins absorb light at 280 nm, the use of UV-Vis bulk measurements limits experimental bulk measurements to single protein experiments.

An alternative to bulk solution measurements of protein concentration is the use of protein assays to measure their activity. Assays of protein activity provide information on protein function on support and active site accessibility, in addition to information regarding loading on the support. Jaladi et.al. (2009) employed the p-nitrophenyl acetate assay as a measure of Burkholderia cepacia lipase (BC Lipase) activity after immobilization onto SBA-15 silica supports.[46] Measurements of protein activity on SBA-15 materials with 24 nm pore diameters was similar to that of the free enzyme in solution, indicating limited diffusional resistance of assay reactants to the protein or denaturation on the support. On 5.5 nm supports, a 20 to 30 percent reduction in protein activity was interpreted as diffusion into porous supports, reducing assay reactant access to enzyme active sites. This work highlights the fact that assay based systems are dependent on both enzyme activity and accessibility. In order to confirm location of proteins within mesopores of SBA-15 silica materials (rod shaped and spherical SBAS particles), protein visualization studies have been employed to confirm protein accessibility and location within pores.

The development of well ordered, large particle sizes of SBA-15 materials has permitted the direct microscopic visualization of fluorescent and fluorescently tagged proteins and guests in materials via Confocal Scanning Laser Microscopy (CSLM).[7, 47, 48] CSLM has been used to visualize and measure the size dependent diffusion of fluorescently tagged Lipase into SBA-15 materials with pore diameters of 5.6, 8.0 and 9.7 nm. [48] Size exclusion is visually apparent in the smallest pore diameter with increasing diffusivity in large pore diameters. In a multiprotein systems using SBA-15 materials, Katiyar et.al. visually demonstrated size selective protein separations of fluorescently tagged Bovine Serum Albumin (BSA) and Lysozyme (Lys) where BSA was excluded from 12.7 nm pores accessible to Lys in SBA-15.[7] While the fluorescent

tagging of proteins is an effective way to locate them, proteins that are naturally fluorescent provide both location[47] and protein activity data via fluorescence. In Chapter 3, the fluorescent protein Enhanced Green Fluorescence Protein (EGFP) is demonstrated as an effective tool to locate and confirm protein activity. A secondary protein, the large protease Pepsin A, is used to actively cleave EGFP from the surface of particles and when accessible in larger pores. This two protein system is used to delineate surface bound from pore located proteins and demonstrates an effective method of both cleaning proteins from particles surface and utilizes fluorescence to confirm protein activity.

2.3 Surface Functionalization of Silica

One of the greatest benefits of mesoporous silica is the ease of surface functionalization. MSMs can be functionalized with a variety of different compounds including metal oxides and a host of organic functionalities for controlled adsorption [49, 50], targeted particle therapies [51], cargo stabilizers [44] and detection and imaging sensors.[52, 53] Functionalization of mesoporous silica with amines, in particular, has been shown to stabilize enzymes in mesopores,[54] to modulate interactions of peptides and proteins with silica[55-58] and to control particle uptake and cytotoxicity[59-61]. The most common methods of surface functionalization are co-condensation and post-synthetic functionalization. The co-functionalization approach to particle functionalization incorporates the addition of functional agents prior to completion of particle synthesis. Efforts have been made to use the co-condensation approach to control functional group location at different periods of particle formation.[62, 63] Depending on time in synthesis, before, during or after particle formation, functional groups can be located in the silica framework, on all surfaces or exterior only surfaces. [62, 63] Co-condensation techniques are employed for the incorporation of fluorescent guests into the silica framework for biological imaging and as contrast agents.[63, 64] Post-synthesis functionalization approaches functionalize particles after synthesis and curing, ensuring sol-gel formation of the silica network without functional group perturbations.[18] Post-synthesis functionalization methods benefit from ensured particle robustness, as surface functional groups do not compromise sol-gel framework

integrity.[65] Additionally, post-synthesis grafting on external surfaces afford greater control in functional group localization as well as the detail of surface chemistries.[65]

2.3.1 Selective surface functionalization approaches

Selective functionalization of mesoporous silica has been approached by a variety of methods, each with mixed success. [8-12, 62, 66-68] Co-condensation, addition of functional groups during particle formation, is generally used to functionalize particle frameworks, generally with guests that aid in visual detection (for medical diagnostics). [62, 63] Kecht determined addition of surface reactants towards the end of particle formation places functional groups on the exterior of the particle surfaces, as opposed to within the framework if added earlier in particle synthesis.[62] On the other hand, Kim et.al. took advantage of the particle growth phase to introduce functional groups within the silica frame work and pore walls and reacting particle exteriors with alternative silanes at the end of synthesis to form hydroxyl coated particles. [63] While confirmation of external particle charges, measurements of pore diameter changes after functionalization, FTIR and Fluorescence Resonance Energy Transfer (FRET) have been used to infer functional group location, direct visualization of functional groups via imaging is prohibited due to nanoscale particle size.[62, 63]

In addition to co-condensation approaches to control functional group location, functionalization of materials with bulky functional groups prohibited from entering pores is also a method of surface functionalization. PEG is frequently used as a surface modifier of silica particles to increase their biocompatibility, although PEG functionalization frequently leads to pore blocking.[68] Therefore, Bouchoucha et.al. used simultaneous deposition of a smaller, spacer silanes with PEG silanes to reduce deposition quantities of PEG silane.[68] While 10% (w/w) PEG coverage lead to significant pore volume loss and blocking, tailoring deposition between the two silanes (<5% (w/w) PEG) resulted in more open, accessible pores, resulting in pore accessible, exterior PEGylated silica particles. Reverse de-protection has also been a method developed to selectively functionalize mesoporous silica materials.[69] Cheng et.al. demonstrated this method by fully functionalizing particles with N-(9-fluorenylmethyloxycarbonyl) (FMOC) tagged amino-silanes and reacting the functionalized materials with the small molecule piperidine, which cleaves the FMOC

leaving amine terminated particle surfaces. Although this method formed selectively functionalized silica surfaces with amine exteriors, pore surfaces were functionalized in FMOC, significantly reducing pore diameters from 3.0 nm to < 2.0 nm.

As opposed to co-condensation, bulky silane deposition or complex unblocking methods, the simplistic pore blocking method of selective functionalization is more frequently used. Pore blocking relies on the use of pore templates within pores to block the accessibility of functional groups to functionalize pore walls, and has been used to selectively functionalize with carboxylic acids, alkanes and amine functional groups.[8-10, 70] In specific regard to amine functionalization, selective functionalization of amines on small pored (<5.5 nm pore diameter) silica has been demonstrated. Critical to this demonstration of selective functionalization is the retention of surfactant templates within pores as well as the use of reduced reactivity amino silanes (3-aminopropyltris(methoxyethoxyethoxy)silane) (APTMEES). These techniques have specifically relied on the reactivity of amino silanes coupled with pore blocking to achieve external only functionalization.[70] In the absence of a pore blocking template, the greatest pore size capable of selective functionalization was 2.9 nm diameter. Silica particles with pore diameters up to 5.5 nm were capable of being selectively functionalized in the presence of the pore blocking pore template, although removal of template prior to functionalization resulted in the grafting of the functional group throughout the particle, regardless of amino-silane used.[70] These results were achieved on silica materials capable of being visualized, although their pore diameters are narrow, prohibiting their use with biologically active systems.

2.3.2 Characterization of selective surface functionalization

Although there are a variety of characterization techniques employed to determine functional group location on mesoporous materials, the vast majority are bulk material measurements in which functional group location must be inferred from indirect measurements. Zeta potential measurements can measure the change of charges on external surfaces, but provide no information on internal grafting. [62] Similarly, nitrogen adsorption measurements can indicate changes in pore diameters, suggesting pore surface functionalization, but cannot differentiate between functionalization a the pore opening or in the pore itself.[62] NMR has been used to determine interactions between surface

functional groups and surface silanols to determine surface functionalization of porous materials.[71] The only direct method of locating surface functional groups is via visualization of functional groups on particles. Gartmann et.al. demonstrated the amine functionalization of large diameter silica particles followed by fluorescent tagging to locate the functional groups on the particle.[65] While this technique confirmed selective functionalization, the pore diameter of the materials investigated (2.9 nm to 5.5 nm) is too small for larger biomolecule applications. Cheng et.al. also used confocal microscopy to visualize surface functionalization of large particle diameter materials, although the pore diameters within the materials were limited to 2.3 nm – 3.0 nm.[66] In this work, particles were fully functionalized with a construct that was later cleaved off to reveal amine functional groups. Controlling exposure times to the cleavage molecule piperidine results in selective, surface cleavage or full particle cleavage with increased exposure times.

Chapter 4 of this dissertation develops methods of selective exterior functionalization of large pore diameter silica materials (>7 nm) that do not rely on the blocking of pores to control external functionalization. When compared to pore blocking methods employed in smaller pore diameter materials, it was determined that pore blocking methods were not effective in selectively functionalizing large pored materials. All functional group locations were confirmed via confocal fluorescence localization of functional groups after fluorescent tagging. The methods described in Chapter 4 are time dependent, bulk diffusion methods, techniques capable of extension into larger pore diameter ranges.

2.4 Lipid Bilayer Membranes Supported on Mesoporous Silica

All eukaryotic cellular systems are surrounded by cell membranes which control cellular signaling, transport in and out of cells and environmental detection. Significant research efforts have focused cell membrane mimicry, in the form of synthetic lipid bilayers, in an attempt to duplicate the function of individual cell membrane systems. A primary problem with synthetic membrane systems is their sensitivity to environmental conditions. Free formed lipid bilayers vesicles are self-assemblies that are sensitive to temperature, pH, and ionic strength, among other environmental parameters. [72] Synthetic supports are used to provide physical support and favorable surface chemistries

to stabilize bilayers.[73] Mesoporous silica is an ideal support for lipid bilayer membrane applications due to its morphological versatility, ease of surface functionalization, tunable porosity and particle dimensions. [3, 15]

2.4.1 Silica supported bilayer membranes – applications

Silica supported membranes on porous silica materials have direct applications in targeted drug delivery, membrane separations and isolation of small molecules for detection. [73-75] Ashley et.al. employed membrane coated silica nanoparticles for targeted drug delivery with membrane associated targeting peptides.[76, 77] Due to the large pore volumes and surface areas of mesoporous silica nanoparticles, multicomponent cargos including SiRNAs and chemotherapeutics can be loaded into nanoparticles for cellular delivery.[76] Pore forming proteins within lipid membranes can be used for single molecule separation processes with the pores of nano-particles acting as small molecule receptacles. [78, 79] The transmembrane proteins Gramicidin A and Cyctochrome C have been used as model transport proteins for selective transport of ATP and ions, respectively, through membranes into nanoporous supports.[78, 79] Receptor-ligand binding events on cellular surfaces are used for environmental sensing and detection. Translated into membrane associated supports, these proteins are used for molecular sensing via fluorescent signaling upon binding. [80]

2.4.2 Tether supported membranes

A variety of membrane tethers have been developed to stabilize membranes and promote binding to synthetic surfaces. The primary method of membrane tethering is via insertion of the tether into the hydrophobic portion of the membrane. The most simplistic membrane tethers include long chain alkane tethers[81] and covalently bound lipid tails[82] on porous membrane supports. Additionally, releasable membrane tethers have been synthesized via reducible phosphatidyl choline tails that release membrane contents upon reduction. Non-porous supports require more comprehensive approaches to membrane tethers. The narrow interstitial water space between the membrane and support induces membrane-support interactions, interfering with membrane activity.[83] PEG cushioned supports have been designed to increase the interstitial water layer between the membrane and support by inclusion of hydrophilic PEG chains between the membrane

tether and support.[84, 85] Membrane tethers in these systems are composed of peptide or protein tethers to mimic the local environment of cell membranes.

2.4.3 Investigation of membrane fluidity on supports

A primary characterization component of lipid bilayer membranes is the fluidity of the lipid bilayer. Membrane fluidity is critical for membrane function as it impacts membrane associated protein insertion, membrane function and small molecule permeability.[86, 87] Bilayer fluidity varies by orders of magnitude between different lipid systems, support chemistries and membrane tethering.[84, 88, 89] The primary supports for investigation of membrane fluidity are non-porous, micron diameter silica particles and non-porous thin films.[88, 90-92] Micron diameter particles are employed for their ability to be visually characterized via Confocal Scanning Laser Microscopy and subsequently use the CSLM technique Fluorescence Recovery After Photobleaching (FRAP) for measurement of bilayer fluidity. Compared to other techniques, such as Fluorescence Correlation Spectroscopy (FCS) and Single Particle Tracking (SPT), FRAP is one of the more robust methods of measurement in supported bilayer systems.[93]

A frequent lipid choice for assembling synthetic bilayer membranes is the lipid 1,2-dipalmitoyl-*sn*-glycero-3-phosphocholine (DPPC). DPPC is a primary lipid component of the cell membrane and uniquely has a gel to fluid phase transition temperature of 41ºC, where most lipids are fluid at or below room temperature. [88, 94] Scomparin et.al. investigated the effect of support chemistry on DPPC bilayer diffusivity after vesicle fusion onto both mica and glass slide substrates.[88] Although both supports are primarily composed of silicon dioxide, subtle differences in metal oxide doping resulted in order of magnitude differences in DPPC diffusivities (Glass: 0.05-0.1 μm^2/g, Mica: 0.00009-0.01 μm^2/g). In addition to surface chemistry effects, surface tethering dramatically affects the fluidity of lipid bilayers. Surface tethers themselves are immobile, therefore in a lipid bilayer they impart a tether density dependent effect on bilayer fluidity, potentially reducing diffusivity by orders of magnitude.[95]

Investigations of porosity effects on supported 1-palmitoyl-2-oleoyl-sn-glycero-3-phosphocholine (POPC) bilayer fluidity have been performed by Claesson et.al. on 2 nm, 4 nm and 6 nm pore diameter silica thin films.[96] A decrease in bilayer fluidity with pore diameter was observed. However, several surfactant systems were used to achieve a

range of pore diameters, each resulting in a different nanopore structure and surface chemistry. Large diameter porous silica particle provide the opportunity to visually investigate lipid properties both on the surface of pores and within particle pores, which is difficult in thin films due to shallow pores. In addition, pore diameters in these particles are tunable over a wider range while keeping constant the templates, pore geometries and surface chemistries. Simple FRAP experiments on the interior of particles have demonstrated bilayers retain their fluidity within mesoporous silica particles, although no diffusivity measurements have been made.[91] Recently, mesoporous silica nanoparticles have been used as fluorescent detection devices with lipid filled pores.[52]With high density lipophilic particle cores, these materials are ideal for sequestering fluorescent molecules in solution for signal production. The application versatility of porous supports with bilayer membranes necessitates investigation into porous support effects on bilayer properties.

Chapter 5 of this dissertation will take into consideration the use of membrane tethers and porosity in the investigation of lipid bilayer fluidity on and within mesoporous silica. Pore diameters will be tuned within a size range capable of excluding and internalizing lipid bilayers within the pore. The FRAP technique, established in section 2.6.2, will be used to investigate bilayer fluidity as a function of pore diameter and surface chemistry.

2.4.4 Investigation of membrane proteins in supported lipid bilayers

Complex protein structures within the plasma membrane of cells control membrane transport, cell signaling and signal transduction pathways within the cell.[97] As described in Section 2.5.1, incorporation of these proteins in synthetic lipid membranes has become an area of growing interest for investigating membrane associate protein and receptor function, protein mediated membrane transport and receptor affinity investigations. [78-80] The incorporation of membrane proteins within synthetic bilayers requires the separation and purification of proteins from biological sources that often lead to protein inactivation.[80] Reincorporation of transmembrane proteins into synthetic lipid systems requires the detergent or organic solvent solubilization of membrane proteins followed by detergent removal or solvent exchange during reincorporation into synthetic membranes which can also lead to denaturation.[98] Incorporation of proteins

within their native lipid membranes onto particle supports for investigation would prevent protein denaturation and retain the physiological surrounds used to retain protein function within the membrane.

Due to recent efforts in molecular biology to understand protein pathways in cells, improved methods to purify cell components have been identified, including separation of the cell plasma membrane from other organelles and cellular components.[99, 100] In Chapter 6, purified plasma membrane vesicles, also known as microsomes, were used to transfer membrane proteins in their physiological lipid mixtures for evaluation of protein function on porous particles supports. Microsomes are formed by rupturing cells via nitrogen cavitation where membranes reform in solution and are purified from cell lysates via ultra-centrifugation. Upon mixing with large diameter particles, microsomes rupture on the particle surface, spanning pores, ideal for visual investigation of membrane protein function. In Chapter 6 a model transmembrane receptor system, epidermal growth factor receptor (EGFR) is expressed within HEK293 cell prior microsome to evaluate function on particle surfaces. Protein function and ligand binding is evaluated on particle surfaces to confirm transfer of active protein function on particle supports. Retaining membrane proteins within their native lipid membranes is envisioned as a method to retain protein function after transfer to particle supports for both investigation of protein function and applications into membrane protein separations and catalysis.

2.5 Fluorescent Characterization Techniques

Confocal scanning laser microscopy (CSLM) is a form of high resolution microscopy that has generally been reserved for imaging of cells. Some of the first demonstrated uses of confocal microscopy with synthetic materials occurred in the later part of the 90's with large diameter porous silica particles. In Ljunglof's work, bulk solution measurements of protein adsorption were correlated with images of protein diffusion into mesoporous silica materials as a function of time.[101] Following this work many authors began to use confocal imaging couple with bulk protein measurements to understand the interaction and adsorption of proteins within mesoporous silica materials. Katiyar visually demonstrated size selective protein separations over mesoporous silica[7] while numerous papers have coupled visual protein accessibility images with controlled adsorption as a function of pore size.[27, 40, 43, 47, 102] In

addition to guest molecules on the surface of silica particles, confocal scanning microscopy has been demonstrated as an effective method of visualizing surface functional groups on mesoporous silica. Some of the first work visually confirming selective surface functionalization on silica particles was demonstrated by Gartmann et.al.[70] This work investigated the use of different amino-silane precursors as well as a pore blocking theory in an attempt to selectively functionalize mesoporous silica. After functionalization, the amino-silane were fluorescently tagged for visual location confirmation using CSLM.   Fluorescence has long been used as a technique for analysis of lipid bilayer membrane systems. In order to investigate lipid bilayer properties on silica particles, non-porous silica particles with large diameters are frequently used as a support for investigation of bilayer fluidity.[90] In order to measure bilayer fluidity, the fluorescence technique Fluorescence Recovery After Photobleaching (FRAP) is employed, which will be covered ins 2.6.2. In Chapter 5 of this work, both CSLM and FRAP will be used to investigate lipid bilayer location and fluidity over a series of pore sizes both too small and large enough to internalize lipid bilayers. Additionally, in Chapter 6 CSLM will be used to confirm the enveloping of these pore size tunable particles in lipid bilayers derived from cell membranes, for investigation of membrane protein function in their native physiological membranes.

2.5.1 Fundamentals of Fluorescence

The beginnings of fluorescence can be found in nature. For example, the fluorescent protein used in Chapter 3 of this dissertation is derived from the jelly fish *Aequorea Victoria*. Fluorescent molecules can be generally characterized by their aromatic rings of double bonds, which are composed of dumbbell shaped π bonds in addition to σ bonds. π bonds are generally weaker as their electron density is further from the positive charge of their nucleus. These less strongly bound electrons can be excited with light of a particular wavelength.[103] When these fluorescent molecules are exposed to light having an energy that matches an electronic transition within the molecule, the light is absorbed, and the electrons within the molecule are considered excited. [103] This transition takes the electron from the Highest Occupied Molecular Orbital (HOMO) to the Lowest Unoccupied Molecule Orbital (LUMO). This phenomenon can be represented in **Figure 2.3**, which is the traditional Jablonski diagram.[104] The excitation of electrons

happens rapidly (10^{-15} seconds). After excitation, electrons vibrate into their LUMO on the order of 10^{-12} seconds. Relaxation into a lower orbital can take on the order 10^{-9} seconds during which time fluorescence occurs via the release of a photon of greater wavelength than received. This lower energy, longer wavelength light is read by the detector as the output of fluorescence.
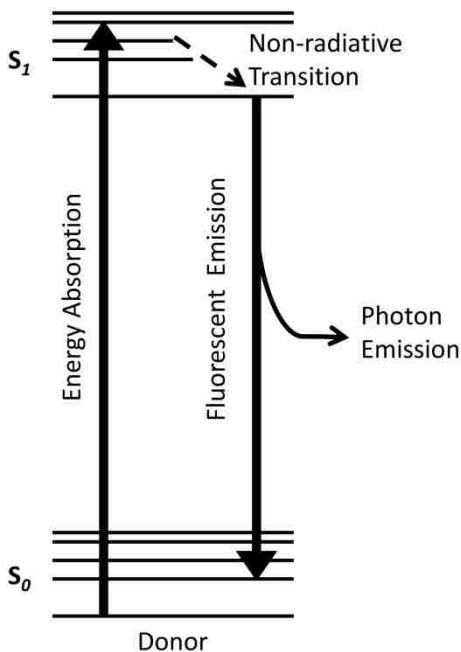
Figure 2.3 A modified Jablonki
diagram demonstrating fluorescence

2.5.2 Confocal Scanning Laser Microscopy (CSLM)

Fluorescence microscopy was developed in the early 1900's by Carl Zeiss.[105] A standard fluorescence microscope floods an entire sample with excitation light and the CCD detector images the entire field of vision. Unfortunately, standard fluorescence microscopy detects significant amount of out of focus light, blurring images taken. The numerical aperture (NA) is a convenient indicator of objective resolution[106]. NA ranges from 0.1 for low magnification objectives to 1.6 for high performance objectives. The equation can be seen in **(2.1).**[106].

$$NA = n(\sin(\theta)) \qquad\qquad (2.1)$$

The numerical aperture is a function of both the refractive index of the observation medium (n) and (θ) which is one-half the objective angular aperture. In

addition to describing objective resolution, the NA is inversely proportional to the square root of the depth of field (DOF) (**Equation 2.2**)[106]. The DOF is the axial range in which the objective can be focused.

$$d = {}^{\lambda n}/_{NA^2} \tag{2.2}$$

In **Equation 2.2**, d is the DOF, λ is the wavelength of light used, n is the refractive index of the medium and NA is the numerical aperture of the objective used. The DOF changes decreases dramatically with increasing NA, from 15.5 µm in a 4x magnification lens to 0.19 µm in a 100x lens.[106] A thinner depth of field has greater resolution as light is being imaged from a thinner slice of the sample. Although the depth of field can be thinner with increasing magnification, out of focus light is still detected by the detector, blurring the image and taking away detail.

CSLM uses two main methods to decrease the amount of out of focus light detected: 1) point by point laser illumination of the sample and 2) rejection of out of focus light using a pin hole aperture before the detector (see **Figure 2.4**).
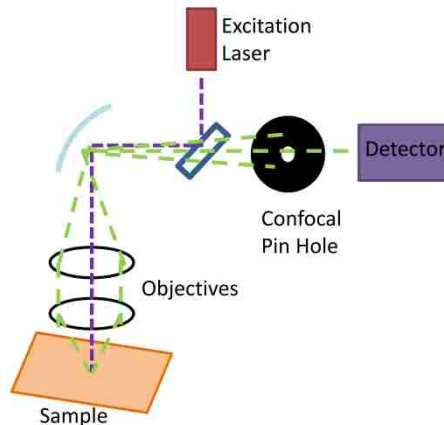
Figure 2.4 Schematic diagram of confocal microscope.

The pin hole is located at the conjugate focal (thus confocal) plane of the sample thus rejecting all out of focus light coming from the remainder of the sample. Any rejection of photons from the sample decreases the intensity of emission light, therefore photomultiplier tubes are used to increase the signal of photons received from the focused sample. The rejection of out of focus light permits the optical slicing of the materials as a

function of sample depth.[107] At any instant in time, there is only one point of sample illumination; the 2-D image is a reconstruction of the individual points. By stacking multiple 2-D images, 3-D reconstructions of images are possible.

2.5.3 Fluorescence Recovery After Photobleaching (FRAP)

In Chapter 5 of this dissertation, the impact of supporting lipid bilayers on and within mesoporous silica pores with and without lipid tethers is evaluated via comparison of bilayer fluidity. Lipid bilayer fluidity can be measured by fluorescence correlation spectroscopy (FCS), single particle tracking (SPT) and most commonly fluorescence recovery after photobleaching (FRAP).[93] FCS requires significant referencing and calibration for correct diffusivity analysis and SPT methods suffer from low accuracy, whereas FRAP is considered a more robust measurement technique.[93]

2.5.3.1 Measurement of Fluorescence Recovery After Photobleaching

FRAP works by photobleaching a section of sample and monitoring the recovery fluorescence as a function of time. Photobleaching is the permanent photochemical destruction of a fluorescent molecule by illuminating the molecule with high intensity fluorescence light of the fluorophores excitation wavelength. After photobleaching, the fluorescence intensity of the area photobleached is scanned over a period of time as unbleached fluorophore from surrounding areas diffuses into the space and fluorescence recovers. The fluorescence recovery is described by a series of differential equations as a function of the diffusivity and fluorescence intensity at $t = \infty$, both of which are obtained after modeling the raw data.

Identification of a photobleach geometry that describes the experimental measurement is necessary geometries available such as squares, rectangles circles etc. In general, squares and rectangles are ideal for measurement of one dimensional diffusion in thin fluorescent strips, such as in a lipid bilayer wrapped around porous and non-porous silica particles.[90, 91] In planar supported bilayers, circular bleach spots are used to account for two dimensional diffusion within the plane.[96, 108] In 3-dimensional bilayer systems, such as bilayer supported throughout porous particles or membrane within colloidal crystals, circular bleach spots are used as well.[109] In this case, the light beam used to bleach the region of interest (ROI) also bleaches all fluorophore above and below the ROI, reducing vertical diffusion effects while the confocal microscope images only

the plane of interest.[109] After identification of an ROI, the area is bleached with high intensity excitation light to permanently bleach the fluorophore. The ROI is then monitored using low intensity excitation light to measure diffusion of fluorophores and fluorescent recovery.

Diffusivity of fluorophores is calculated by modeling data to an equation that fits the general photobleach geometry and bleach pattern. Bleach shapes are also affected by light beam profile, either Gaussian or circular.[110] Modern laser excitation sources achieve bleach spots by high speed rastering of the laser light, providing uniform, non-Gaussian bleach profiles. For circular bleach profiles assuming an exponential recovery curve, zero immobile lipids and full fluorescence recovery, a simplified single exponential equation can be used to determine the lipid diffusivity (**2.3**).[108, 110]

$$D = (\frac{r^2}{4 * \tau_{1/2}})\gamma_D \qquad \text{2.3}$$

Where diffusivity, *D*, is a function of the bleach radius, *r,* half time of recovery $\tau_{1/2}$ and a correction factor, γ_D that is dependent on the bleach time and laser beam geometry (0.88 for circular beams). For more accurate results, where post-bleach fluorescence is greater than zero and recovery values may not reach pre-bleach values, fluorescence recovery results can be modeled to the recovery data using the differential equations used to describe the circular bleach spot. This model for a circular bleach profile is derived in section **2.5.3.2**. Equation **2.3** is the simplified three point fit solution to the differential equation outlined in **2.5.3.2,** with the assumptions of full fluorescence recovery and known halftime fluorescence recovery developed by Axelrod.[110]

2.5.3.2 Modeling of Fluorescence Recovery After Photobleaching

The following derivations were adapted from Minchul Kangs and Anne Kenworthy's *Complex Application of Simple FRAP on Membranes*.[111] Before understanding the recovery of fluorescence, fluorescence must be defined as a function of concentration of the diffusing species. Fluorescence of the tagged lipids is defined by **(Equation 2.4)**

$$F(x, y, t) = qI(x, y)C(x, y, t) \qquad \textbf{(2.4)}$$

In **Equation 2.4**, F is fluorescence intensity, I is the intensity of the excitation light, C is the concentration of fluorescent species and q is the quantum yield, i.e. how many photons are emitted per photon of excitation light. The fluorescence over the region of interest can be described as in **Equation 2.5**.

$$F(t) = q \iint_{ROI} I(x, y)C(x, y, t)dxdy$$

(2.5)

where, $I(x,y) = I_0 / \pi\omega^2$ and which describes the FRAP curve evolution as a function of time within the ROI.

Deriving the diffusion of fluorescent species within lipid bilayers from raw FRAP data requires a model that accurately describes the diffusion geometry and species. From Fick's first law, the diffusion of fluorescent species will move into the bleach area across a concentration gradient while the mass within the bleach area will remain conserved. Therefore the net change in the number of fluorescent molecules and the total flux of species will be equal to one another **(Equation 2.6)**.

$$\frac{\partial}{\partial t} \iint C(x, y, t)dxdy = - \iint \left(\frac{\partial F}{\partial x} + \frac{\partial F}{\partial y} \right) dxdy$$

(2.6)

Ficks law states that $\mathbf{F} \propto -\nabla C$ therefore for some constant D, $\mathbf{F} = -D\nabla C$ and the differential equation can be evaluation to produce **(Equation 2.7)**

$$\frac{dC(x, y, t)}{dt} = D\nabla^2 C(x, y, t)$$

(2.7)

Where, the laplacian operator defines $\Delta = \nabla^2 = \partial^2/\partial x^2 + \partial^2/\partial y^2$. The equation can be changed to into radial dimensions by changing the spatial variables $x = r\cos(\theta)$ and $y = r\sin(\theta)$.

FRAP for a three dimensional geometry in x,y and z can be described by **Equation 2.5** and C can be solved from equation **(Equation 2.7)** with the appropriate initial conditions. From PDE theory, the solution to **(Equation 2.7)** takes the form **(Equation 2.8)**

$$C(x, y, t) = \iint C(x, y, 0)\Phi(x - x'), y - y', t)dx'dy'$$

(2.8)

where $\Phi(x,y,t)$ satisfies **(Equation 2.9):**

$$\frac{\partial \Phi(x,y,t)}{\partial x} = D\Delta\Phi(x,y,t) \qquad \textbf{(2.9)}$$

In **Equation 2.9**, the initial condition of Φ at $t = 0$, $\Phi(x,y,0)$, is the Dirac function, δ_o. The δ_o function states every point on a line is zero, except at 0, which has an integral value of 1. Therefore, this describes our initial concentration at $t=0$ prior to any diffusion. Φ is solved by taking the Fourier transform to obtain an equation only in t and is then transformed back to a function of x,y and t by taking the inverse transform (**Equation 2.10**).

$$\Phi(x,y,t) = \frac{1}{4\pi Dt} e^{-\left(\frac{x^2+y^2}{4Dt}\right)} \qquad \textbf{(2.10)}$$

$F(t)$ is solved for using equation (**Equation 2.5**) after solution of $C(x,y,t)$ (**2.7**) with uniform laser profile $I(x,y)$ is solved using (**Equation 2.10**). The solution is an infinite series which can be converted into the explicit equation (**Equation 2.11**).

$$f(t) = \exp\left(-\frac{2\tau_d}{t}\right)\left[I_0\left(\frac{2\tau_d}{t}\right) + I_1\left(\frac{2\tau_d}{t}\right)\right] \qquad \textbf{(2.11)}$$

In (**Equation 2.12**), I_0 and I_2 are the modified bessel functions, τ_d is the characteristic diffusion time and $f(t) = (F(t) - F_o)/(F_{inf} - F_o)$. Diffusion (D) can be obtained from the relationship $\tau_d = \omega^2/(4D)$. The raw fluorescence data is modeled using the MATLAB function lsqcurvefit, which is a nonlinear curve-fitting function using a least squares method.

2.5.4 General Fluorescence Techniques

In addition to FRAP, confocal scanning laser microscopy is a valuable tool for a variety of other fluorescence based characterization techniques. Techniques such as fluorescence resonance energy transfer (FRET), fluorescence loss in photobleaching (FLIP) and fluorescence lifetime imaging microscopy (FLIM) are frequently employed in materials and biological characterization applications. While not used in this work, it is worthwhile to review them in the context of this work.

FRET is a frequently used fluorescence technique used to measure the proximity of fluorophores and understanding fluorophore interaction within mesoporous silica using two distinct fluorophores with overlapping emission and excitation wavelengths.[63, 104, 112] A donor fluorophore in its excited state can transfer energy to an accepting fluorophore, thus exciting the acceptor (**Figure 2.5**). The emissions wavelength of the

acceptor fluorophore can then be monitored to confirm energy transfer. [2] The excited state energy transfer between the donor and acceptor fluorophores occurs via a dipole-dipole coupling, making the distance between donor and acceptor interaction very short (nanometers). [113] This tool has been recently employed by Wang et.al. to confirm fluorophores incorporated within the silica framework during co-condensation are accessible as the materials surface within the pores. [63]
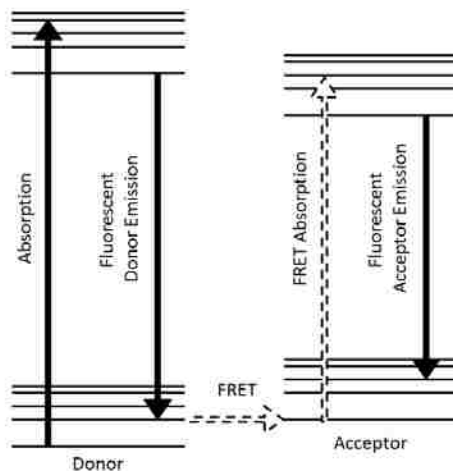
Figure 2.5 A modified Jablonksi diagram of the basic FRET interaction between two fluorophores. (Adapted from Jakowicz [2])

FLIP is used to determine the colocalization of fluorescent components. In FLIP, the biomolecule of interest carries two fluorescent labels, one of which is bleached and the second which is used as reference for localization. Two distinct regions of interest are identified on the sample. One ROI is repeatedly bleached while the second ROI, in a separate location, monitors fluorescence intensity.[114] This method is used to determine the flow and exchange of species between different portions of a sample and is often used to verify membrane continuity and determine exchange rates between different reservoirs.

In addition to FRAP, FRET and FLIP, FLIM uses the difference in exponential decay rates to produce an image from a sample. As opposed to using the fluorescence

intensity to image samples, the lifetime of the fluorescence decay is used to produce images. This method makes possible the observation of the local fluorescent environment, and its impact on environmentally sensitive fluorophores.[114] In addition to understand local environments, lifetime imaging is used to understand fluorophore interactions with other molecules, in a manner similar to FRET.

CHAPTER 3

Pore-Size Dependent Protein Adsorption and Protection from Proteolytic

Hydrolysis in Tailored Mesoporous Silica Particles

3.1 Abstract

Protein adsorption and interactions with mesoporous silica are of interest for a broad range of applications including drug delivery, chemical synthesis, biosensors and bioseparations. A major challenge in designing mesoporous silica supports for tailored protein interaction is the differentiation of protein interactions at the surface of the particle from interactions within the pore, important features when considering mesoporous silica as a protective support for active proteins. In this investigation, the location of Enhanced Green Fluorescent Proteins (EGFPs) adsorbed on tailored mesoporous silica particles is examined as a function of pore diameter using proteolytic hydrolysis to distinguish between accessible and inaccessible proteins. Pore size control is achieved by tuning the hydrothermal aging temperature (60°C - 110°C) during synthesis, where the synthesis results in 5 - 15 µm diameter spherical particles appropriate for imaging by confocal scanning laser microscopy (CSLM). In low pH environments, EGFP unfolds within pores and on the surface of particles, rendering it susceptible to proteolytic hydrolysis by the protease Pepsin A. Upon return to neutral pH, un-hydrolyzed EGFP regains it fluorescence and can be visualized within the mesoporous particles. The pore-size dependent loading and protection of EGFP (2.4 nm diameter x 4.2 nm) from proteolytic attack by Pepsin A (7.3 nm x 3.6 nm x 5.4 nm) is demonstrated by the retention of fluorescence in 7.3 nm pores. Larger-pored materials (> 9 nm) provide diminishing protection for EGFP, and the protection is greatly reduced with increasing pore size and pore size distribution breadth. Proteolytic hydrolysis is used to delineate the activity of pore-loaded versus surface-bound proteins and to establish that there is an optimal pore diameter for loading EGFP while protecting it from attack by a larger proteolytic enzyme.

3.2 Introduction

Significant interest in the development of nano-scale protein encapsulation platforms has coincided with advances in the synthesis of mesoporous silica, which provide the ability to engineer nanoscale materials with fine control of the surface and

pore environments. Mesoporous silica materials (MSMs) are inexpensive to produce, robust and employ well known aqueous-based synthesis chemistry with existing applications as platforms for separations and catalysis. [16, 17] The structures of MSMs can withstand high temperatures and pressures, are finely tunable, and synthetically versatile, allowing for a broad range of bulk forms (particles, monoliths, thin films), pore structures, and organic functional group incorporation. While the applications of MSMs for the separation and reaction of small molecules are well established, more recent interest in separations, catalysis and controlled release using larger biomolecules has grown as advances in synthesis techniques have made pore diameters greater than 5 nm in spherical particles readily achievable. [32, 115]

Approaches to increasing the pore diameters of MSMs for the encapsulation of proteins include the use of mixed cationic and non-ionic surfactant systems as well as aging the templated silica materials at increased temperatures before pore template removal. [4-7, 25, 47, 102, 116] Originally, Zhao et. al. reported the first large-pore mesoporous materials with well-ordered hexagonal close-packed pores having diameters as large as 30 nm. [3] These materials were denoted SBA-15 (Santa Barbara Amorphous batch 15). Initially developed using tri-block copolymer surfactants, such as Pluronic surfactant P123, these materials have significantly increased pore diameters as a function of synthesis temperature due to use of the large tri-block copolymers as the pore templating micelle. [25] Increasing the temperature of the micelles during particle formation incorporates more of the hydrophilic chain ends of the non-ionic triblock copolymer into the core of the micelle, thus increasing micelle size and subsequently pore diameter with increased aging temperatures. [3, 25, 117] The use of cationic surfactants such as CTAB as a cosurfactant along with P123 in acidic conditions yields spherical particles, with particle diameters dependent upon CTAB concentrations in solution. [4, 25] Acidic conditions are used due to the lower rate of silica condensation at low pH, allowing the shape of the particle to assume a sphere to minimize surface area and surface free energy. [118] Large pore diameters capable of protein adsorption (> 6 nm) have been reported in micron-scale spherical P123-templated silica particles (5 µm -20 µm diameter) by adjusting the temperature during hydrothermal aging (from 80°C to 125°C). [25, 115]

Due to the generally negative charge of silica materials and positive charge of most biological proteins at neutral pH, an inherent attraction is present between the surface of silica materials and proteins in solution. [33, 34, 119] The adsorption of proteins on the particle exterior and interior of pores provides different environments for the activity and stabilization of these adsorbates. The stabilization of proteins in biotechnology is dependent upon keeping the proteins active in an unnatural environment. [32] The confining effects of pore walls provide conformational stability to adsorbed proteins, thus protein encapsulation within the pores is desirable. [39] The ability to functionalize the exterior and interior of these structures extends their potential uses into biomimetic *in vitro* applications, using surface functional groups for drug delivery and targeted therapies. [120] Recently published reviews outline many of the applications of mesoporous silica as a biomaterial for encapsulating proteins as well as the potential for biological catalysis, size selective protein separations, biological signaling and drug delivery. [32-37]

Several research groups have demonstrated the use of tailored pore diameters for size selective adsorption of proteins, concluding that large pore diameters increase the accessibility of interior surface area for protein adsorption. [5-7, 48] Previously, protein depletion measurements in solution have been used to deduce protein loading on particles. [5, 6] High resolution confocal scanning laser microscopy (CSLM) has recently been employed to visualize proteins throughout mesoporous silica particles. [7, 43, 47, 102, 121] The diffusion of fluorescently tagged proteins and biomolecules is easily imaged in the well-ordered hexagonal close packed columnar pore structures of MCM-41 and SBA-15 materials. [47, 48, 70] CSLM imaging has been used to demonstrate the diffusion resistance of enhanced green fluorescent proteins (EGFP) (2.4 nm x 4.2 nm) in the pore openings of random shaped (4.1 nm pores), rod shaped (2.9 nm pores) and spherical (5.5 nm pores) particles. [47] Size selective protein adsorption within large pored silica materials has been visualized using fluorescently tagged lysozyme and bovine serum albumin (BSA). Pores of 7.4 nm and 12.7 nm diameter are fully accessible to lysozyme (3.0 x 3.0 x 4.5 nm) while prohibiting diffusion of BSA (4.0 x 4.0 x 14.0 nm). [7] A pore diameter of 2.8 nm prohibited the diffusion of both lysozyme and BSA. Visualization studies have been complemented by computational

studies of biomolecular diffusion, which suggest that significant diffusion resistance occurs in the boundary layer at the entrance to pores in which the pore diameter approaches the size of the proteins diffusing. [48]

Limiting active proteins to porous structures and confirming the location of proteins within the pores of the materials requires a technique to inactivate proteins that are located on the surface of the particles and not protected within pores. Proteases are common proteins that hydrolyze other proteins, rendering them inactive. EGFP, for example, is susceptible to proteolytic hydrolysis and inactivation by the porcine protease Pepsin A. [122] Hydrolysis of EGFP by Pepsin A results in a permanent loss of protein activity and fluorescence due to the preferential cleavage of peptide bonds between hydrophobic aromatic amino acids. [122] Nearly the entire protein sequence is required for chromophore formation, therefore cleavage of 1 of the 45 available hydrophobic aromatic amino acids provides inactivation of EGFP fluorescence. [122] The quantitative reproducibility of EGFP fluorescence inactivation by Pepsin A has led to its use in an assay to determine active Pepsin A concentrations. [122] The size of Pepsin A (7.3 nm x 3.6 nm x 5.4nm) is slightly larger than that of EGFP (2.4 nm x 4.2 nm barrel), suggesting a range of pore diameters for size exclusion of Pepsin A, ensuring proteolytic hydrolysis of only surface bound proteins. [123] Pepsin A activity on SBA-15 mesoporous silica materials with 7.0 nm diameter pores is consistent with limited accessibility of larger substrates in the pores. [124] Small substrates (Z-L-glutamyl-L-tyrosine) demonstrated significantly increased Pepsin A activity compared to the larger hemoglobin, which showed diminished activity, suggesting steric hindrance of the protease. [124]

The inactivation of proteins located on the surface of the particle using proteases is a novel approach to examine the protective environment of proteins in porous materials as well as to achieve materials with only pore-loaded active proteins. The concept is demonstrated in this work for a fluorescent protein (EGFP) / protease (Pepsin A) system using pore-diameter tunable silica particles appropriate for CSLM. EGFP is used both as a probe to visualize protein position and as a functional protein that will become non-fluorescent upon degradation by Pepsin A. CSLM is used to investigate protein protection as a function of pore diameter based upon imaging both before and after exposure of fluorescent protein loaded particle to a proteolytic environment. EGFP

loaded particles with pore diameters ranging from 5.4 nm – 11.6 nm are exposed to a solution of Pepsin A at low pH, rendering EGFP susceptible to hydrolysis by active Pepsin A. The dimensions of EGFP, Pepsin A and the pore diameter are used to interpret the results and to demonstrate size selective protein adsorption, protection and localization within spherical mesoporous silica particles.

3.3 Materials and Methods

3.3.1 Materials

Enhanced Green Fluorescent Proteins (EGFP) (≥97%) were purchased from BioVision and were received in a 1 mg/mL solution of PBS. Acetone (≥99.5%), ACS certified HCl (12.1M), and citric acid (≥99.9%) were purchased from Fisher Scientific. Lyophilized Pepsin A (≥2,500 units per mg dry) was purchased from Worthington Biochemical. Tetraethyl orthosilicate (TEOS, ≥98%) and crystalline trichloroacetic acid (TCA, ≥99%) were purchased from Acros Organics. Cetyltrimethylammonium bromide (CTAB, 98%) was purchased from Research Organics. 200 proof ethanol (ETOH, 200 proof) was purchased from Decon Labs. Pluronic P123 triblock copolymer $((EO)_{20}(PO)_{70}(EO)_{20}$ where EO is an ethylene oxide unit and PO is a propylene oxide unit, $MW_{avg}= 5800$) was purchased from Sigma Aldrich. All materials were used as purchased and dilutions were made using deionized, ultra filtered water purchased from Fisher Scientific.

3.3.2 Materials Synthesis

Spherical SBA-15 (SBAS) materials were prepared using an adapted version of Gartmann's synthesis procedure, as modified from the work of Katiyar. [7, 70] Initially, 3.10 grams of P123 was heated in a round bottom flask in a 50°C oven until melted. After this, 0.465 g of CTAB dissolved in 20 mL of deionized water was added to the P123. This solution was placed in a water bath at 30°C and stirred vigorously while 7.8 mL of 200 proof ETOH and 45.9 mL of 1.5 M HCl were added. After the P123 completely dissolved, 10 mL of TEOS was slowly added drop wise. This solution was mixed for 2 hours. At the end of 2 hours, the solution was poured into a Parr 4748 Teflon lined bomb, which had been acclimated to the hydrothermal aging temperature, between 60°C and 120°C, prior to use. The sample was kept at the desired hydrothermal aging temperature in an oven for 3 days. At the end of the 3 day period, the sample was

removed from the bomb and mixed in a high speed mixer to homogenize the solution. After homogenization, the sample was filtered and rinsed with 50 mL of deionized water. After filtration, the sample was placed into a single walled Whatmann cellulose extraction thimble and the surfactants were removed using Soxhlet extraction with 200 mL of acetone over 24 hours. The extracted particles are designated as SBASx, where x is hydrothermal aging temperature in °C, which is the independent synthesis variable.

3.3.3 Materials Characterization

Pore diameter and surface area were measured from nitrogen adsorption experiments (Micromeritics Tristar 3000) conducted at 77 K. Samples were degassed at 120 °C for a minimum of 4 hours under flowing nitrogen gas before analysis. Specific surface area was estimated using the Brunauer, Emmett and Teller (BET) isotherm and the pore diameter was estimated as the peak in the pore size distribution calculated by the method of Barrett, Joyner and Halenda (BJH). [125-127] The particles were imaged using a Hitachi S-4300 Scanning Electron Microscope (SEM). SEM samples were prepared by sprinkling the particles onto double sided carbon tape and attached to 15 mm aluminum mounts with M4 threads. Excess silica materials were blown off of the sample with nitrogen. Samples were prepared 24 hours in advance and left in a desiccator prior to being sputter coated in a gold-palladium alloy before analysis.

3.3.4 EGFP pH Based Denaturation and Renatuaration

The fluorescence of aqueous EGFP at room temperature was measured using a Varian Cary Eclipse fluorescence spectrophotometer. The "activity" of EGFP is interpreted from its fluorescence in the protein's folded state. Fluorescence experiments were performed at an excitation wavelength of 398 nm and excitation slit width of 5 nm, with the emission spectra measured at 508 nm. The stability of EGFP fluorescence was confirmed by monitoring its intensity in solution (11 µg/mL EGFP in 10 mM Tris-HCl at pH 7.5) in the absence of silica particles at room temperature for 30 hours. After an initial decrease of fluorescence intensity of 20% over the first 2 hours, the fluorescence intensity of EGFP remained constant. EGFP was denatured and renatured by pH using a combination of citric acid and Tris-HCl, as adapted from Malik et al. [122] Concentrated EGFP was diluted to 22 µg/mL in 10 mM Tris-HCl at pH 7.5. Upon use, 500 µL aliquots were denatured using 100 µL of 0.1 M citric acid solution to adjust the pH to 2.5. After

10 minutes, the fluorescence of the denatured sample was measured. The EGFP sample was renatured by returning the solution to pH 7.5 using 400 µL of 1M Tris-HCl at pH 8.5 and protein fluorescence while renaturing was monitored as a function of time.

All silica samples were pre-wetted before introduction of EGFP. Thirty milligrams of each SBAS material was first shaken with 1 mL of 10 mM Tris-HCl in a 1.5 mL centrifuge vial for 24 hours. After 24 hours these materials were centrifuged at 13,300 RPM for 3 minutes and the supernatant was discarded. The wetted particles were re-dispersed in 0.5 mL of 22 µg/mL EGFP and shaken for 24 hours to allow for EGFP diffusion into the particles. The silica particles were used to prepare three types of samples for CSLM; EGFP-adsorbed particles, pH-denatured/renatured EGFP particles, and pH denatured/Pepsin A exposed/pH renatured EGFP particles. Denaturation/renaturation of the protein adsorbed to the particles was performed by introducing 0.1 mL of 0.1 M citric acid to the protein loaded particles, reducing the pH to 2.5, and shaking for 10 minutes followed by raising the pH to 7.5 with the addition of 0.4 mL of 1 M Tris-HCl. Hydrolyzed EGFP-adsorbed particles were obtained by conducting the pH denaturation step, with shaking in the presence of 30 µg/mL Pepsin A in 0.1 M citric acid. The pH was raised in the same manner through the addition of 0.4 mL of 1 M Tris-HCl.

Samples of each type of EGFP/particle solution were prepared by dropping the suspended particles in EGFP solution onto glass slides and covering them with standard cover slips. The edges of the samples were sealed and samples were immediately imaged using a LEICA TSP SP5 Confocal Microscope. An argon laser was used to excite the fluorescent proteins over a 63X objective. The gain voltage on the photo multiplier tube detector was held between 995 and 1200 V. The scan speed was 400 frames per second. The CSLM images presented are slices through the center of a single particle or a pair of particles, where the scan corresponding to the approximate "center" of the spherical particles was established from greater than 20 scans of the spherical particles in the z-direction. Fluorescence intensity profiles were extracted by scanning along a line through the center of each particle in the CSLM images using ImageJ software (National Institutes of Health). Each set of images comparing the fluorescence of EGFP loaded into the particles at pH 7.5 and the subsequent image after exposing the same particles to

Pepsin at pH 2.5 and increasing the pH back to 7.5 were obtained under the same microscope conditions.

3.4 Results and Discussion

Spherical SBA-15 (SBAS) silica materials were chosen as the encapsulating structure for proteins based on their large particle size and sphericity, making them appropriate for imaging, as well as their large, tunable pore diameter range appropriate for protein loading. SEM images establish an average particle diameter range of 5 µm – 15 µm for these spherical particles (**Figure 3.1**). As seen in **Figure 3.1A,** particles synthesized at 60°C are characterized by a rough particle surface. SBA-15 particles transition from "gyroid" to spherical morphology when synthesized between room temperature and 80°C, therefore the rough surface of SBAS60, synthesized at 60°C, could be attributed to this transitional structure (**Figure 3.1A**). [118] Materials synthesized at higher temperatures are smooth relative to materials synthesized at lower temperatures (for instance, SBAS120 in **Figure 3.1B**).
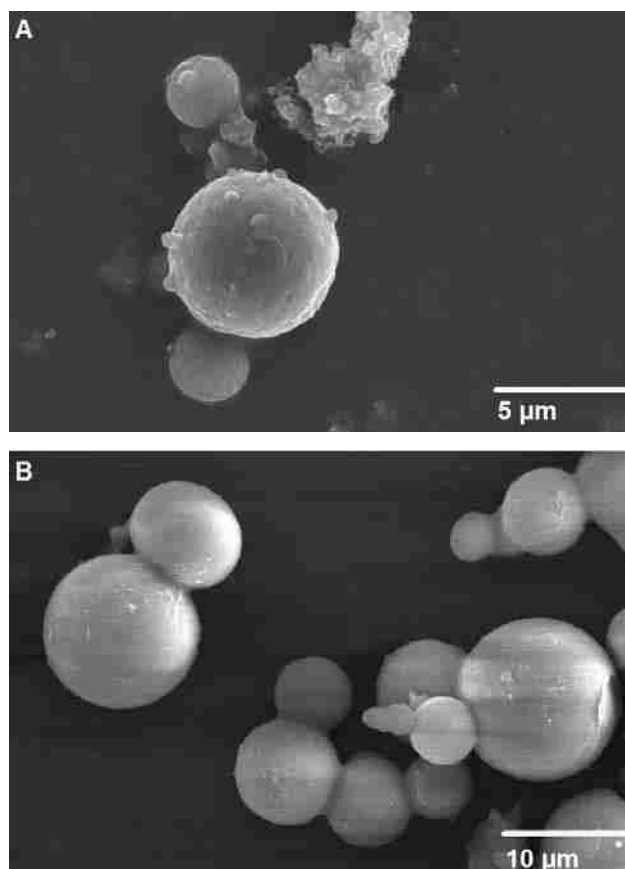
Figure 3.1 SEM images of SBAS materials synthesized at A) 60°C and B) 120°C.

A key feature of these materials is the large, temperature-tunable pore diameter range appropriate for protein loading that can be achieved using the same surfactant template system (P123 and CTAB). [25] Increasing temperatures during hydrothermal aging increases the hydrophobic volume of the micelle templates, thus increasing micelle and template pore diameters. [25] The pore diameter of the synthesized materials, as determined by the Barrett-Joyner-Halenda (BJH) method, range from 5.4 nm to 11.6 nm over the range of hydrothermal aging temperatures (60°C – 120°C) (**Table 3.1**). All materials have type IV isotherms, which are consistent with the well-defined mesoporous nature of these materials. The BJH pore diameter distribution for all synthesized materials is provided in **Figure 3.2**. Materials synthesized between 60°C and 110°C exhibit sharp pore diameter distributions, while a broader distribution is found at 120°C.

The presence of small mesopores is apparent in SBAS60 materials in **Figure 3.2** and is due to the ethylene oxide units of the large P123 copolymer extending from the templating micelle and into the walls of the silica matrix. [3, 25, 117] At higher temperatures, these small mesopores disappear as the ethylene oxide units are incorporated into the hydrophobic core of the micelle. [115] The pore diameters could be tuned in a range spanning from a diameter near to size of the protein to be encapsulated (EGFP 2.4 nm x 4.2 nm barrel, 26.9 KDa) to a diameter large enough to accommodate both the protein and protease (Pepsin A, 7.3 nm x 3.6 nm x 5.4 nm, 34.6 KDa). [122, 123, 128, 129]

Table 3.1 Surface area and pore diameter (mode of the pore size distribution) as a function of synthesis temperature determined by BET and BJH methods, respectively.

Sample	Synthesis Temperature (°C)	Surface Area (m^2/g) [a]	Pore Diameter (nm) [b]
SBAS60	60	819	5.4 ± 0.6
SBAS90	90	654	7.3 ± 1.5
SBAS100	100	532	9.2 ± 1.5
SBAS110	110	441	11.3 ± 1.2
SBAS120	120	311	11.6 ± 4.4

[a] The uncertainty of the BET regression of a single measurement is less than ± 2 m^2/g

[b] The value in parenthesis is the half of the full width at half maximum in the pore distribution peak
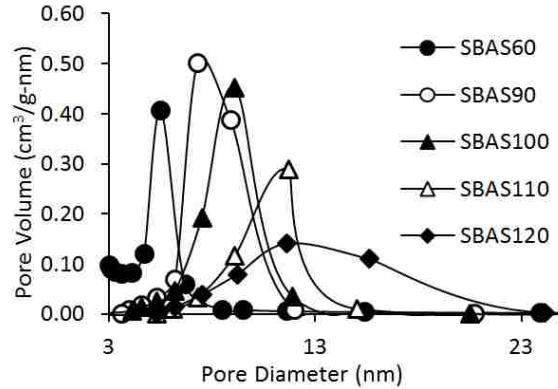
Figure 3.2 Effect of hydrothermal aging temperature on pore diameter distributions.

The pore diameter of SBAS60 (5.4 nm) is slightly larger than the largest dimension of EGFP (4.2 nm) while the pore diameter of SBAS90 is the same as the largest dimension of Pepsin A (7.3 nm). The pore diameters of SBAS100, 110 and 120, 9.2 nm, 11.3 nm and 11.6 nm, respectively, are large enough for both the diffusion of EGFP and Pepsin A, potentially limiting the size selective protective abilities of the pores. Thus, this pore range is ideal to test the hypothesis that an optimal pore diameter exists that is adequate for loading and protection of only the target protein within the pores of these materials.

Enhanced green fluorescent protein (EGFP) was chosen for this protein encapsulation study because of its robust renaturing abilities during pH changes as well as its significantly greater stability over wild type GFP, minimizing the effect of time dependent protein unfolding over the period of the experiments. [122, 130] Pepsin A is active below pH 4, a pH where EGFP is unfolded and non-fluorescent. In the presence of Pepsin A in acidic environments, EGFP undergoes proteolytic hydrolysis, rendering it incapable of refolding, thus permanently eliminating fluorescence. [122, 130] Visualization of EGFP not hydrolyzed at low pH by Pepsin A requires an increase of pH back to pH 7.5, permitting recovery of fluorescence and subsequent visualization in CSLM. The hydrolysis of EGFP by protease Pepsin A at pH 2.5 and the ability of EGFP to regain fluorescence after exposure to pH 2.5 (in the absence of the protease) was confirmed in solution (**Figure 3.3**). In the absence of protease, full recovery of EGFP fluorescence is observed in going from pH 7.5 to pH 2.5 to pH 7.5. In contrast, a total

loss of EGFP fluorescence is observed in an identical sample exposed to this denaturing and renaturing pH cycle in the presence of Pepsin A. The residual fluorescence intensity observed in the hydrolyzed protein solution is consistent with the background fluorescence from the solution.
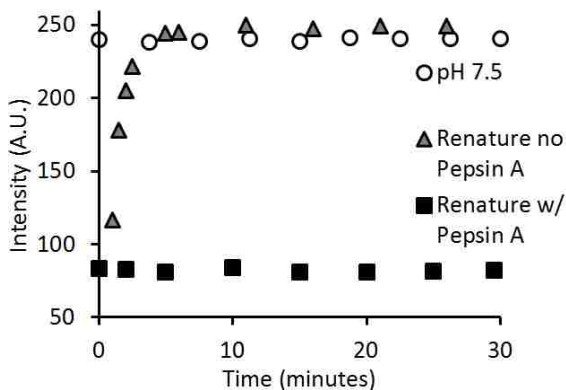
Figure 3.3 Fluorescence intensity of EGFP at pH 7.5, after denaturation at pH 2.5 and during renaturation via pH increase to pH 7.5, and after exposure to Pepsin A at pH 2.5 and renaturing at pH 7.5.

CSLM was used to establish the location of fluorescently active EGFP in the 5 µm to 15 µm diameter silica particles. **Figures 3.4 and 3.5** present the representative CSLM images and the corresponding fluorescence histograms taken across the center of a single spherical particle or pair of particles, respectively, as a function of the SBAS material. The first column in these figures is the fluorescence of the EGFP loaded particles prior to Pepsin A exposure. The second column is of the protein loaded particles after exposure to Pepsin A at pH 2.5 and renaturation at pH 7.5. The exception to the imaging of individual particles is the SBAS60 material (presented at 4x lower magnification). The particle clustering observable by CLSM is similar to SEM (**Figure 3.1A**), making this material less ideal for direct visualization of protein adsorption in pores. The histogram taken in **Figure 3.5** is over one particle that was located within the cluster image of SBAS60 in **Figure 3.4**.
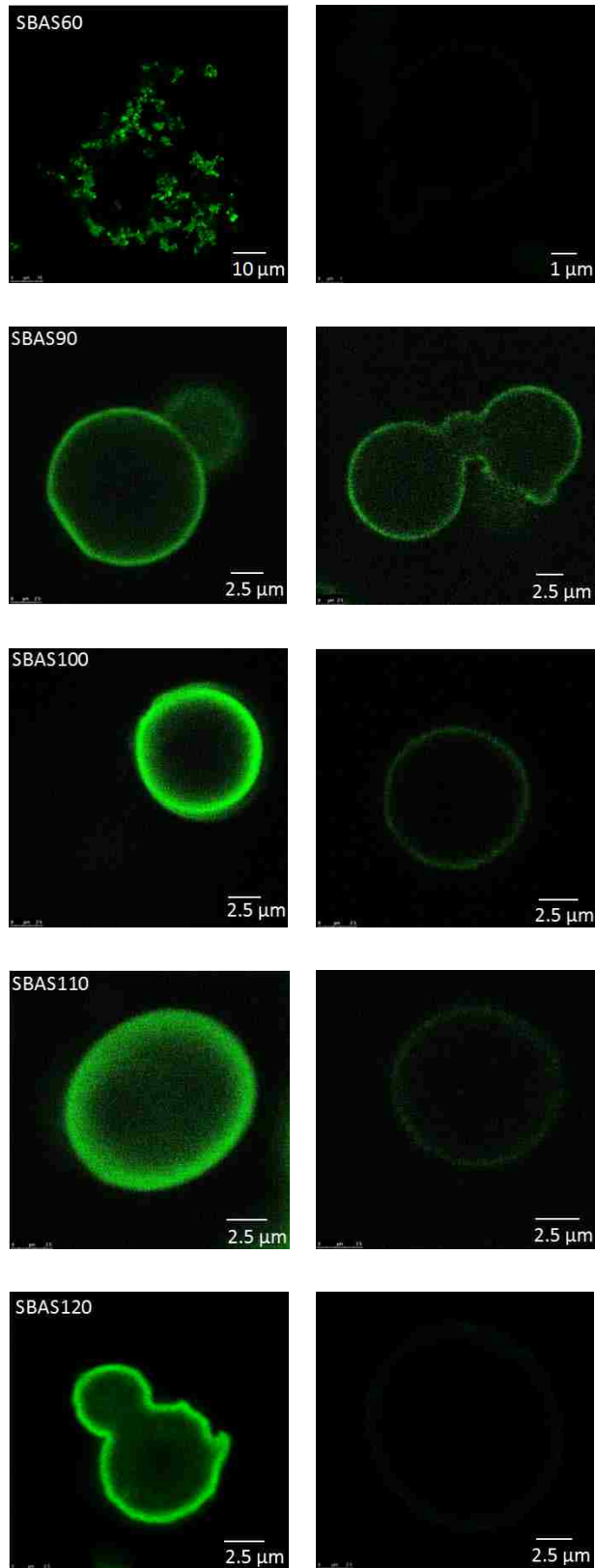
Figure 3.4 CSLM images of EGFP loaded

41

mesoporous silica materials (column 1) and EGFP loaded materials after exposure to active protease (column 2). The contrast of SBAS90, SBAS100 and SBAS110 images were enhanced by .1% for the clarity. The contrast of image groups SBAS60 and SBAS120 were unmodified.

SBAS60

SBAS90

SBAS100

SBAS110

SBAS120
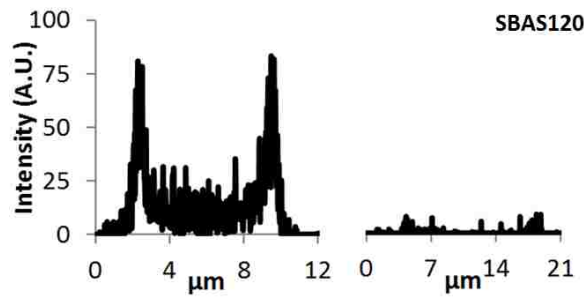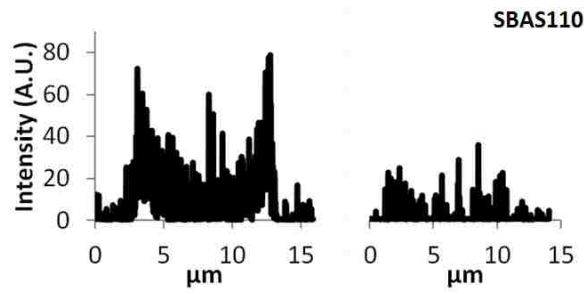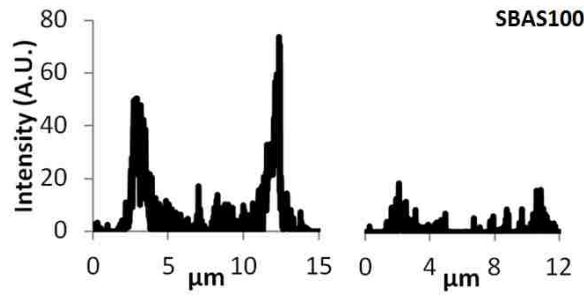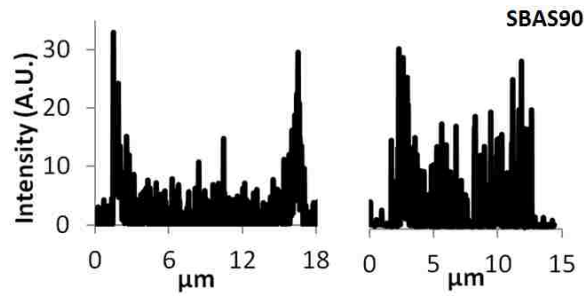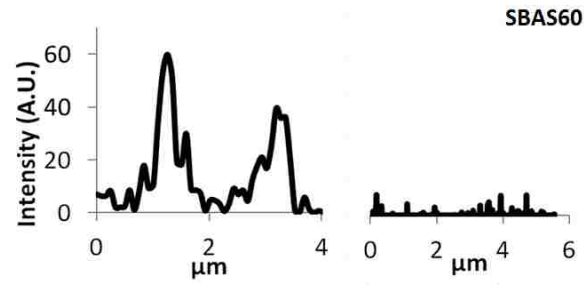
Figure 3.5 Histograms of the fluorescence intensity of EGFP loaded mesoporous silica materials (column 1) and EGFP loaded materials after exposure to active protease (column 2). Histograms correspond to images in Figure 4 without contrast enhancement, with the exception of the histogram for SBAS60 taken for a single particle from the cluster image in Figure 4.

The CSLM images can be used to interpret the accessibility of the pores to EGFP and the size-dependent protection of the EGFP from proteolytic attack. Minimal diffusion of the protein into the smallest pore material synthesized (SBAS60, 5.4 nm pores) is observed, as indicated by a sharp ring of fluorescence intensity at the surface of the particles after exposure to EGFP for 24 hours. The fluorescence of this surface bound protein is completely lost upon 10-minute exposure to Pepsin A, indicating that the standard protocol for EGFP hydrolysis by Pepsin A[28] is effective at hydrolyzing the surface protein. Although the pore diameter is greater than the largest dimension of EGFP (2.4 nm x 4.2 nm), the pores of SBAS60 are too narrow for the diffusion of active EGFP molecules over a 24 hour period. Protein accumulation on the surface of particles where protein dimensions approach the pore diameter has been attributed to the inability of native folded proteins to pass each other at the pore entrance. [48] While these images are similar to previous reports of GFP loading in porous silica, [47] our results uniquely establish the removal of surface proteins by proteases.

Increasing the pore diameter of the SBAS materials to 7.3 nm (synthesized with hydrothermal aging temperature at 90°C) allows for significant EGFP loading within the pores as well as protection against proteolytic attack of the pore-loaded protein. Greater loading of EGFP within the pores is indicated by a more diffuse fluorescence intensity profile in the CSLM image that extends into the interior of the particles. Although the pore diameter is theoretically sufficient to permit diffusion of both EGFP (2.4 nm x 4.2 nm) and Pepsin A (7.3 nm x 3.6 nm x 5.4 nm), these pores provide the best protection

against proteolysis (indicated by the highest level of fluorescence after Pepsin exposure relative to the intensity before exposure in **Figure 3.5**). The accessibility of the protease to a pore of similar dimension may be hindered, as in the case of protein buildup of EGFP at the surface of materials with 5.4 nm pores. Alternatively, the pore diameter must also be sufficient to allow for access of the active site of the enzyme to the protein in its unfolded state, dimensions that are not predicted by protein size.

Higher hydrothermal treatment temperatures lead to larger pore diameters, 9.2 nm and 11.3 nm for SBAS100 and SBAS110, respectively. The pore diameters of these carriers allow for even more effective diffusion of EGFP, which leads to a greater fluorescence intensity throughout the entire cross section of the protein-loaded particles in **Figures 3.4 and 3.5**. However, the large pores of these materials also permit diffusion of Pepsin A into the pores as indicated by the hydrolysis of EGFP within pores. The decreased fluorescence of the EGFP after exposure to hydrolysis conditions is more pronounced for EGFP-loaded SBAS120, although the mode pore diameter of this material, 11.6 nm, is only 0.3 nm larger than SBAS110. Complete loss of fluorescence intensity throughout the spherical particles is observed after exposure to active Pepsin A at pH 2.5. The broad distribution of pore diameters in the SBAS120 material may contribute to its inability to protect EGFP towards proteolysis. Although 11.6 nm is the predominant pore diameter in this material, a significant fraction of pores of larger size (greater than 20 nm) are available for diffusion of EGFP and Pepsin A.

Protein protection from proteolytic hydrolysis would be overestimated and underestimated, respectively, if the pores of mesoporous silica materials provide conformational stability to encapsulated proteins [34, 37, 39, 131], suggesting that protein unfolding may be less favorable relative to bulk solutions. Our description of size selective protein adsorption and protection from proteases assumes that EGFP undergoes pH denaturation (unfolding) and renaturation (refolding) in mesoporous silica. In support of our described mechanism of size-selective protein protection, EGFP loaded SBAS90 was subjected to pH denaturation/renaturation in the absence of the protease. SBAS90 materials have the smallest pore diameter (7.3 nm) capable of significant EGFP loading in this study. The potential that the unfolding or refolding of EGFP is constrained by the pore size would be most evident in SBAS90 relative to the larger pore materials

(SBAS100, SBAS110, and SBAS120). The fluorescence intensity histogram of EGFP within SBAS90 materials prior to lowering the solution pH (**Figure 3.6A**) and after denaturation at pH 2.5/renaturation at pH 7.5 (**Figure 3.6B)** are similar. The fluorescence of intermediate confocal images of EGFP loaded SBAS90 at pH 2.5 is indistinguishable from background noise, indicating denaturation of EGFP in the silica pores at low pH. The effective pH denaturation/renaturation of EGPF within silica pores is consistent with observations in silica gels that the difference in kinetics of unfolding are not distinguishable for GFPs confined in pores or in solution. [132] Stability of EGFP in SBAS90 is not due to confinement within the pores, but due to the pore diameter limiting the accessibility of Pepsin A to the unfolded EGFP.
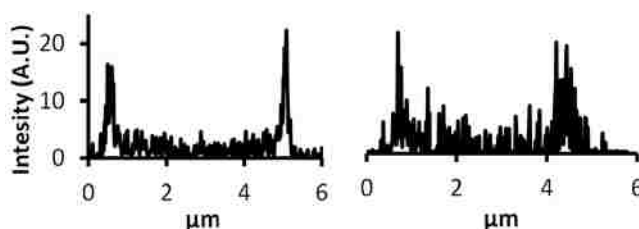
Figure 3.6 Histograms of the fluorescence intensity of EGFP loaded SBAS90, a) at pH 7.5 b) after lowering to pH 2.5 and returning to pH 7.5 in the absence of a protease. The lack of EGFP fluorescence at pH 2.5 is not shown.

3.5 Conclusion

This investigation provides direct evidence of size selective protein adsorption on porous spherical silica particles, a phenomenon that can be used to convey protective capabilities to pore loaded proteins or selectively remove proteins from particle surfaces using proteases. For the system of EGFP and Pepsin A, mesoporous silica with pore diameters greater than the diameter of the target protein provide for effective diffusion of the protein into the pores, while preventing rapid proteolytic attack within the pores even for a protease similar in size to the protein loaded in the pore. As the pore diameter increases beyond this optimal diameter, the loading of the target protein increases, but diffusion of the protease into the pores also increases, with the subsequent hydrolysis of the target protein. Increasing the synthesis temperature of SBAS materials increase the

pore diameter, and also increases the pore size distribution at the highest synthesis temperature. Materials with a broad pore size distribution (SBAS120) provide significantly less protection of the target protein from hydrolytic attack, although the mode pore diameter of 11.6 nm represents only a slight increase in pore size relative to materials synthesized at a lower temperature (SBAS110, 11.3 nm).

      The direct visualization of size selective protein protection and localization in porous materials made use of spherical SBAS materials, which were specifically chosen for this purpose based on their morphological homogeneity, narrow pore diameter distribution and most importantly, particle size, allowing them to be imaged using CSLM. The use of EGFP, which is stable, robust to pH changes and the use of Pepsin A to hydrolyze EGFP not protected within the pores, were also critical to this investigation. However, the interpretation of size selectively and protein protection against hydrolysis is applicable to mesoporous materials in general. Our results show that, consistent with some of the earliest studies of protein loading into mesoporous silica, merely having a pore size slightly larger than or similar in size to the protein being adsorbed is not always adequate for protein loading.[5] The use of a protease allowed us to more clearly demonstrate that the protein is indeed loaded into the pore, and that co-diffusion of proteins follows a similar trend to single protein diffusion – namely, that the pore diameter must be larger than the combined diameters of the pair of proteins to permit significant entry of the larger protein to occur. Thus, when tuning mesoporous materials for protein loading and delivery applications, the optimal pore size for loading with protection is likely to be found between the diameter of the target protein and the sum of the diameters of the target protein and the smallest proteolytic enzyme able to attack that protein. Also, when co-diffusion of proteins is desirable (for example, when co-locating enzymes for sequential reactions in mesopores), the optimal pore diameter for protein loading is likely to be larger than the sum of the diameters of the two proteins. These findings demonstrate the value of techniques that provide complementary information to bulk adsorption, release and activity measurements– namely tuned micron-scale particles for visualization of protein location, and introduction of proteolytic enzymes for removal of surface-bound protein from the particle surface and confirmation of protein protection.

These techniques are suggested to be broadly applicable in the design of mesoporous protein nanocarriers.

CHAPTER 4

Selective External Surface Functionalization of Large Pored Silica Materials Capable of Protein Loading

4.1 Abstract

Differentiating the chemical properties of the external and pore surface of sol-gel derived mesoporous materials by selective functionalization is important to advancing their application as platforms for biological catalysis, sensing and drug delivery. Prior selective functionalization techniques have been limited to small pores (≤ 5.5 nm diameter) incapable of loading large biological molecules. This work investigates the selective exterior surface functionalization by amines of larger-pored (>7 nm diameter) mesoporous silica particles, which are synthesized by dual surfactant templating and hydrothermal aging. Previously developed selective functionalization techniques rely on choice of functionalization precursor, functionalization reaction time, or pore blocking (by leaving pore templates in as-synthesized materials). The effectiveness of these strategies are compared for larger-pored materials using the precursors (3-aminopropyl)trimethoxyethoxyethoxy silane (APTMEES) and (3-aminopropyl)triethoxy silane (APTES). The extent of amine functionalization is determined as a function of precursor reaction time (10 or 20 minutes) in both as-synthesized and template-extracted materials by confocal laser scanning microscopy of the ~10 mm diameter particles tagged with fluorescein isothiocyanate. Reaction time, regardless of pore template presence, is demonstrated to be the controlling variable for achieving selective exterior functionalization in these larger pored mesoporous materials. Under the conditions used, 10 min of functionalization with APTMEES localizes amine groups at the exterior of the particles, while 20 min functionalizes both the exterior and the interior pore surfaces. Protein accessibility within pores, before and after selective and full functionalization, is visually confirmed by confocal fluorescence imaging of Rhodamine B tagged lysozyme probed particles.

4.2 Introduction

Complementary advances in the synthesis of mesoporous silica materials (MSMs) and the uses of proteins in biotechnology present new opportunities for enzyme catalysis, protein delivery, and protein-based sensing using silica platforms. [38, 45, 133-137] The

synthesis of templated mesoporous silica materials with tunable ordered pores of size appropriately large for protein loading (5 nm – 12 nm) has become routine. [3, 138] These materials can be synthesized in a variety of morphologies such as thin films and particles. [4, 15] The uses of enzyme loaded mesoporous silica materials range from biosensors to biocatalysts for the detection of a variety of compounds such as carbohydrates, aromatics and aquatic toxins. [34, 37, 119, 139-141]

The benefits of using mesoporous silica materials for the entrapment of proteins stem from the tunable properties of the materials. SBA type materials, synthesized with the tri-block copolymers such as Pluronic P-123 ((ethylene oxide)$_{20}$(propylene oxide)$_{70}$(ethylene oxide)$_{20}$), have transformed the synthesis of ordered large-pored metal oxides with a variety of tunable morphologies such as thin films and particles with different ordered mesostructures. [4, 15, 26] The addition of the ionic surfactant cetyltrimethylammonium bromide (CTAB) permits the synthesis of SBA-15 particles with spherical morphology and diameters in the micron range. [4] Hydrothermal aging of particles has proven to be an effective means of tuning pore diameters from 3.5 nm to 11.6 nm using temperatures between 60°C and 130°C. [25, 27, 142] Tunable pore sizes within mesoporous silica particles can be used for protein protection, protein separations and to sustain protein activity. [7, 27]

Protein loading within the pores of mesoporous silica is frequently established by bulk measurements of protein concentration or activity assays before and after exposure to particles. [46, 119] However, activity measurements can be difficult to interpret clearly due to limited accessibility of the substrate to the enzyme within pores. In addition, neither method can directly determine the location of proteins within the materials. Confocal laser scanning microscopy (CSLM), on the other hand, has the benefit of using fluorescent imaging to visualize the location of proteins on the surface or within the particles. [7, 70] For example, the diffusional resistance of enhanced green fluorescent proteins has been visualized within particles with pore sizes between 2.9 nm and 5.5 nm in both rod shaped and spherical particles. [47] Size selective protein separations have been visually confirmed using fluorescently tagged lysozyme and bovine serum albumin within 12 nm diameter pores of SBA-15 silica. [7] Recently, our group has demonstrated the use of spherical MSMs for pore-size dependent protection of

proteins within SBA-15 spherical particles in the presence of hydrolyzing proteases. [27] Hydrothermal aging was used to tune pore sizes between 5.4 nm and 11.6 nm in diameter where an optimum diameter of 7.3 nm permitted access of a smaller fluorescent protein, while protecting it from a larger protease. CSLM provided both confirmation of fluorescent activity and location of the protein within the particles.

The synthesis of separate organic functional domains, either on the exterior particle surface or in the pores, has the potential to further enhance the application of large-pored organic – inorganic porous structures for protein applications. Selective functionalization could regulate particle interactions with their environment, covalently anchor proteins either within pores or on the exterior surface of particles, screen molecules entering and exiting pores or be used in particle targeting with antibodies. Functionalization of mesoporous silica with amines, in particular, has been shown to stabilize enzymes in mesopores,[54] to modulate interactions of peptides and proteins with silica[55-58, 143] and to control particle uptake and cytotoxicity[59-61, 144].   Due to the versatile chemistry of primary amines on the surface of silica, amine functionalization allows for direct tagging with fluorophores or use as a building block for more advanced functionalization. [70, 145, 146] Precursors typically used to modify mesoporous silica are aminopropyl alkoxysilanes (e.g. 3-aminopropyltriethoxysilane (APTES) and 3-aminopropyltris(methoxyethoxyethoxy)silane (APTMEES)).

 Selective interior or exterior functionalization of ordered mesoporous silica has been demonstrated by using pore blocking in mesoporous silica (where an organic functionality is grafted while the pore template still resides in the pores),[8-12] by functionalizing non-selectively followed by diffusion-limited deprotection[66], by adding combinations of precursors at different times to generate layers with different functionality[62, 67], by intentionally functionalizing with bulky functional groups, sterically hindered from pore accessibility[68] and by passivating the external surface with an inert organic group followed by adding a second reactive silane to functionalize the internal pore surface.[8] Specifically for amines, selective external functionalization of silica with small mesopores (less than 5.5 nm) has been demonstrated through the selection of an amino silane precursor of suitable size and reactivity, and via pore blocking by the templating surfactant. [62, 65, 71, 147] For example, Gartmann et.al.

demonstrated exterior functionalization using the larger and less reactive aminosilane APTMEES for particles with 2.9 nm pores. [70] By functionalizing mesoporous materials in the presence of the unextracted P123/CTAB template, exterior surface functionalization was demonstrated for pore sizes up to 5.5 nm using APTMEES as the precursor. Selective exterior aminosilane functionalization has been interpreted from FTIR and NMR data, [71, 147] and visual confirmation of functional groups location via fluorescent tagging has been demonstrated with CSLM. [66, 70, 146]   However, the techniques used to functionalize small pored materials (pore blocking, choice of aminosilanes, and reaction time for functionalization) have not been translated to selective functionalization of large pore porous materials (pore diameter > 5.5 nm). [62, 70, 71]   Pores for protein loading and protection from environmental destabilization are required to be large in diameter (in excess of 5 nm) to accommodate protein dimensions, so a need exists to test and develop methods for selective functionalization to large pored materials. [27, 39]

The goal of this work is to demonstrate strategies for the selective exterior functionalization of large pore (>7 nm diameter) mesoporous silica particles with aminosilanes. SBA-15 sphere (SBAS) materials are employed in this study, which are micron-scale particles with tunable large mesopores obtained through dual-surfactant templating and hydrothermal aging. Synthesis conditions have been chosen (90°C hydrothermal aging temperature) to obtain 5 µm – 15 µm particles, appropriate for imaging by CSLM, with 7.4 nm diameter pores. The aminosilanes, APTES and APTMEES, are selected for their differing reactivity and size. The density of amine functional groups on the silica particles as a function of reaction time with the precursor (10 or 20 minutes) is examined for both as-synthesized (materials with the pore template left in the pores) and template extracted materials using FTIR and by a fluorescamine assay following dissolution of the particles. Functional group location and protein accessibility in the functionalized material is confirmed via imaging using confocal microscopy after fluorescent tagging.

4.3 Materials and Methods

4.3.1 Materials

ACS Certified Hydrochloric Acid (12.1 M) and hexanes were purchased from Fisher Scientific. Tetraethyl orthosilicate (TEOS , ≥98%) and Fluorescamine (Synthetic, 100% pure) were purchased from Acros Organics. Cetyltrimethylammonium bromide (CTAB, 98%) was purchased from Research Organics. Ethanol (200 proof) was purchased from Decon Labs. Rhodamine B isothiocyanate (TRITC), fluorescein isothiocyanate (FITC, 90%), 3-aminopropyltriethoxy silane (APTES, 99%) and Pluronic P123 triblock copolymer $((EO)_{20}(PO)_{70}(EO)_{20}$ where EO is an ethylene oxide unit and PO is a propylene oxide unit, $MW_{avg}= 5800$) were purchased from Sigma Aldrich. 3-aminopropyltris(methoxyethoxyethoxy) silane (APTMEES, 95%) was purchased from Gelest Inc. Lyophilized lysozyme (LYS, ≥20,000 units/mg) was purchased from MP Biomedicals. Proteins were purified after tagging with TRITC using Thermo Scientific Pierce polyacrylamide desalting spin columns with 6K MW cutoffs from Fisher Scientific. All dilutions were made using 18.2 MΩ DIUF water purchased from Fisher Scientific.

4.3.2 Materials Synthesis

Spherical SBA-15 particles were prepared using synthesis procedures adapted from Gartmann and Brühwiler, as modified from the work of Katiyar and Pinto. [7, 70] Initially, 3.10 g of P123 were heated in a 250 mL round bottom flask in a 50°C oven until melted. After this, 0.465 g of CTAB dissolved in 20 mL of deionized water was added to the P123. This solution was placed in a water bath at 30°C and stirred vigorously while 7.8 mL of 200 proof ethanol and 45.9 mL of 1.5 M HCl were added. After the P123 completely dissolved, 10 mL of TEOS was slowly added drop wise. This solution was mixed for 2 hours. After 2 hours, the solution was poured into a Parr 4748 Teflon lined reactor, sealed, and heated at 90°C for 3 days. The sample was then homogenized in a high speed mixer and filtered over Whatman #5 filter paper in a 55 mm Büchner funnel. The synthesized material was split into two portions prior to amine functionalization (described below). In one portion (labeled 'extracted'), the template was removed via Soxhlet extraction with 200 mL refluxing ethanol over 24 hours. The extracted materials were then filtered and dried in the oven at 80°C. The 'as-synthesized' sample was placed in an oven at 80°C overnight, leaving the template present in the materials.

4.3.3 Amine Functionalization of Mesoporous Silica

Extracted or as-synthesized material (200 mg) was dispersed in 10 mL of hexane in a 50 mL nitrogen-purged two-necked flask. To this solution, 190 µL of either APTES or APTMEES was added under vigorous mixing. This solution was stirred for either 10 or 20 minutes under a nitrogen atmosphere. The materials were labeled as AsSyn- XM or Extracted- XM for as-synthesized or extracted, functionalized for X Minutes (0M (non-functionalized), 10M or 20M). After the functionalization period, the particles were filtered from solution over Whatman #5 filter paper in a 55 mm Buchner funnel and rinsed with 25 mL hexane. These materials were then cured at 80°C for 24 hours. After curing, the materials were washed for 24 hours in 100 mL ethanol to remove any remaining surfactant (in both as-synthesized and extracted materials), filtered, and dried in an oven at 80°C overnight.

Washed and dried functionalized APTMEES materials were re-suspended in 10 mL hexane in a nitrogen-purged 50 mL two-necked flask. To this solution, 15 mg of FITC was added and mixed for 10 minutes. After mixing, particles were filtered over Whatman #5 filter paper, rinsed with 25 mL hexane and immediately placed in 100 mL ethanol under vigorous mixing to remove excess FITC. After 24 hours, materials were filtered from solution again and rinsed with copious quantities of ethanol over filter paper until the supernatant became colorless, indicating that the non-covalently bound FITC had been removed. After rinsing with ethanol, the materials were dried in an 80°C oven for 24 hours. APTES functionalized materials were tagged immediately following functionalization with 15 mg of FITC for 10 minutes followed by filtration over Whatman #5 paper and curing at 80°C overnight. Samples were washed in 100 mL 200 proof ethanol for 24 hours, centrifuged out of solution and dried.

4.3.4 Particle Characterization

Pore diameter and surface area were measured from nitrogen adsorption measurements (Micromeritics Tristar 3000) conducted at 77 K. Samples were degassed at 120°C for a minimum of 4 hours under flowing nitrogen gas before analysis. Specific surface area was estimated using the Brunauer, Emmett and Teller (BET) isotherm and the pore diameter was estimated as the peak in the pore size distribution calculated by the method of Barrett, Joyner and Halenda (BJH) using the adsorption branch of the nitrogen adsorption-desorption isotherm. [125-127] The particles were imaged using a Hitachi S-

4300 Scanning Electron Microscope (SEM). SEM samples were prepared by sprinkling the particles onto double sided carbon tape and adhering the tape to 15 mm aluminum mounts. Excess silica materials were blown off of the sample with nitrogen. Samples were prepared 24 hours in advance and left in a desiccator prior to being sputter coated using an Emscope SC400 with a gold-palladium alloy before analysis. Particle diameters were measured from the captured SEM images using ImageJ software.

FTIR was used to observe the removal of template during the functionalization procedure. The removal of the surfactant pore template was examined by exposing as-synthesized particles to hexane (the solvent used during functionalization) for 10 and 20 minutes. The FTIR spectra of the original as-synthesized particles and the hexane-exposed particles were analyzed for the presence of the pore template. FTIR also provided a complementary method to particle dissolution (below) for the determination of the extent of aminosilane functionalization of the materials. All FTIR samples were ground at a concentration of 0.5 – 1.0 % by weight in anhydrous KBr. Pellets were pressed and spectra taken using a desiccated and sealed ThermoNicolet Nexus 470 with a DTGS detector at room temperature.   Within the FTIR spectra, the areas beneath the CH_2 stretching (2800 cm^{-1} to 3000 cm^{-1}), Si-OH stretching (900 cm^{-1} to 984 cm^{-1}), and N-H bending (1570 cm^{-1} to 1740 cm^{-1}) bands were calculated using Thermo OMNIC software, and were normalized using the area of the Si-O-Si stretching (980 cm^{-1} to 1330 cm^{-1}) band to account for small changes in the mass of the bulk silica sample being prepared.

The amount of amine incorporated on the particles was quantified from the presence of amines in solution following particle dissolution at basic conditions. Fluorescamine, which covalently binds to primary amines to form a fluorescent pyrrolinone, was used to quantify the amines in solution. [148] Functionalized particles were dissolved over a 4 hour period in 30 mL of 0.02 M NaOH at room temperature under vigorous stirring. A 100 µL aliquot of the dissolved particle solution and 1.0 ml of 1.0 mM solution of fluorescamine in acetone was added to 2.0 mL of phosphate buffered saline (PBS) at pH 7.4. The maximum fluorescence of this solution at 480 nm was monitored after excitation at 366 nm using a Varian Cary Eclipse fluorescence spectrophotometer. Both excitation and emission slits were held at 5 nm. A calibration

curve with known amounts of aminosilanes was prepared by dissolving 30 mg of extracted, non-functionalized material in 30 mL of 80, 160 and 320 µM APTMEES solutions in 0.02 M NaOH. These calibration solutions (100 µL) were added to the PBS solution with fluorescamine and analyzed as described above.

4.3.5 TRITC-labeled Lysozyme to Probe Pore Accessibility

Lysozyme, at a concentration of 10 mg/mL in 1 mL PBS, was labeled at a ratio of 1:1 molar with TRITC for 24 hours at 4°C. After 24 hours, samples were purified in 100 µL aliquots according to the instructions provided with the Thermo Scientific spin columns (#89849). [149] New columns were unsealed and centrifuged for 1 minute at 1,500 x g to remove excess gel liquid. Columns were equilibrated in PBS by applying 100 µL PBS to columns and centrifuging at 1,500 x g for 1 minute. Proteins were purified by pipetting 100 µL of TRITC-Lys solution on the columns followed by centrifugation at 1,500 x g for 2 minutes. The accessibility of the particles to TRITC-labeled lysozyme before and after amine functionalization was examined by diluting the protein solution to 200 µg/mL in ethanol and mixing 1 mL of the protein solution with 10 mg of particles for 1.5 hours. After 1.5 hours, samples were imaged using confocal microscopy.

4.3.6 Confocal Scanning Laser Microscopy (CSLM)

Particles were prepared for CSLM (with a LEICA TSP SP5 confocal Microscope) by dispersing 10 mg of fluorescently tagged silica particles in 1 mL ethanol via vortex shaking for 24 hours. After 24 hours, one or two drops of the solution was placed on a glass slide, covered with a glass cover slip and sealed to prevent ethanol evaporation. An argon laser was used to excite the fluorophores over a 63X objective. The gain voltage on the laser was between 400 and 700 V. The scan speed was 400 frames per second. FITC emission was detected via a standard photomultiplier tube detector. Particles exposed to TRITC-labeled lysozyme were used as prepared and dropped onto glass slides for imaging, as described above. TRITC emission was detected with a photon counting high definition detector.

4.4 Results and Discussion

Selective external amine functionalization of mesoporous silica has previously been demonstrated for pore diameters ranging from 2.9 nm to 5.5 nm. [8, 62, 70, 71]

Selective functionalization for the largest pore diameter (5.5 nm) was achieved with APTMEES using as-synthesized (pore blocked) materials and verified visually using CSLM. [70] For the purpose of extending selective functionalization techniques to larger-pore materials appropriate for protein loading, spherical silica particles with tunable pore sizes are synthesized by combining mixed cationic and non-ionic surfactant templating methods with hydrothermal aging. [4, 7] In our previous work, 5 µm to 15 µm spherical particles were synthesized with a pore size range of 5.4 nm to 11.6 nm (corresponding to hydrothermal aging temperatures between 60°C and 120°C). [27] These spherical particles are appropriate for the visualization of protein loading by CSLM based on their large pore sizes and easily recognizable spherical morphology. Adsorption of proteins into pores with diameters that are greater than the largest diameter of the protein by 1 nm to 2 nm was demonstrated. Here, a synthesis temperature of 90°C was chosen to produce pore diameters of 7.4 nm, with a goal of producing accessible mesoporous silica materials for the model protein, lysozyme (3.0 nm x 3.0 nm x 4.5 nm).

The pore diameters and surface areas of as-synthesized and pore template extracted mesoporous silica particles synthesized by mixed surfactant templating were measured using nitrogen adsorption. Surface areas were calculated using the BET method and modes of the pore diameter distribution were determined from the BJH pore size distribution plots. Pore size distribution plots can be seen in **Figure 4.1.** As-synthesized samples have 59 m^2/g of external surface area with pore diameters of 6.0 ± 1.1 nm. As expected, template removal from the porous materials increases the measured surface area and pore diameter. The surface area and pore diameter of template extracted samples increases to 587 m^2/g and 7.4 ± 1.0 nm, respectively. Particles with spherical morphology and diameter of 7.34 ± 1.76 µm (n = 21 particles for this estimate) are obtained from this synthesis procedure, as seen in the representative SEM micrograph in **Figure 4.2.** This morphology makes the particles easily identifiable under a confocal microscope. Additionally, locating fluorescent protein probes and functional groups on the surface or interior of the particle is possible with spherical particles by performing z-scans in the third dimension to define particle boundaries during imaging.
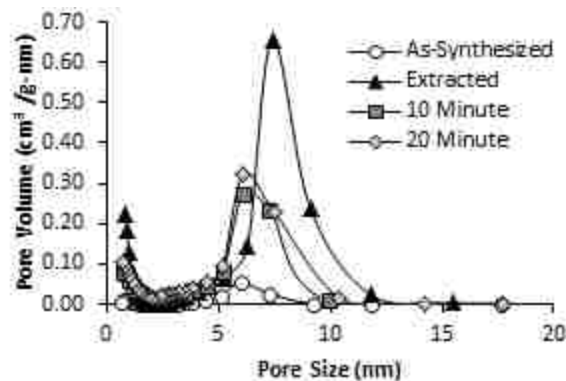
Figure 4.1 B.J.H. pore size distributions for materials synthesized after varying synthesis steps – as-synthesize, after extraction of the templates, and after 10 or 20 minutes of functionalization by APTMEES in hexane.
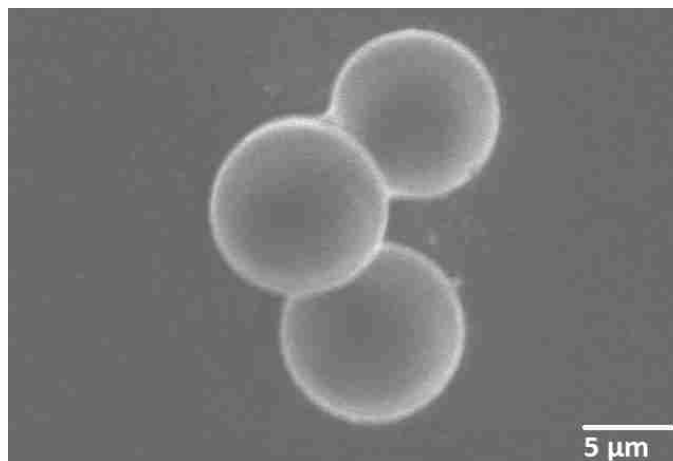
Figure 4.2 SEM image of non-functionalized, extracted mesoporous silica (denoted Extracted-0M).

A time-dependent functionalization method was chosen to selectively modify both as-synthesized and template extracted materials. The location of the grafted aminopropyl silane groups on the particles was determined by tagging the amine groups

with the fluorescent probe (FITC) and imaging the particles using CSLM. The effects of functionalization time (10 and 20 minutes) on the location of aminopropyl groups for APTMEES functionalization of as-synthesized and extracted materials are compared in **Figure 4.3**. The removal of FITC from non-functionalized materials with ethanol washing is effective, resulting in no fluorescence of non-functionalized particles after washing. Selective, exterior functionalization is evident in **Figure 4.3** for both as-synthesized and extracted materials after 10 minutes of exposure to APTMEES in hexane. In contrast, after 20 minutes of exposure to APTMEES in hexane, incorporation of the amine group both on the exterior of the particles and in the pores throughout the particles is observed. Similarly, grafting of another common aminosilane, APTES, was examined in extracted particles after 10 minutes of functionalization. Relative to APTMEES, APTES has significantly higher hydrolysis reactivity due to the reduced size of its alkoxy groups. [150] In spite of higher reactivity of APTES, selective surface functionalization is also observed for APTES grafted material after 10 minutes of exposure to particles in hexane (**Figure 4.4)**, suggesting a similar time-dependence for selective functionalization as in APTMEES.
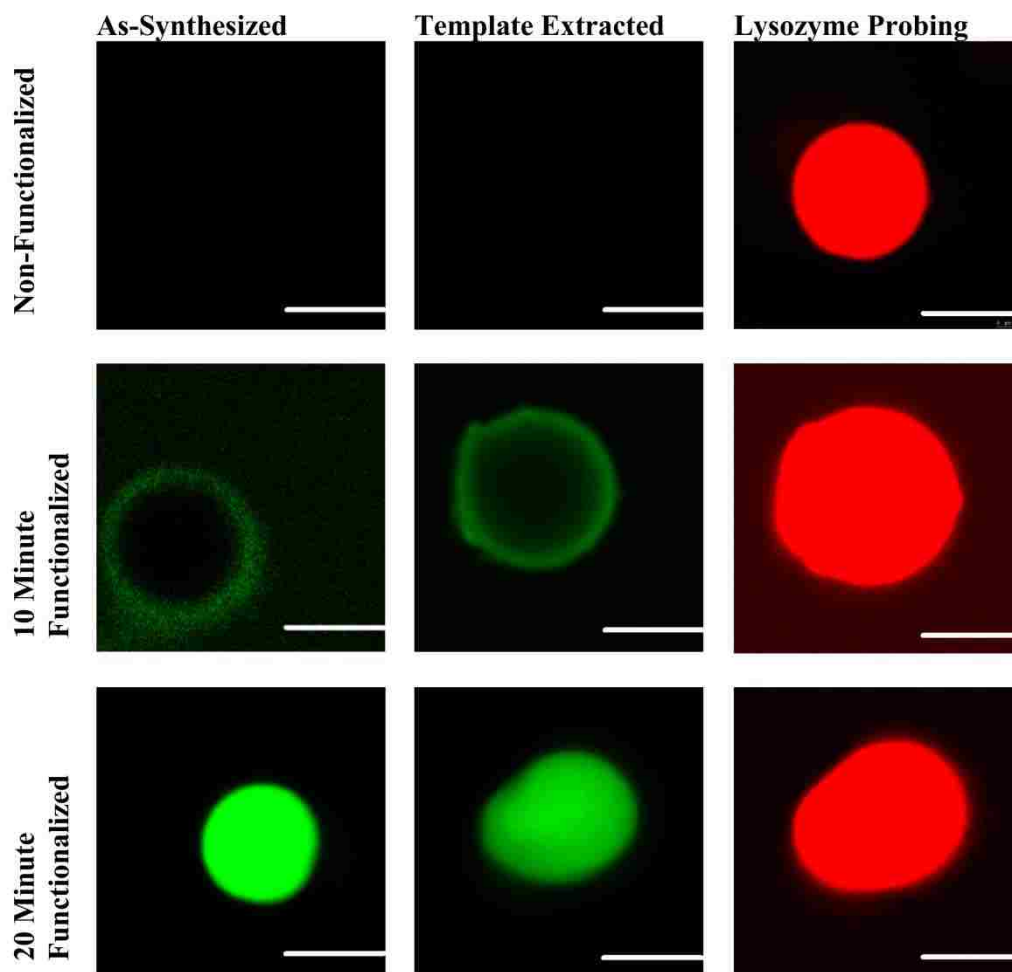
Figure 4.3 CSLM images of FITC tagged amine functional groups (green) before and after template extraction (left and center columns) for varying functionalization time. The materials after template extraction are simultaneously probed with TRITC tagged Lyszome (red). All scale bars are 5.0 µm wide.
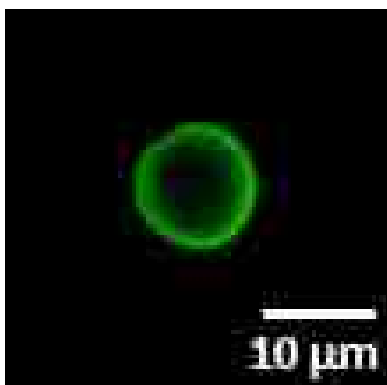
Figure 4.4 APTES functionalized
mesoporous silica particles after
FITC tagging.

Characterization of the effects of the reaction time for amine functionalization (0 (no functionalization), 10 or 20 min) on the surface area and the overall extent of functionalization was performed using nitrogen adsorption, FTIR, and an amine assay on the dissolved particles. Only template extracted materials were characterized due to potential effect of remaining templating agents on the FTIR and nitrogen adsorption results. The effect of APTMEES functionalization on the pore diameters for extracted particles is similar for 10 and 20 minutes of functionalization (**Table 4.1**). Pore diameters of non-functionalized and APTMEES functionalized samples are 7.4 nm and 6.1 nm, respectively. The reduction in pore size can be attributed to the presence of amine functional groups either on pore walls or at the edge of the pore openings, where they can extend approximately 0.5 nm into the pore space, although pore diameter differences after before and after functionalization approach the associated error of measurement. [151] The accumulation of aminosilane functional groups at the pore opening of smaller, 3.1 to 3.9 nm pores is well documented as a known artifact of post-synthesis functionalization. [151, 152]

Table 4.1 Pore diameter of materials after template extraction as a function of functionalization time using APTMEES

Functionalization Time	Pore Diameter (nm)
0 min. (as extracted)	7.4 ± 1.0
10 min.	6.1 ± 1.3
20 min.	6.1 ± 1.4

FTIR was used to qualitatively evaluate the functionalization of the particle surface with aminopropyl silane functional groups. Specific vibrational modes analyzed were the CH_2 stretching associated with the aminopropyl silane, Si-OH stretching of surface silanols and the Si-O-Si stretching of the bulk silica sample. All spectra are normalized by the area of their Si-O-Si stretching peaks (980 cm^{-1} -1330 cm^{-1}), which is representative of the amount of bulk silica prepared in each KBr crystal sample. The FTIR spectra in the region 800 cm^{-1} to 1500 cm^{-1} (**Figure 4.5A)** highlights the Si-O-Si stretching (1085 cm^{-1}) and the Si-OH stretching (970 cm^{-1}). The greatest absorbance at 970 cm^{-1} occurs prior to functionalization and is attributed to hydroxyl groups on the surface of the particles. This peak decreases as the surface silanols react with silanes to form siloxane bonds bound to aminopropyl silane groups during functionalization. After 10 minutes of functionalization the normalized peak area is reduced by 72 %, followed by a further reduction to 19% of the original silanol content after 20 minutes of functionalization, indicative of increased surface functionalization as a function of time. As can be seen in **Figure 4.5B**, minimal CH_2 stretching (2800 cm^{-1} – 3000 cm^{-1}) occurs in non-functionalized, extracted samples. CH_2 stretching associated with the propyl portion of the aminopropyl silanes increases fourfold after 10 minutes of functionalization, as compared to non-functionalized samples (as seen in **Figure 4.5B**). After an additional ten minutes of functionalization, a small increase of 3% in CH_2 stretching is seen. Although FTIR qualitatively describes particle functionalization, a

more quantitative method of particle dissolution was employed to measure the amount of aminosilane grafted to the particles.
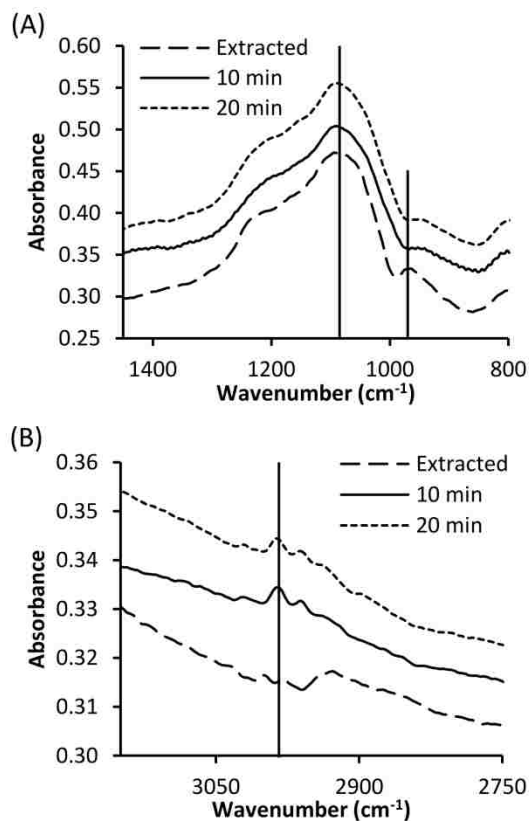
Figure 4.5 FTIR spectra of extracted (non-functionalized) silica particles and silica particles after 10 or 20 min of functionalization using APTMEEES. The regions are selected to highlight (A) the Si-OH stretching band (970 cm^{-1}) and (B) the CH$_2$ stretching band (2985 cm^{-1}). The FTIR spectra are normalized to the Si-O-Si stretching (1085 cm^{-1}) indicated in part in A.

Quantification of grafted APTMEES was performed via a fluorescence based amine assay following the dissolution of the silica particles in dilute sodium hydroxide.[151] After particle dissolution, fluorescamine, which covalently binds to the free primary amines to create a fluorescent pyrrolinone product, was added to the solution. The quantity of APTMEES grafted to the particles was determined from the fluorescence intensity of the solution and quantified using a calibration curve (**Figure 4.6**) developed from known quantities of APTMEES. After 10 minutes of APTMEES functionalization, grafting quantities reached 623.4 mg APTMEES per gram of silica sample (**Figure 4.7**). After an additional 10 minutes of grafting, the amount of amine increased by 45% to 906.0 mg/g. Each aminosilane covalently bound to the silica surface covers approximately 50 Å^2 of surface area when present in a monolayer [153]. The quantities of grafted amines at functionalization times of 10 and 20 minutes correspond to 3 - 5 times excess of monolayer coverage for the entire (internal and external) particle surface. This is consistent with the reaction conditions during particle functionalization. Although anhydrous solvents were used in nitrogen purged reaction flasks, water physiosorbed to the particle surface or minutely present in the reaction flask could induce hydrolysis and condensation between amino-silanes in solution and on the surface of particles, leading to multilayer formation. Although the deposition of aminosilane is significantly higher than monolayer coverage, the quantity of amine groups between 10 and 20 minutes is in qualitative agreement with the visualization of amine functionalization presented in **Figure 4.3.** Increased quantities of amines are deposited after 20 minutes of functionalization, as compared to 10 minutes of functionalization.
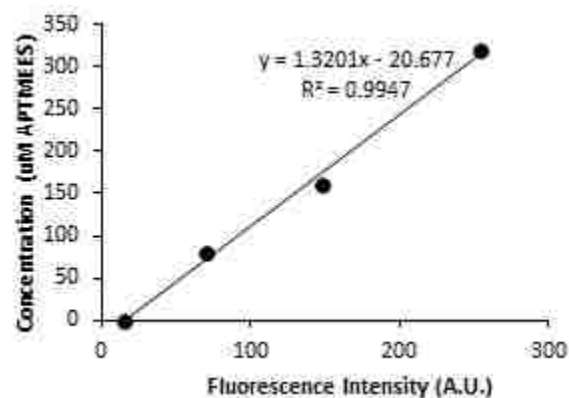
Figure 4.6 Calibration curve used for amine dissolution assay. Fluorescence from known quantities of APTMEES mixed with fluorescamine reagent is shown.
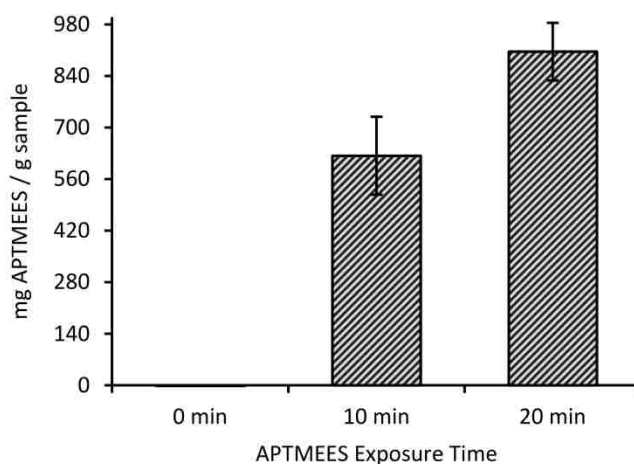
Figure 4.7 Quantity of amines grafted onto extracted particles as determined by the fluorescence emission of the fluorescamine-aminosilane derivative after particle dissolution.

Amine functionalization is observable in the pores deep within the particles after 20 minutes of functionalization for both the as synthesized and template-extracted materials (**Figure 4.3**). This finding is in contrast to an accepted approach to exterior-only functionalization of mesoporous silica - functionalizing as-synthesized materials while leaving the template in the pores to limit the accessibility of the reactive organic silanes to the interior pore walls. For small-pore silica materials (less than 5.5 nm), selective exterior functionalization using pore blocking with silanes has been confirmed with combinations of NMR, nitrogen adsorption, CSLM and FTIR. [8, 70, 71] The effectiveness of this pore-blocking approach for the larger-pore silica materials was examined by quantifying the presence of the pore template in the materials after exposure to hexane, the solvent used for the functionalization with APTMEES. FTIR spectra were measured for as-synthesized, 10 minute hexane-exposed, 20 minute hexane-exposed and Soxhlet extracted samples to compare the CH_2 stretching band associated with the pore template. A quantitative comparison between each sample can be made by normalizing the CH_2 stretching (between 2800 cm^{-1} and 3000 cm^{-1}) to the bulk silica samples by dividing the area under the CH_2 stretching band by the area under the Si-O-Si stretching band (980 cm^{-1} to 1330 cm^{-1}). The raw FTIR spectra with marked CH_2 and Si-O-Si stretching ranges are presented in **Figure 4.8** of the supporting information. The normalized CH_2 stretching associated with the pore template can be seen in **Figure 4.9.** There is a minor reduction in the quantity of template present after exposure to hexane; after 10 and 20 minutes of exposure to hexane, 92% and 83%, respectively, of the template present in the as-synthesized sample remains. In contrast, the Soxhlet ethanol extraction process removes over 90 percent of the original pore template. These results suggest that the while some template may be extracted by hexane during functionalization, its removal is largely incomplete during the amine functionalization procedure used for the as-synthesized silica particles. These results suggest that interior pore functionalization occurs independently of pore template presence in these hydrothermally processed, large-pored materials.
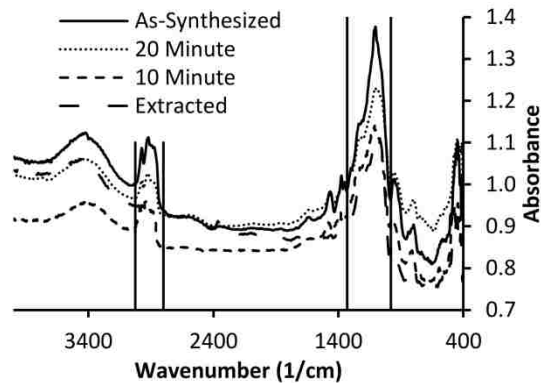
Figure 4.8 FTIR spectra of as-synthesized, extracted and hexane treated (10 or 20 minutes) samples.
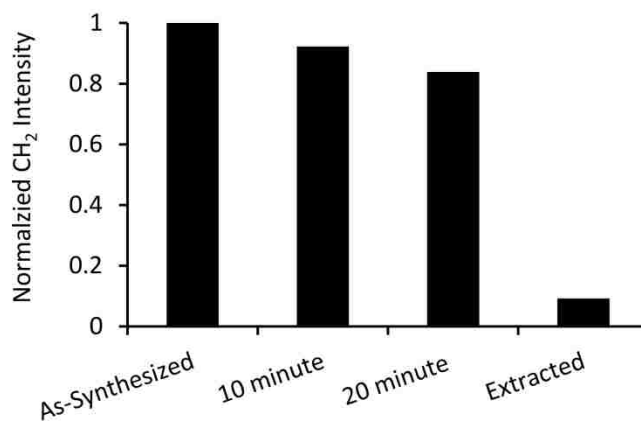
Figure 4.9 Normalized CH_2 stretching of the pore template in as-synthesized material as a function of duration of exposure to hexane. Materials washed by Soxhlet extraction are presented as a reference, and denoted "extracted."

The demonstrated functionalization of the silica pores in the presence of pore template suggest that the pore blocking techniques used to achieve selective exterior functionalization of small pore mesoporous silica may not be effective in materials

prepared by hydrothermal expansion of P123 micelles. Prior researchers have used mesoporous materials with smaller pore diameters, 2 nm – 4 nm, with CTAB as a pore blocking agent, and found evidence for selective external functionalization even with relatively long (on the order of hours) exposure periods to silanes in solution. [8, 71] Extended functional group exposure periods on the hour time scale are incompatible with the selective functionalization of the large-pored materials used here, which can be seen with full particle functionalization after 20 minutes. Aminosilanes have previously been shown to remove pore template by displacing surfactants within 4.9 nm pores and to rapidly hydrogen bond to surface silanols within pores. [154, 155] APTES, as well as the similarly structured 3-aminopropyltrimethoxysilane (APTMES), have been shown to displace the positively charged head group of CTAB (the templating surfactant) during a 10-hour period of refluxing, thus simultaneously displacing the template and functionalizing the pore walls [155]. This method of template removal and surface functionalization would not be evident in hexane exposure studies (**Figure 4.9)** due to the absence of aminosilane functional groups in the solution**.** Functionalization of both the external surface and the interior pore surface at longer functionalization times is consistent with the greater diffusion of aminosilanes into the pores, and perhaps increased template replacement with aminosilanes. In addition to displacement of the pore template, more rapid diffusion of APTMEES in the hydrothermally expanded CTAB and P123-based particles may be possible due to greater separation of the PEO blocks of the template from the silica walls due to increased hydrophobicity at elevated temperature. [25] At increased temperatures, water becomes a poorer solvent for the ethyleneoxide blocks of P123. Therefore at higher temperatures they retract into the hydrophobic core of the micelle, reducing their pore wall interactions. This reduced pore template – pore wall interaction, caused by high temperature synthesis, may increase the accessibility of aminosilanes to pore wall surfaces in the presence of P123 based templates.

This work establishes through visualization a selective, surface functionalization strategy for mesoporous particles with pore sizes appropriate for the protein loading. The accessibility of the pores of these functionalized particles is verified using a model protein, fluorescently tagged lysozyme, which has previously been used to demonstrate pore accessibility in non-functionalized mesoporous silica materials as well as size

selective protein separations in these materials. [7, 119, 156] Lysozyme, a 14.6 kDa protein with dimensions of 4.5 nm x 3.0 nm x 3.0 nm [157], has been shown in literature to adsorb into pore diameters as narrow as 6.5 nm. [7, 119] In this study, the favorable properties of the silica particles for CSLM imaging are used to visualize the accessibility of TRITC-tagged lysozyme for functionalized particles. The difference in the excitation and emission wavelengths of the TRITC tagged lysozyme and FITC tagged amine groups on the surface of the particles allow their location to be imaged simultaneously.

The location of TRITC tagged lysozyme within non-functionalized particles shows full penetration through the particles after 1.5 hours of passive protein loading (**Figure 4.3**). Although there is a pore diameter reduction after 10 and 20 minute functionalization, this reduction does not have an impact on the diffusion of lysozyme into the pores. Both selectively functionalized and fully functionalized materials are capable of loading lysozyme within pores throughout the particle. Previous reports using CSLM have visually confirmed accessibility of lysozyme within non-functionalized particles with 7.4 nm diameter pores, but this is the first documentation of simultaneous protein localization with selective external or full particle functionalization. [7] Similar amino-silane grafting attempts on smaller pored silica materials (4.0 nm pore diameter) block pores and significantly reduced pore accessibility to proteins – to the extent they have been used to permanently trap proteins within pores. [158] Similar to selectively functionalized materials, full functionalization of pore walls after 20 minutes of functionalization does not result in the clogging of pores, which would prohibit lysozyme diffusion into the pores. This observation is significant not only because it suggests that protein-accessible particles with engineered external surfaces can be prepared by controlling silane exposure times, but also because simultaneous imaging of functional groups attached to pore walls within close proximity to proteins inside of pores is an enabling technology for future studies of functional group / protein interactions in confined nanopore spaces.

4.5 Conclusion

The selective placement of functional groups on mesoporous particles allows for two distinct local interactions of a particle with a solute or with its environment. Selective functionalization of large-pored, protein accessible materials has been shown to be

69

primarily dependent on the reaction time of the functionalization, where shorter exposure time (10 minutes vs. 20 minutes) to aminosilane precursors led to localization of functional groups only at the exterior of the particles. As indicated by CSLM, the location of grafted amine groups (on the exterior surface or in the pores) is identical for as-synthesized (non-extracted) materials and extracted materials, indicating the ineffectiveness of the pore blocking method in selectively functionalizing large-pored materials prepared in this case by hydrothermal expansion of a P123 template. Although extended functionalization periods (in excess of an hour) can provide selective exterior functionalization in small pore blocked materials, aminosilanes in larger pored materials effectively replace template along pore walls, leading to pore wall functionalization.

The accessibility of pores after functionalization is critical in maintaining the applicability of large pored-mesoporous particles. Pore diameters were found to be somewhat reduced after functionalization, from 7.5 nm to 6.1 nm, in both selectively and fully functionalized materials. This reduction is consistent with the length of an aminopropyl functional groups extending into a pore opening. Although pore diameters were reduced, pores were still accessible to the model protein(fluorescently tagged lysozyme (14.6 kDa 3.0 nm x 3.0 nm x 4.5 nm)). Using both red and green fluorescent dyes, respectively, to tag proteins and particles, CSLM was used to simultaneously confirm the presence and full accessibility of lysozyme throughout non-functionalized, selectively external functionalized and fully functionalized particles.   Mesoporous silica materials have proven to be versatile platforms for biological interactions, although the ability to selectively locate functional groups on distinct particle surfaces can be difficult to verify. As demonstrated here, the selective functionalization of mesoporous silica with pore sizes appropriate for protein loading permits tailored interactions on the particle surface while providing the opportunity for protein based biological function within pore environments.

CHAPTER 5

Effect of Pore Size on the Diffusivity of Tethered and Supported Lipid Bilayers in Mesoporous Silica

5.1 Abstract

Incorporation of lipid bilayers on the surface and within pores of mesoporous silica particles provides for biomimetic approaches to analyte sensing and separations on high surface area platforms. The small diameter of typical mesoporous silica supports (50 nm – 300 nm) limits direct investigation of bilayer properties. In this work, lipid mobility in lipid-filled mesoporous silica is investigated as a function of pore size using spherical, large diameter (greater than 5 μm) mesoporous silica (SBAS) particles. Large diameter particles provide for the visual characterization of fluorescent lipid location and lipid bilayer diffusivity via confocal scanning laser microscopy (CSLM) and fluorescence recovery after photobleaching (FRAP), respectively, as a function of location in the particle (surface, mid-core, and core). SBAS materials with 3.0 nm, 5.4 nm and 9.1 nm pores were filled with dipalmitoylphosphatidylcholine (DPPC) by evaporation deposition, followed by hydration and sonication to form bilayers. Steric constraints restrict the DPPC bilayers (approximately 4 nm in thickness) to the surface of the SBAS with 3.0 nm diameter pores, while bilayers were present throughout the 5.4 nm and 9.1 nm pore diameters materials.. FRAP measurements indicate a pore size dependence on bilayer fluidity, with a 4.6 and 9.4 fold increase in bilayer diffusivity at the surface from 3.0 nm pores to 5.4 nm and 9.1 nm pores, respectively. Functionalizing silica surfaces with covalent lipid tethers (such as the lipid-like silane 13-(chlorodimethylsilylmethyl)heptacosane (CDSMH)) can promote bilayer adhesion and stability as well as affect bilayer fluidity. Formation of bilayers within mesoporous silica functionalized with CDSMH was prohibited in both 3.0 nm and 5.4 nm pore diameter materials, and only permitted throughout 9.1 nm particles. The diffusivity of tethered bilayers was significantly compared to supported bilayers, by a factor of 3.4 in 5.4 nm pore diameter materials and a factor of 1.4 in 9.1 nm materials. Diffusivity was reduced below the limit of detection in in 3.0 nm pored materials. This work presents a framework for interpreting high density loading of lipid bilayers within large pore diameter materials for bilayer based applications, as well as a platform for investigation

of bilayer location and function within these chemically and physically tunable, high surface area silica materials.

5.2 Introduction

Lipid bilayer membranes are synthetic analogues of the ubiquitous cell membrane found in biological systems. These biological membranes, coupled with numerous membrane associated proteins, control cell to cell signaling, selective membrane permeability, isolation of small molecules for detection and environmental sensing. [74] Mimicking these individual membrane functions in synthetic supported lipid bilayers is being explored for new molecule discovery, small molecule separations and catalysis.[74, 75] Solid surfaces provide physical stabilization of bilayers, tunable morphology and surface chemistry for applications, and allow for the use of surface characterization techniques to probe bilayer structure and function. [73] Mesoporous silica is morphologically versatile, capable of being synthesized in particles, thin film and membrane platforms, physically robustness and easily functionalized, making it an ideal support for lipid bilayers.[4, 15]

Mesoporous silica nanoparticles, typically synthesized with particle dimensions of 50 – 300 nm in diameter, have large surface areas and pore volumes which are suitable for drug loading and delivery [76]. Lipid bilayer enveloping of drug loaded nanoparticles have been used to design stealth particles and to develop therapies using membrane associated targeting peptides.[77]   Lipid bilayer membranes and membrane associated proteins have been incorporated in a variety of biosensor and small molecule sensing applications on nanoparticles due to their selectivity in molecular binding.[80] Membrane-based single molecule and ion transport devices have also been assembled around porous silica nanoparticles, using the large pore volumes as reservoirs for molecular transport.[78, 79]

The self-assembled structure of supported lipid bilayers (SLBs) renders them sensitive to environmental stressors, particularly those found in biological environments. In order to stabilize these nano assemblies, functionalization of silica with moieties that mimic lipids is used to promote bilayer adhesion, increasing stability against pH, temperature, ionic concentration gradients and other environmental factors that destabilize bilayers.[72] Silica can be easily functionalized for the purpose of forming

tethering bilayers (TLBs) using long chain alkane tethers[81], covalently bound lipid tails [82] and PEG-cushioned protein and peptide supports.[84, 85, 159]

While silica nanoparticles have been effectively employed as bilayer and membrane protein supports, limited techniques exist to characterize bilayer – particle interactions both at the surface and in the interior of the particles. In particular, the fluidity of bilayers on supported surfaces is an important property in their application and has been demonstrated as a key modulator of membrane permeability and membrane protein insertion and activity in bilayers.[86, 87] Fluidity is dependent not only on the specific lipid composition of the bilayer, but also on temperature and support surface chemistry. [88, 89] The tethering of lipid bilayers effects bilayer mobility, reducing bilayer diffusivity as a function of tether density.[84, 85, 95, 160]

Non-porous, micron diameter particles and non-porous thin films are common supports for the measurement and characterization of supported lipid bilayer diffusivity due to their respective large particle diameters (micron scale), suitable for microscopic visualization and surface characterization techniques.[88, 90-92] Confocal scanning laser microscopy (CSLM) has been employed for the characterization and visualization of a bilayer formation on non-porous supports, as well as the measurement of membrane fluidity via fluorescence recovery after photobleaching (FRAP) in both large diameter non-porous particles [90, 91] and non-porous planar thin films.[161] The fluidity of lipid bilayers on porous silica thin films has recently been measured for 1-palmitoyl-2-oleoyl-sn-glycero-3-phosphocholine (POPC) bilayers as a function of pore size (2 nm, 4 nm and 6 nm). [96] Multiple templating chemistries and synthesis strategies were required to achieve this range of pore sizes.   Deposition of the lipid bilayers on the porous surfaces by vesicle rupturing resulted in sometimes inconsistent bilayer membranes across the pores, as determined from AFM and QCM-D.   Both the changes in surface chemistry due to synthesis conditions [88, 162] and the method of bilayer coating [163] could contribute to inconsistent bilayer formation. While a trend of increasing pore diameter lead to increasing bilayer fluidity, these factors make the results difficult to interpret.

Recent materials development has made possible the synthesis of spherical, large diameter (5µm to 15µm), pore size tunable (3 nm – 12 nm diameter) SBA-15 (SBAS) silica particles appropriate for characterization by CSLM. [7, 27] SBAS synthesis utilizes

both a dual surfactant templating system and hydrothermal aging to form spherical particles and tune pore size using a single synthesis approach. Coupled with CSLM, these materials make possible the nano-scale investigation of the interaction of both small and larger, biologically relevant molecules with silica as a function of pore size. SBAS particles have been used to investigate pore size dependent protein separations as well as protein protection in hydrolytic environments. [7, 27]

Lipid bilayer coating of silica particles, both nonporous and porous, is traditionally achieved by rupturing preformed bilayer vesicles on particle surfaces, enveloping particles. While effective at producing pore spanning supported lipid membranes, this method is ineffective of forming bilayers within pores. [109, 164] On the other hand, the evaporation deposition of lipids into nano-pores and subsequent rehydration and sonication into bilayers is an effective method to form bilayers within nano-porous colloidal crystals.[109] Evaporation deposition of lipids has been used for increased bilayer loading and membrane associated isolation of small molecules for detection in nanoparticle platforms.[52] In regard to nano-confinement of lipid bilayers, diffusivity effects on membranes have been evaluated by Ratto and Longo, using gel phase lipid rafts as physical barriers to diffusing fluid bilayers, discovering order of magnitude reductions depending on gel phase density. [165] Lipid bilayer confinement within nano-pores may exhibit similar effects with reduced bilayer fluidity in narrow pore diameters.

Large diameter spherical SBAS mesoporous silica particles are capable of visual characterization using CSLM, which can be used to both confirm bilayer location within particles as well as measure the diffusivity of lipids at the surface of the particle and also within nano-confined pore spaces within the particle interior. The lipid dipalmitoylphosphatidylcholine (DPPC) is used as a model membrane system in this work to form bilayers (4 nm thickness) on the surface of and within particle pores. Lipids are deposited on particle surfaces via evaporation deposition and bilayers are formed via rehydration and sonication. Pore size tunable SBAS particles are synthesized using hydrothermal aging temperatures of 60°C, 70°C and 120°C to produce respective pore diameters of 3.0 nm, 5.4 nm and 9.1 nm, ranging above and below bilayer thickness. Fluorescence recovery after photobleaching (FRAP) is used to determine the fluidity of

bilayers supported on the particle surface as well as within pores in the particle interior. The effect lipid tethering on bilayer formation and mobility in porous nanoparticles is investigated using the lipid silane (13-(chlorodimethylsilylmethyl)heptacosane (CDSMH)), which is lightly deposited on particles surfaces. Using confocal scanning laser microscopy, thin optical slices can be taken throughout particles in different locations, making possible the location confirmation and measurement of bilayer fluidity within particle pores. Coupled with surface measurements of bilayer fluidity, this information provides a more complete understanding of lipid dynamics within nanoporous silica materials.

5.3 Materials and Methods

5.3.1 Materials

ACS certified hydrochloric acid (12.1 M), 200 proof ethanol, chloroform (ACS Grade), phosphate buffer tablets (0.01M phosphate buffer, 0.0027M KCl, and 0.137M NaCl at pH 7.4) and 18.1 MΩ de-ionized ultra-filtered water were purchased from Fisher Scientific. Tetraethyl orthosilicate (TEOS, ≥98%) was purchased from Acros Organics. Cetyltrimethylammonium bromide (CTAB, 98%) was purchased from Research Organics. Pluronic P123 triblock copolymer ($(EO)_{20}(PO)_{70}(EO)_{20}$ where EO is an ethylene oxide unit and PO is a propylene oxide unit, $MW_{avg}= 5800$) was purchased from Sigma Aldrich. 1,2-dipalmitoyl-*sn*-glycero-3-phosphocholine (DPPC) was purchased from Avanti Polar Lipids (Alabaster, AL). The fluorescent lipid *N*-(Fluorescein-5-Thiocarbamoyl)-1,2-Dihexadecanoyl-*sn*-Glycero-3-Phosphoethanolamine (DHPE-FITC) was purchased from Life Technologies (Carlsbad, CA). The lipid silane 13-(chlorodimethylsilylmethyl)heptacosane (CDSMH) was purchased from Gelest Inc. (Morissville, PA).

5.3.2 Materials Synthesis

Spherical SBAS-15 particles were prepared using synthesis procedures adapted from Gartmann and Brühwiler, as modified from the work of Katiyar and Pinto. [7, 70] Initially, 3.10 g of P123 were heated in a 250 mL round bottom flask in an 80°C oven until the P123 melted. This was then placed in a 30°C water bath and stirred vigorously while 7.8 mL of 200 proof ethanol, 45.9 mL of 1.5 M HCl, 0.465 grams of CTAB and 20 mL of deionized water were added. After complete dissolution of P123, 10 mL TEOS

was added dropwise. This solution was then mixed for 2 hours. After mixing the solution was transferred to a Teflon lined bomb and kept at either 60°C, 70°C or 120°C in an oven for 3 days. After three days, the mixture was broken up under a high speed mixer and filtered over Whatmann #5 filter paper in a 55 mm Buchner funnel. The pore template of the material was then extracted in a Soxhlet extractor with 200 mL of refluxing 200 proof ethanol. The final sample was dried at 80°C and stored for use.

5.3.3 Materials Characterization

Pore diameter and surface area were measured from nitrogen adsorption measurements (Micromeritics Tristar 3000) conducted at 77 K. Samples were degassed at 120°C for a minimum of 4 hours under flowing nitrogen gas before analysis. Specific surface area was estimated using the Brunauer, Emmett and Teller (BET) isotherm and the pore diameter was estimated as the peak in the pore size distribution calculated by the method of Barrett, Joyner and Halenda (BJH) using the adsorption branch of the nitrogen adsorption-desorption isotherm. [125-127] The particles were imaged using a Hitachi S-4300 Scanning Electron Microscope (SEM). SEM samples were prepared by sprinkling the particles onto double sided carbon tape and adhering the tape to 15 mm aluminum mounts. Excess silica materials were blown off of the sample with nitrogen. Samples were prepared 24 hours in advance and left in a desiccator prior to being sputter coated using an Emscope SC400 with a gold-palladium alloy before analysis.

5.3.4 Lipid Silane Surface Modification

For the formation of tethered lipid bilayers, particles were functionalized with 13-(chlorodimethylsilylmethyl)heptacosane (CDSMH), which was added in amount significantly less than monolayer coverage in an attempt to lightly functionalize particle surfaces without blocking pores. Monolayer coverage was calculated using the approximate surface area of 59 Å^2 for tethered silane attachment [83, 166] and assuming a 800 m^2/g accessible surface area on all materials. Sufficient CDSMH was used to functionalize 10% of the calculated monolayer surface coverage. In a 15 mL centrifuge tube, 10 mg of silica particles were combined with 5.5 mL of $CHCl_3$ and 1.4 µL of CDSMH in a nitrogen purged bag. After sealing of the tube and removal from the nitrogen bag the sample tube was vortexed for 1 hour while CDSMH reacted with the particle surface. The $CHCl_3$ was then blown off the sample under flowing air and the

sample was washed 3 times with 5.5 mL ethanol through repeated centrifugation cycles. After washing, the sample was dried in air at 80°C overnight. Surface functionalization of particles with the lipid silane CDSMH was confirmed using Fourier Transform Infrared (FTIR) spectroscopy. All FTIR samples were ground at a concentration of 0.5 – 1.0 % by weight in anhydrous KBr. Pellets were pressed and spectra taken using a desiccated and sealed ThermoNicolet Nexus 470 with a DTGS detector at room temperature.   Within the FTIR spectra, the identified bands of interest were the CH_2 stretching (2800 cm^{-1} to 3000 cm^{-1}), Si-OH stretching (980 cm^{-1}), and Si-O-Si vibration (1070 cm^{-1}) which identified the lipid silane, non-functionalized surface groups and bulk silica particle, respectively. For qualitative analysis of surface functionalization the areas beneath the CH_2 stretching (2800 cm^{-1} to 3000 cm^{-1}) and Si-OH stretching (915 cm^{-1} to 980 cm^{-1}) bands were calculated using Thermo OMNIC software, and were normalized using the area of the Si-O-Si stretching (980 cm^{-1} to 1330 cm^{-1}) band to account for small changes in the mass of the bulk silica sample being prepared.

5.3.5 Supported and Tethered Lipid Bilayers (SLBs and TLBs)

Particles were coated in supported lipid bilayers of DPPC containing 0.5 % DHPE-FITC in a method adapted from Wang et.al.[82] In one 2 mL centrifuge vial, 10 mg of particles (non-functionalized or lipid silane modified) were place in 0.5 mL $CHCl_3$. In a second 2 mL centrifuge vial 20 mg of DPPC and 0.12 mg of DHPE-FITC were placed in 0.5 mL $CHCl_3$. Solutions were sonicated separately for 5 minutes, combined and sonicated for an additional 30 minutes. After sonication, the $CHCl_3$ was evaporated by blowing air over the centrifuge tube and then placing samples under high vacuum for a minimum of 12 hours. To form bilayers, samples were sonicated at 47°C for 1 hour in 1 mL phosphate buffered saline (pH 7.4). Samples were shook and sonicated for an additional 15 minutes while cooling to 25°C. Excess lipid was removed from the samples by washing with PBS, centrifuging at 1,000 x g and repeating 3 times.

5.3.6 Differential Scanning Calorimetry (DSC)

DSC was used to confirm the formation of lipid bilayers on particle surfaces by measuring the gel to fluid phase transition temperature of DPPC bilayers on particles. Following the preparation of supported and tethered lipid bilayers on particles, particle suspensions were centrifuged at 1,000 x g to form a soft pellet. After formation of a soft

pellet, 10 uL of the pellet was hermetically sealed in a DSC sample pan. Thermograms were run on a TA Instruments Q600 DSC between 20ºC and 70ºC at a ramp rate of 10ºC/min and returned to 20ºC at a cooling rate of 10ºC/min.

5.3.7 Confocal Microscopy and FRAP

Samples of supported or tethered lipid bilayer particles were imaged within 2 hours of preparation using a Leica TSP SP5 confocal microscope. DHPE-FITC was excited at 496 nm with an argon laser at 6% laser power for imaging and emission was collected between 505 nm and 600 nm. Experiments were performed at 28°C over a x63/1.3 oil immersion objective. For FRAP experiments, one image was captured prior to bleaching, a 500 nm diameter disk was bleached once at 75% laser power, 5 images were captured at the fastest capture rate (1.3 seconds), 5 images were captured at 3 second intervals and finally 20 images were captured at 10 second intervals. Diffusivity was measured in three locations throughout the particle, at the particle cap, middle and core of the particle, (**Figure 5.1).**
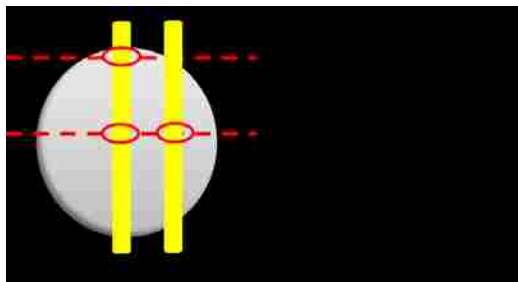
Figure 5.1 Location of FRAP measurements for determination of lipid diffusivity throughout the particle. Yellow columns indicate the path of photobleach light.

Pixel intensity data for the 500 nm diameter bleach spot was collected as a function of time and averaged via the Leica FRAP Wizard software. The diffusivity of the lipid bilayers was calculated from raw FRAP data modeled with the solution of the differential equation describing diffusion in a disk shaped (bleach) spot [111]:

$$f(t) = \exp\left(-\frac{2\tau_D}{t}\right)\left[\mathbf{I}_o\left(\frac{2\tau_D}{t}\right) + \mathbf{I}_1\left(\frac{2\tau_D}{t}\right)\right] \tag{5.1}$$

where f is the relative fluorescence recovery intensity as a function of time (t), I is the modified Bessel function and τ_D is the characteristic diffusion time. The relative fluorescence recovery is related to the measured fluorescence:

$$f(t) = \frac{F(t) - F_o}{F_{inf} - F_o} \tag{5.2}$$

F_o = fluorescence intensity at $t = 0$ and F_{inf} is the fluorescence at $t = \infty$ and $F(t)$ is the raw fluorescence intensity as a function of time, t. The diffusivity is a function of the bleach spot radius, r, and the characteristic diffusion time:

$$D = \frac{r^2}{4 * \tau_D} \tag{5.3}$$

The parameters of characteristic diffusion time and the fluorescence intensity at $t = \infty$ (F_{inf}) were determined by fitting the time-dependent diffusion data using MATLAB version R2012a and the lsqcurvefit function. Modeled diffusivity values and their 95% confidence intervals are reported in **Tables A1-A11** in Appendix A.

5.4 Results and Discussion

Large diameter spherical SBA-15 (SBAS) mesoporous silica particles were chosen for this study due to their large particles size and spherical morphology, making them appropriate for imaging, and their tunable diameters, appropriate for investigating lipid bilayer formation and fluidity within nano-pores. SEM images of particles (**Figure 5.2**) confirm their spherical shape and large diameters between 5 µm and 15 µm. The diameters of the hexagonally oriented pores formed in the dual templating surfactant system can be tuned using the hydrothermal aging temperature. Pores are templated from P123 and CTAB in the aqueous synthesis sol, where the hydrophobic cores of the pore templates expands with increasing synthesis temperature creating larger pore diameters.[25] In this study, hydrothermal aging temperatures of 60°C, 70°C and 120°C resulted in pore diameters of 3.0 nm, 5.4 nm and 9.1 nm (**Table 5.1**). Materials were named to indicate the particle type and pore diameter (in nm), with SBAS indicating non-

functionalized material after preparation and TLB indicating functionalization with the lipid bilayer tether (CDSMH), followed by the pore diameter. Synthesized pore diameters are below, near and above the thickness of the DPPC lipid bilayer (4.0 nm).[166] Surface area decreases and pore volume increases with increasing pore diameters (Table 1), expected trends for mesoporous silica. [126] TLB materials functionalized with CDSMH containing 12 and 14 carbon tails, similar in length to the 15 and 16 carbon tails of DPPC. After functionalization, pore diameters did not change, although surface areas and pore volumes decreased. This is consistent with the blocking of some of the pores during functionalization, thus lowering the overall surface area while not significantly reducing the pore diameter.
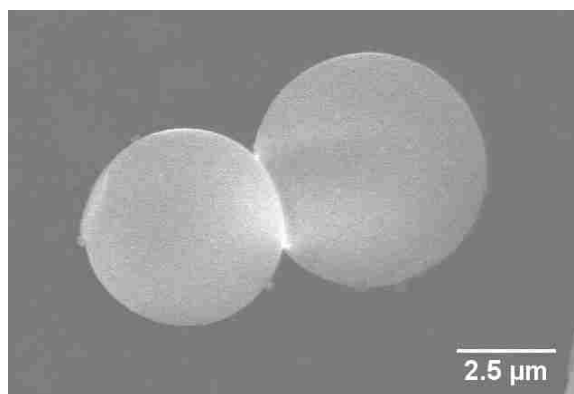
Figure 5.2 SEM image of SBAS mesoporous silica particles synthesized at 70°C.

Table 5.1 Surface area, pore diameter and pore volume as a function of pore diameter on bare silica (SBAS) and silica following lipid silane tethering (TLB).

Sample	Surface Area (m^2/g)	Pore Size (nm)	Pore Volume (cm^3/g)
SBAS-3.0	885	3.0	0.80
TLB-2.9	579	2.9	0.51
SBAS-5.4	866	5.4	1.28
TLB-5.4	626	5.4	0.91
SBAS-9.1	541	9.1	1.81
TLB-9.0	488	9.0	1.63

Particle surfaces were lightly functionalized with the lipid silane to not block pores and to retain the properties of a primarily DPPC bilayer. Thermogravimetric analysis of materials was used to determine the surface coverage of CDSMH functional groups of TLB materials relative to their non-functionalized SBAS starting materials (**Figure 5.3**). Analysis revealed the lipid silane functionalization density was approximately 120 mg CDSMH / g particles, which equates to 9%, 14%, and 11% of surface area coverage for TLB-2.9, TLB-5.4 and TLB-9.0, respectively, after functionalization (**Figure 5.4**). For comparison, full CDSMH coverage of materials with 800 m^2/g surface area is approximately 1100 mg CDSMH / g silica material.[83, 166]
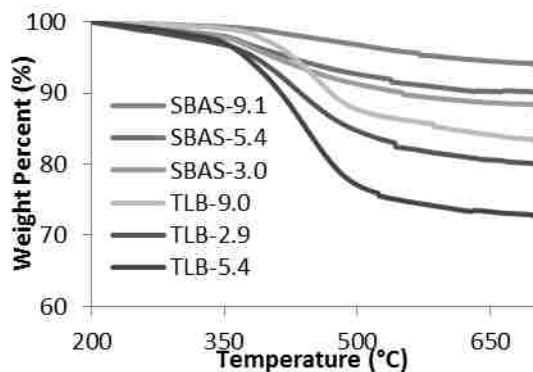
Figure 5.3 Thermogravimetric analysis (TGA) plots of materials before and after surface functionalization with CDSMH.
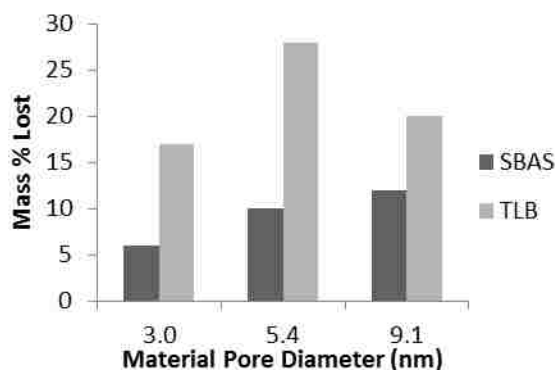
Figure 5.4 Weight percentage difference between non-functionalized SBAS and functionalized TLB materials after thermogravimetric analysis at 700ºC.

Fourier transform infrared (FTIR) analysis of samples is used to verify attachment of CDSMH to the particle surface (**Figure 5.5**). Two sharp peaks associated with the C-H vibration of the long hydrocarbon chains of the lipid silane are clearly present at 2850 cm^{-1} and 2930 cm^{-1} after functionalization. Additionally, the Si-O-Si network of the silica particles as well as remaining un-functionalized surface Si-O-H group vibration can be

seen at 1070 cm^{-1} and 960 cm^{-1}, respectively. A qualititative comparison of functionalization between each sample can be made by normalizing the CH_2 stretching band (between 2800 cm^{-1} and 3000 cm^{-1}) area of each sample by the Si-O-Si stretching band (980 cm^{-1} to 1330 cm^{-1}) area of each sample (**Figure 5.6**) The area beneath the CH_2 stretching peaks increases approximately by a factor of two due to the functional group presence. The reduction of surface silanol groups as they are replaced by tethered CDSMH can also be used to compare the extent of functionalization by a tethered silane. A similar factor of two decrease in the Si-O-H peak area (915 cm^{-1} to 980 cm^{-1}) relative to the Si-O-Si stretching band (980 cm^{-1} to 1330 cm^{-1}) area of each sample also occurs after functionalization (**Figure 5.6**).
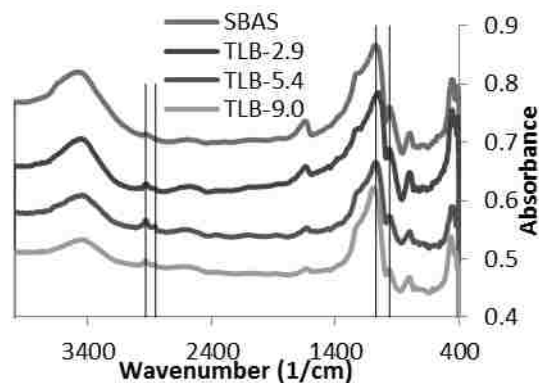
Figure 5.5 FTIR analysis of materials before
and after CDSMH functionalization
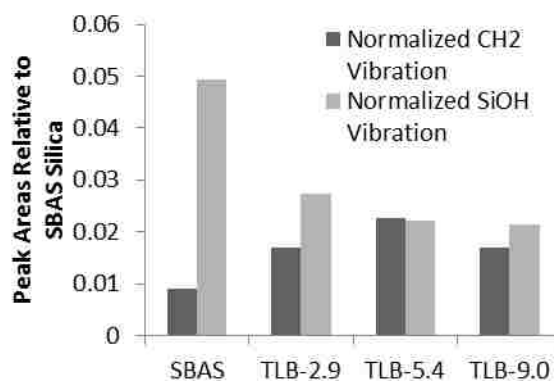
Figure 5.6 Normalized CH2 and SiOH vibration areas of CDSMH functionalized TLB materials compared to non-functionalized SBAS.

The lipid 1,2-dipalmitoyl-*sn*-glycero-3-phosphocholine (DPPC) was chosen for this study because DPPC membrane are frequently used as model membranes and primary constituent of cell membranes [94, 167] and because it has a phase transition temperature of 41°C, ensuring all bilayer measurements are made in the gel phase.[88] In addition to DPPC, the fluorescein-isothiocyanate tagged lipid DHPE-FITC is incorporated within the DPPC lipid mixture at 0.5% for visualization and FRAP measurements. Unilamellar vesicles for enveloping silica particles can be pre-formed from multilamellar vesicles by sonication or extrusion through polycarbonate membranes, which when mixed with nanoparticles adhere and wrap around the particle but do not enter the pores. [77, 90, 92, 109] Lipid enveloped SBAS materials with 9.1 nm pore diameters were prepared to demonstrate that, at even the largest of pore diameters investigated in this study, the particle is enveloped in a bilayer but preformed bilayers are not present in the pores (**Figure 5.7**).   In contrast, the solvent casting method of bilayer coating forms bilayers within nanoporous spaces, providing the opportunity to investigate bilayer mobility within pores at locations across the mesoporous particle. Solvent casting deposits lipid in pores via evaporation from chloroform, and uses sonication and rehydration to form bilayers within porous domains, when sterically feasible. The

bilayers formed by this method have been demonstrated previously to be unilamellar, as indicated via TEM imaging of stained bilayers on 100 nm diameter silica nano-particles with 2.4 nm pore diameters.[72] DSC was used to confirm the bulk phase transition temperature of all supported bilayers within pores and on the outside of particles to be between 41°C and 43°C (**Figure 5.8**), which agrees with the phase transition temperature of pure DPPC bilayer vesicles. [167]
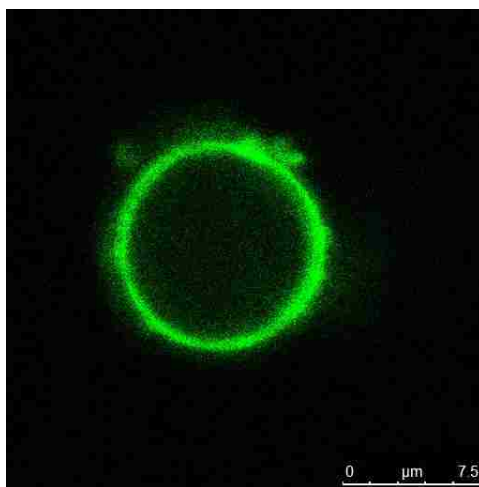
Figure 5.7 Lipid enveloped SBAS material with 9.1 nm pore diameter.
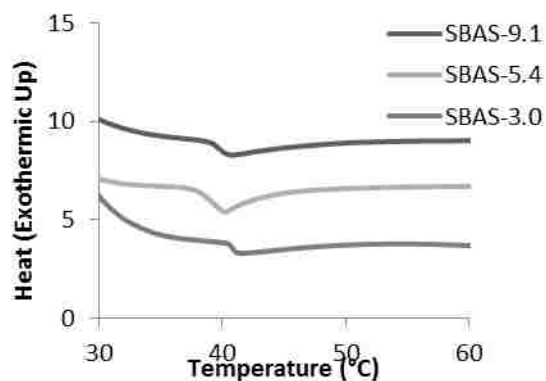
Figure 5.8 Differential Scanning Calorimetry analysis of lipid bilayers supported on particles.

After rehydration and bilayer formation of lipids deposited within the pores of SBAS-3.0 materials, bilayers are formed on the exterior of particles, as indicated by the halo of fluorescence around the particle. (**Figure 5.9**). The enveloping of particles with 3 nm pores most likely is due to the thickness of DPPC bilayers when fully hydrated, which is approximately 4.0 nm thick, prohibiting bilayer formation within the particles.[166] Rehydration of lipids with the pores of SBAS-5.4 and SBAS-9.1 materials results in lipid bilayer formation within pores (**Figure 5.9**).

Figure 5.9 Confocal microscopy images of Supported Lipid Bilayers (Column 1) and Tethered Lipid Bilayers (Column 2) on mesoporous silica with varying pore diameters.

CDSMH functionalized TLB particles were coated in lipid bilayers to form tethered bilayers using the same solvent casting method as used for SBAS materials. Following a similar trend to SBAS-3.0 particles, bilayers in TLB-2.9 materials were

formed only on the surface of particles (**Figure 5.9**). Ho et.al. confirmed a similar result on 200 nm diameter particles with 3.7 nm diameter pores by staining and imaging bilayers under TEM after formation, although a 70 fold increase in CDSMH used during synthesis relative to our study could have resulted in increased blocked pores and affected the interpretation of these results.[82]

Bilayers formed on TLB-5.4 materials were excluded to the exterior particle surface, which is unexpected considering their pore accessibility in SBAS-5.4 materials (**Figure 5.9**). Lipid tethers have the potential to alter the interstitial water space between the lipid and support surface as well as decrease the diffusivity of the bilayer upon formation. [83, 159] . The relatively narrow pore diameter (5.4 nm) approaching the bilayer membrane thicknesses (4.0 nm) coupled with perturbations in the membrane – support interstitial space may cause the available diameter of the pore to become too narrow to support bilayer formation within TLB-5.4 pores, resulting in exterior only bilayers on TLB-5.4 surfaces. Within TLB-9.0 materials, bilayers form within pores as well as the surface of particles due to the significantly larger pore space, providing room for bilayers to organize within the pores (**Figure 5.9**).

The diffusion of lipids on the surface of particles and throughout different locations within particles was measured using FRAP. In order to determine the diffusivity of lipids within pores of the materials, thin optical slices of particles were made through the equator of particles for core and mid-core FRAP measurements (**Figure 5.1**). For determination of bilayer diffusivity on the particle surface, and for particles that were enveloped by the bilayer (SBAS-3.0, TLB-2.9 and TLB-5.4 materials), cap FRAP measurements were made through thin optical slices of the top of particles (**Figure 5.1**).

The diffusivity of supported bilayers on the surface of particles varies with pore diameter, with increasing mobility with increasing pore size (**Figure 5.10A**). Bilayers on SBAS-3.0 enveloped the external particle surface, therefore measurements were only made on the particle cap, where the measured diffusivity is 0.044×10^{-3} μm^2/s. On SBAS-5.4 and SBAS-9.1 materials, which possessed bilayers throughout the particles, average diffusivities between the core, mid and cap of the particles were 0.326×10^{-3} μm^2/s and 0.574×10^{-3} μm^2/s, respectively. Interestingly, diffusivities were statistically identical between the core, mid and cap in each respective pore diameter, although were

statistically different between different pore diameters. These are the first measurements of bilayer diffusivity in lipid filled pores as a function of pore size and demonstrate consistent bilayer diffusivity throughout particles and on surfaces as a function of pore size. These results suggest long range, similar mobility of the bilayer throughout particles and at the surface. For comparison, POPC bilayers (T_m = -2ºC) on the surface of porous silica thin films with 2 nm, 4 nm and 6 nm pores also show a pore size dependence on diffusivity, increasing with pore diameter.[96] The pore size tuning methods in this work (hydrothermal aging) result in similar support surface chemistry and pore structure (hexagonal) for pore size comparison, where tuning in thin film systems required multiple different synthesis methods to achieve the reported pore size range, also resulting in different pore structures (Im3m and Pm3n). [96] Differences in support chemistry can result in orders of magnitude differences in measured bilayer diffusivity on planar supports.[88] Previous work highlights the surface-dependence of gel phase DPPC diffusivity on planar supports, where DPPC bilayers on mica and glass slide supports have diffusivities of 0.00009 μm^2/s - 0.05 μm^2/s, respectively.[88] DPPC fluidity within unsupported membrane vesicles is approximately 0.014 μm^2/s, approximately two orders of magnitude larger than particle supported membranes, although within range of planar supported membranes.[168] Our measured diffusivities of gel phase DPPC fluidity on mesoporous silica are within these values. Additional FRAP measurements of DPPC fluidity in multibilayers on glass slides reveal diffusivity of ≤0.05 μm^2/s, also a few orders of magnitude above the measured diffusivity in porous particles. Not surprisingly pore confined and supported DPPC bilayers possess reduced diffusivities as comparisons between supported POPC bilayers on non-porousr vs porous planar supports indicate higher diffusivities on planar supports as well.[96]

A
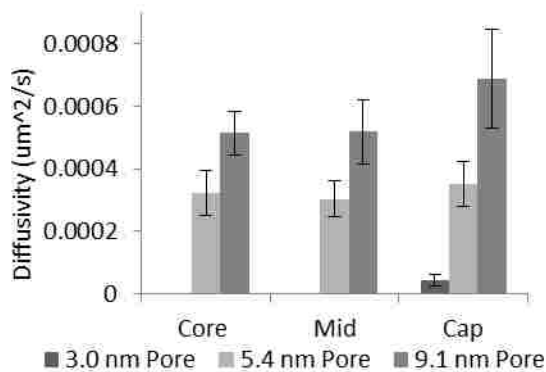
B
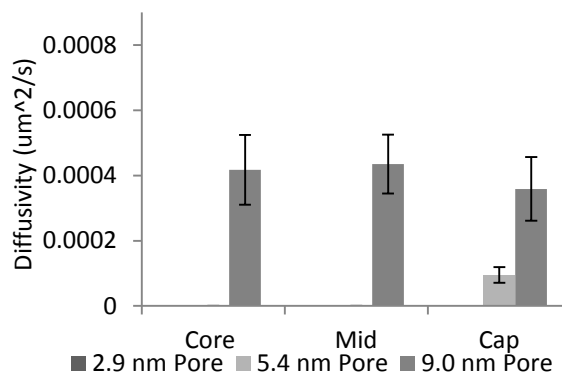
Figure 5.10 Diffusivity of DPPC bilayers
A) freely supported on particle surfaces or
B) tethered to particle surfaces on varying
pore diameter (3.0 nm, 5.4 nm and 9.1 nm)
materials. Error bars are representative of a
minimum of 7 fluorescence measurements.

In addition to impacting the location of formed bilayers on porous particles, bilayers immobilized on lipid tethered surfaces have decreased diffusivities compared to non-tethered systems. TLB-9.0 diffusivity, where bilayer is present throughout particles, is reduced by a factor of 1.4 to 0.404 $\times 10^{-3}$ μm^2/s compared to SBAS-9.1 supported bilayers. As was previously discussed in TLB-5.4 images, constraints within pores prohibited the formation of bilayers within pore spaces, leaving bilayers only on external

particle surfaces. The diffusivity of this bilayer was reduced by a factor of 3.4 to 0.095 $x10^{-3}$ µm^2/s throughout untethered particles as compared to SBAS-5.4 supported bilayers, indicating a clear reduction of diffusivity on the surface of particles due to tethering. Bilayer diffusivity on the surface of TLB-2.9 materials was below the limit of detection, as there was no recovery of fluorescence after monitoring for 180 seconds. This reduction in mobility is an indication of a combined effect of pore size and lipid tether on bilayer mobility, as lipid tethers reduce the overall fluidity of bilayers due to their inherent reduced as a function of tether density.[95]

This work is the first investigation of the behavior of lipid membranes within porous silica materials, with demonstrations of bilayer dynamics within particles, not limited to exterior surfaces only. Traditionally, lipid bilayers have been thought of as a surface coating on particle and planar systems to act as an interface between synthetic particles and their biological environments. Lipid-loaded mesoporous silica takes advantage of the high density hydrophobic core of bilayers upon loading into high surface area porous particles. Potential applications of lipid-loaded silica include small molecule separations, capable of sequestering hydrophobic small molecules, such as PCBs, from aqueous solutions, an area of active investigation for environmental remediation.[169] Additionally, small molecule transporters, such as boronic acids, have been used for the transport of hydrophilic small molecules across membranes.[170] These molecules are used to non-covalently bind and impart a lipophilic property to hydrophilic molecules, increasing their octanol:water partition coefficient and likelihood of bilayer uptake. Lipid filled porous silica particles with high density hydrophobic membrane cores are capable of sequestering lipophilic molecule from solution for hydrophobic molecule uptake, an active area of research for aqueous separation and purification applications.

5.5 Conclusion

The diffusivity of lipids in nano-porous regions is dependent on both the diameter of the nano-pore to which it is confined as well as to the surface chemistry upon which the bilayer is interacting. The large particle, tunable pore size platform used in this work provides the opportunity to visualize and study bilayers within particle pores and is the first demonstration of bilayer diffusivity investigation within multiple locations

throughout the same particle and across a variety of pore diameters. Bilayer diffusivity increases with increasing pore size and is independent of bilayer location within the core, mid or cap of the particle, suggesting uniform long range bilayer mobility in lipid filled pores. Tethering bilayers with the lipid silane CDSMH, significantly reduces the diffusivity of bilayers throughout the largest pore diameter particles by a factor of 1.4. In pore diameters (5.4 nm) approaching the thickness of a lipid bilayer (4 nm), lipid tethers within the pore forced lipid bilayers from forming permitting particle surface only formation, reducing bilayer diffusivity on the cap by a factor of 3.4. This is potentially due to perturbations in the interstitial membrane supporting water space reducing the working diameter of the pore, prohibiting bilayer formation. Large diameter particles are uniquely capable of optical slicing, permitting inner pore measurements of bilayer dynamics in nano-pores capable of extension into understanding membrane protein dynamics within membranes or the diffusion of guest small molecules through membranes and into lipid filled pores.

CHAPTER 6

Mesoporous Silica Micro-Particles as Whole Cell Plasma Membrane Supports

6.1 Abstract

The potential applications of supported lipid bilayers for sensing and separation are limited by the ability to incorporate functional transmembrane proteins in synthetic lipid bilayer vesicles, the traditional starting point for adhering the bilayer to the support. This work demonstrates the formation of supported lipid bilayers on mesoporous silica particles using plasma membrane microsomes as the source of the lipid bilayer. Direct transfer of these microsomes, vesicles composed of cell plasma membranes and membrane associated proteins expressed from mammalian cell lines, to the support have the advantage of maintaining proteins in their physiological lipid environment for increased stability. The synthetic versatility of silica particles, with tunable surface chemistries, particle sizes (50 nm – 15 µm) and pore diameters (2 nm – 30 nm), makes them an ideal platform for the investigation of bilayer integrity and membrane protein functionality. In this work, epidermal growth factor receptor (EGFR) is expressed in HEK293 cells, which are used to form plasma membrane microsomes via nitrogen cavitation, rupturing cells for membrane microsome reformation in solution, and purification via ultra-centrifugation. Microsome bilayers are adhered to spherical mesoporous silica particles (5.4 nm pore diameter) of large particle diameter (5 µm – 15 µm) appropriate for confocal imaging, and the integrity of the bilayer, and presence and selective ligand binding to the protein receptor is confirmed visually using a fluorescently tagged Epidermal Growth Factor (EGF) ligand. This work establishes an approach to synthesize supported bilayers on porous substrates that is generally applicable to the incorporation of membrane associated proteins and provides stabilization in their physiological lipid mixture throughout the process of bilayer adherence on the support.

6.2 Introduction

Mesoporous silica materials (MSMs) are a versatile support for investigating lipid bilayer membranes and their applications. [80] MSMs can be synthesized in a variety of morphologies, including thin films, particles and membranes, versatile for specific supported lipid membrane applications.[3, 15] Traditional formation of supported lipid bilayers on particle surfaces is performed via enveloping particles in preformed vesicles

composed of synthetic lipids. [76, 109] Both extrusion and sonication can be used to form vesicles and, upon mixing with particles, vesicles rupture on particle surfaces, enveloping the exterior. [76, 109] Lipid bilayers supported on spherical silica particles have been used for isolation of small molecules for detection, to investigate ligand binding to membrane proteins and to separate small molecules.[73-76, 78] In addition to their synthetic versatility, porous silica systems are physically robust and can be chemically tailored for specific applications. Specifically, silica surfaces can be modified with lipid-like alkane tethers to promote membrane adhesion to solid supports.[81, 82] These covalent tethers are used to enhance membrane stabilization on supports against pH, temperature and ionic strength gradients as well as influence bilayer fluidity.[72]

Although non-porous particles can be enveloped with lipids to form lipid membrane supports, their surface can limit membrane transport and function, particularly the function of membrane proteins. Non-covalent interactions between membrane associated proteins and non-porous surfaces limit protein function and fluidity within supported bilayers.[160] In contrast, the porosity at the surface of porous supports provides space for the incorporation of transmembrane proteins through the lipid bilayers, potentially limiting the protein / support interactions.[91] For small molecule separation applications, the pores of mesoporous silica particles act as reservoirs for membrane transport and storage or release of small molecules through the bilayer.[78] Small molecule separations have been performed on the surface of nanoporous silica nanoparticles using the transmembrane proteins Gramicidin A and Cyctochrome C for selective transport of ATP and ions, respectively, through lipid bilayer membranes and the pores of the silica support.[78, 79] In addition to molecular transport, pore associated proteins have been demonstrated as effective molecular sensing devices using fluorescent responses from ligand-receptor binding in particle supported membranes.[92]

The incorporation of functional proteins on supported lipid membranes requires the retention of protein function after removal from the physiological environment of the cells used to express the protein and reincorporation into synthetic lipid bilayers, which is often challenging for integral proteins.[80] Supporting cell derived membranes on particle surfaces is preferred as it keeps all membrane proteins in their native physiological lipid mixture, aiding in retention of functionality.[80] Nonporous silica

particles have been used to support natural yeast membranes, where membrane functionality was demonstrated by the synthesis of chitin in solution.[171] Hemolysed red blood cells have also been coated on the surface of nonporous and porous (400 nm pore diameter) silica chromatography packing (3 µm to 5 µm in diameter) and adsorption was confirmed via fluorescent antibody staining.[163] Most recently, porous silica particles (100 nm pore diameter) were used as supports for cell organelles (sarcoplasmic reticulum), containing the transmembrane protein Ca^{2+}-ATPase which hydrolyses ATP. [172] Reticulum coated particles were demonstrated as effective biocatalytic reactors in a packed column for flow through ATP hydrolysis.

Recent efforts in separating cell organelles have led to methods of purifying cell membranes into plasma membrane vesicles potentially ideal for transfer onto particle supports.[100] Gene transfection, introducing foreign nucleic acids to produce genetically modified cells, has made the expression of a variety of membrane proteins and components of interest possible, a powerful technique for investigation of protein function and gene regulation.[173] Cell plasma membranes separate intracellular components from the extracellular environment and possess many complex protein structures involved in signal transduction and transport.[97] Direct cell membrane deposition techniques on synthetic supports are crude. When membranes do not directly transfer by mixing particles with cells, methods of covalently tethering membranes on particle surfaces and shearing off the remaining cell have been employed.[163, 174] Transfer of cell-derived plasma membranes from genetically unmodified or modified cells onto silica particle supports has yet to be demonstrated.

Formation of cell membrane vesicles, microsomes, from mammalian cells can be performed via nitrogen cavitation, where whole cells are ruptured and membrane microsomes are allowed to self-assemble in solution. [175] Purification via ultracentrifugation results in pure microsomes composed of the original cell membrane and membrane associated proteins and molecules in their physiological lipid mixtures. Recent work has demonstrated the effectiveness of this method in the formation of microsomes from HEK293T cells, demonstrating the versatility of gene transfection via controlled receptor expression to evaluate receptor-ligand binding and membrane protein function in vesicles via single molecule fluorescence correlation spectroscopy.[176] The

incorporation of cell derived membrane microsomes on particle platforms is envisioned as possible via microsome enveloping of particles similar to traditional synthetic vesicle enveloping methods. This work demonstrates the formation of supported lipid bilayers onto mesoporous silica particles directly from microsomes containing a membrane protein receptor. Mesoporous (5 nm pore diameter) spherical silica particles are synthesized with particle diameters (5 µm – 15 µm) appropriate for visual confirmation of bilayer immobilization and ligand binding via confocal scanning laser microscopy (CLSM). Using nitrogen cavitation, microsomes are formed from HEK293T plasma membranes and purified using ultra centrifugation, resulting in cell membrane vesicles composed of original plasma membrane lipid mixtures and membrane associated proteins. Microsomes derived from cells with and without the membrane receptor epidermal growth factor receptor (EGFR) are adhered to the silica surface by vesicle rupturing. Confocal microscopy is used to confirm membrane adhesion to particle surfaces, receptor orientation and activity via ligand binding and membrane integrity via ligand exclusion from particle pores.

6.3 Materials and Methods

6.3.1 Materials

ACS Certified Hydrochloric Acid (12.1 M) and 18.2 MΩ DIUF water were purchased from Fisher Scientific. Tetraethyl orthosilicate (TEOS , ≥98%) was purchased from Acros Organics. Pluronic P123 triblock copolymer ($(EO)_{20}(PO)_{70}(EO)_{20}$ where EO is an ethylene oxide unit and PO is a propylene oxide unit, MW_{avg}= 5800) and phosphate buffered saline tables (Product P4417) were purchased from Sigma Aldrich. Cetyltrimethylammonium bromide (CTAB, 98%) was purchased from Research Organics. Ethanol (200 proof) was purchased from Decon Labs. The membrane dye 3,3-dioctadecyloxacarbocyanine perchlorate (DiO) was purchased from AAT Bioquest. Plasma membrane microsomes produced by nitrogen cavitation from HEK293T cells and HEK293T cells transfected with Epidermal Growth Factor Receptor (EGFR) were provided from the laboratory of Dr. Chris Richards (University of Kentucky, Department of Chemistry). These microsomes were produced as described in [176]. Epithelial Growth Factor (EGF) conjugated with biotin and linked via streptavidin to the fluorophore Alexa647 were purchased from Life Technologies (# E-35351).

6.3.2 Materials Synthesis

Spherical SBA-15 particles were prepared using synthesis procedures adapted from Gartmann and Brühwiler, as modified from the work of Katiyar and Pinto. [7, 70] Initially, 3.10 g of P123 were heated in a 250 mL round bottom flask in a 50°C oven until melted. After this, 0.465 g of CTAB dissolved in 20 mL of deionized water was added to the P123. This solution was placed in a water bath at 30°C and stirred vigorously while 7.8 mL of 200 proof ethanol and 45.9 mL of 1.5 M HCl were added. After the P123 completely dissolved, 10 mL of TEOS was slowly added drop wise. This solution was mixed for 2 hours. After 2 hours, the solution was poured into a Parr 4748 Teflon lined reactor, sealed, and heated at 70°C for 3 days. The sample was then homogenized in a high speed mixer and filtered over Whatman #5 filter paper in a 55 mm Büchner funnel. Pore templates were removed via Soxhlet extraction with 200 mL refluxing ethanol over 24 hours. The extracted materials were then filtered and dried in the oven at 80°C. Materials were crushed in a mortar and pestle and then sieved through a 50 μm sieve prior to use.

6.3.3 Materials Characterization

Pore diameter and surface area were measured from nitrogen adsorption measurements (Micromeritics Tristar 3000) conducted at 77 K. Samples were degassed at 120°C for a minimum of 4 hours under flowing nitrogen gas before analysis. Specific surface area was estimated using the Brunauer, Emmett and Teller (BET) isotherm and the pore diameter was estimated as the peak in the pore size distribution calculated by the method of Barrett, Joyner and Halenda (BJH) using the adsorption branch of the nitrogen adsorption-desorption isotherm. [125-127] The particles were imaged using a Hitachi S-4300 Scanning Electron Microscope (SEM). SEM samples were prepared by sprinkling the particles onto double sided carbon tape and adhering the tape to 15 mm aluminum mounts. Excess silica materials were blown off of the sample with nitrogen. Samples were prepared 24 hours in advance and left in a desiccator prior to being sputter coated using an Emscope SC400 with a gold-palladium alloy before analysis. Particle diameters were measured from the captured SEM images using ImageJ software.

6.3.4 Microsome Preparation and Adhesion

Purified membrane microsomes were passed through a 200 nm polycarbonate membrane extruder (Avestin LipoFast, Ottawa Canada) two times prior to use. Extruded microsomes were then tagged with DiO (stock solution 1 mg/mL in DMSO) at a final concentration of 11 µM for imaging. Prior to microsome immobilization to particle surfaces, dry particles were pre-wet with PBS. To 1 mg of particles, 500 µL of PBS was added and vortex mixed overnight. Particles were centrifuged for 2 minutes at 17,000 x g. Particles were then mixed with extruded microsomes (250 µL) for 1 hour prior to imaging.

6.3.5 Microparticle imaging of bilayer and ligand

To image EGF ligand binding to membranes on particles, 1 µL of a 33µM EGF-Alexa647 solution was added to particles and mixed for 5 minutes to allow for binding. Approximately 15 uL of particle sulitions were placed on a glass slide, covered with a cover slip and sealed prior to imaging on a Leica TSP SP5 confocal microscope. An argon laser at 488 nm was used to excite DiO while a helium neon laser at 633 nm was used to excite Alexa647. The gain voltage on photomultiplier tubes was kept at 750 V for all imaging. The DiO excitation laser was turned off while imaging Alexa647.

6.4 Results and Discussion

Materials synthesis procedures result in the formation of spherical, large diameter SBA-15 (SBAS) silica particles. SEM imaging of particles after synthesis confirms their uniform, spherical morphology and particle diameter (**Figure 6.1**). BET analysis of these materials confirms the pore size as 5.4 nm with a surface area of 866 m^2/g. Although SBAS materials were chosen for this investigation, previous publications from our laboratory group have demonstrated the synthetic versatility of these materials.[27] Pore diameters between 3 nm and 12 nm are possible by hydrothermally aging materials at different temperatures between 50ºC and 120ºC. Previous work in our lab has used tuned pore diameters between 3.0 nm and 9.1 nm for the investigation of lipid bilayer properties in nano-porous domains and the effect of bilayer immobilization method on location within particles.(**Schlipf 2015**) Solvent evaporation of lipids (DPPC) and rehydration into bilayers permit bilayer formation within particle pores and on particle surfaces within 5.4 nm pored materials. On the other hand, formation of lipid vesicles via extrusion and rupturing on particle surface lead to exterior only lipid bilayers on much larger, 9.1 nm

pored materials, with similar results expected of microsome adhesion on narrower pored 5.4 nm materials.
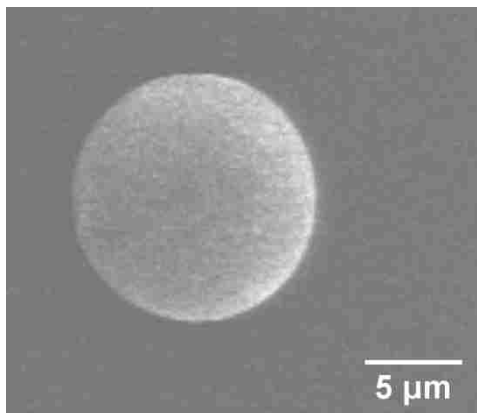
Figure 6.1 SEM image of SBAS materials after synthesis and template extraction.

Preparation of plasma membrane vesicles (microsomes) is performed via nitrogen cavitation where cells are lysed and membrane microsome components reform in solution spontaneously. Microsomes were purified from other cell lysates via ultracentrifugation of solutions to produce purified microsomes of approximately 180 ± 20 nm diameter.[100, 176] . HEK293 cells were used for microsome preparation and were expressed with epidermal growth factor receptor (EGFR) to confirm the ability to retain receptor activity (via ligand binding) after isolation in microsomes and adhesion to particles surfaces.[176] EGFR is a model receptor for the demonstration of transfer of protein function from the microsome to the supported bilayer via active ligand binding from solution, indicating receptor activity and correct receptor orientation in the membrane.[177] Receptor orientation within the membrane is believed to be random as microsomes form spontaneously in solution after rupturing of cells via nitrogen cavitation. Also, receptor binding is seen in microsomes prior to adhesion on particles[176] and herein after rupturing, indicating receptor accessibility on both membrane faces.

Confocal scanning laser microscopy (CSLM) was used to confirm both membrane bilayer location on particles and locate the ligand using two distinct fluorescent tags for simultaneous visual confirmation on particles. The membrane dye, DiO preferentially orients itself within bilayers where it becomes fluorescent upon insertion, confirming bilayer presence. Upon exposure to particles without lipid bilayers, DiO exhibits minimal fluorescence, where only background noise is apparent in **Figure 6.2A**. Additionally. The ligand affinity for silica particles was investigated in absence of membranes as well, **Figure 6.2B**, showing significant nonspecific interactions. The adsorption and diffusion of the Alexa647tagged ligand appears similar to that of the Enhanced Green Fluorescent Protein (EGFP) penetration into pore diameters approaching protein dimensions.(**Chapter 6.3**). The EGF ligand is a 53 amino acid structure, approximately 6 KDa in molecule weight attached via biotin to streptavidin which has approximately 2-3 linked Alexa647 fluorophores. Within this complex, the 52.8 KDa streptavidin is the largest molecule with approximate dimensions of 5.8 nm x 7.3 nm x 6.4 nm.[178] With dimensions slightly larger than the pore diameter of 5.4 nm, build-up of ligand on particle surface is expectedly seen (**Figure 2B**).

A   **B**
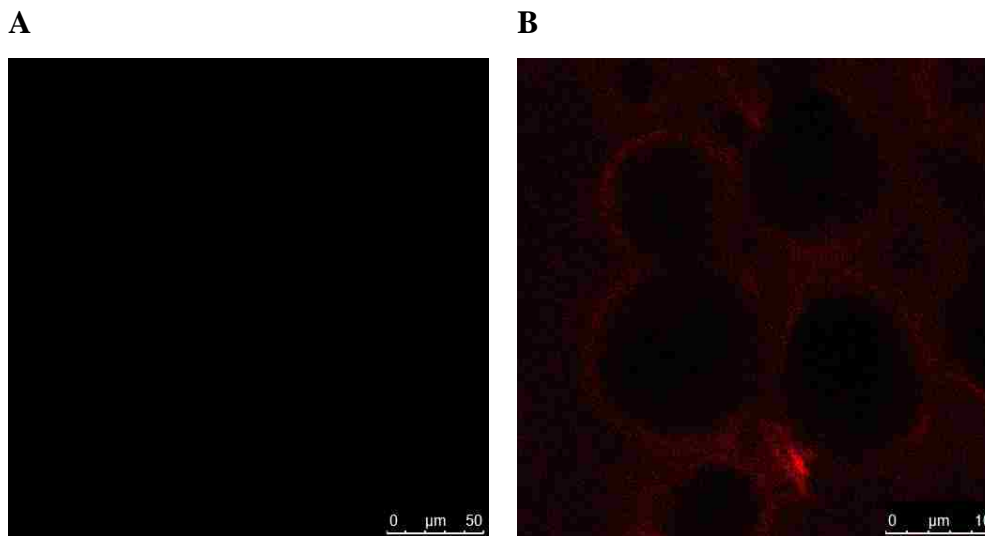
Figure 6.2 A) Membrane tag DiO non-fluorescent in solution with particles. B) Ligand EGF-Alexa647 shows nonspecific binding to silica particles and diffusion within cores.

Membrane adhesion to particles was visually confirmed (**Figure 6.3A** and **C)** via DiO fluorescence after membrane incorporation. Both non-EGFR expressed and EGFR expressed membranes on particles possess continuous bilayers around the outside of particle supports. In EGFR expressed microsomes, locations of high intensity DiO emission potentially signal differences in membrane composition.

EGF affinity for non-expressed microsomes was evaluated to ensure membrane association in EGFR expressed samples is receptor mediated. Non-EGFR expressed microsomes were adhered to particle surfaces and exposed to EGF (**Figure 6.2B)** confirming no EGF ligand association with non-expressed membranes. Although no ligand association is seen on membranes, the Alexa647 fluorescent tag of the EGF ligand can be seen in the surrounding environment confirming its proximity in solution. Upon exposure of EGF to supported EGFR expressed membranes, clear EGF association can be seen on the membrane surface as intense local fluorescent spots from the Alexa647 tag at the membrane surface (**Figure 6.3D**). Ligand binding with EGFR on particle surfaces demonstrates receptor binding site accessibility to the ligand, indicating a rite site out protein orientation, accessible to EGF in solution.[177] Receptor orientation is critical, and many membrane immobilization methods, such as tethered cell shearing and particle mixing cells, result in distinctly inside out membrane orientation.
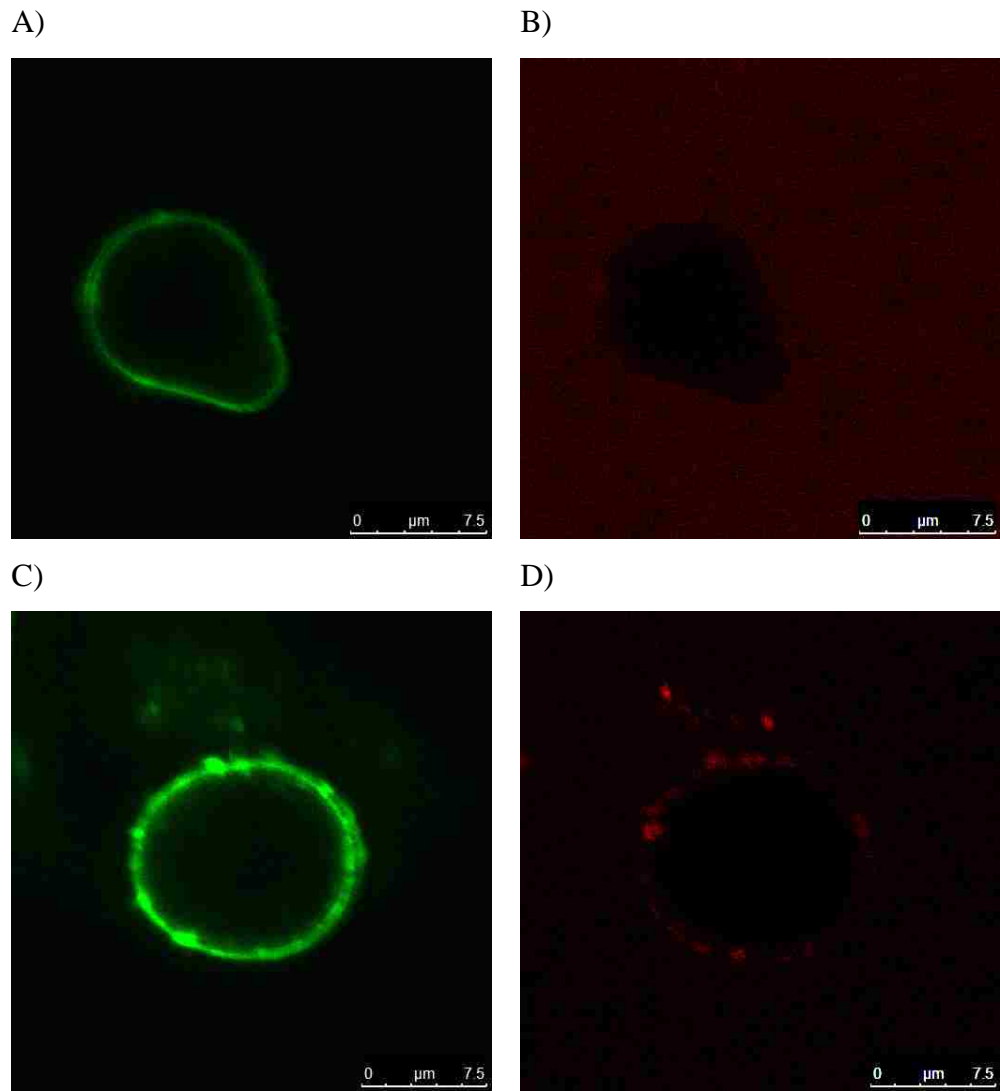
Figure 6.3 A) Non EGFR expressed microsomes adhered to particles B) Non EGFR expressed microsomes on particle surface in presence of EGF ligand without binding C) EGFR expressed microsomes adhered to particle D) EGF ligand binding to EGFR on membrane surface

In addition to determining ligand association with both non-expressed and EGFR expressed supported membranes, membrane integrity can be inferred from **Figures 6.2 and 6.3.** Substantial non-specific binding of EGF ligand onto silica particles can be seen in **Figure 6.2B** with significant build-up of ligand at the surface of the particles. In contrast, in both non-expressed and expressed supported membranes there is no build-up

of ligand at the membrane surface. Membrane sealing of porous particle cores is important as our future work progresses toward evaluating membrane protein transport functions, such as that of the chloride channel cystic fibrosis transmembrane receptor (CFTR), expressed and preliminarily investigated in HEK293 microsomes.[176]

6.5 Conclusion

This work presents a direct method of transmembrane protein incorporation onto synthetic platforms for investigation, circumventing the often troubled method of re-incorporation of purified proteins in synthetic membranes. Mesoporous silica materials are an ideal support for lipid bilayer membrane immobilization as pores permit membrane flux, surface porosity promote membrane protein function and morphological versatility provide application specific support structures. Unfortunately, incorporation of functional membranes proteins into synthetic lipid bilayers has proven difficult. Methods of membrane protein separation from biological sources and reincorporation, using detergents to solubilize the protein, lead to protein denaturation and loss of functionality. Incorporation of cell membrane microsomes via fusion to silica particles permits the incorporation of transmembrane proteins in their native physiological membrane.

Herein we demonstrate a method of adhering cell derived membranes onto particles in a similar method used to adhere synthetic lipid vesicles via vesicle rupture and enveloping on particle surfaces. Cell membranes vesicles (microsomes) were derive from cell membranes via nitrogen cavitation and purified via ultracentrifugation for adhesion to particle supports. Prior to microsome formation, cells were genetically modified to express the epidermal growth factor receptor as a model membrane protein to confirm transfer of functioning, ligand accessible receptors on particles supports. Membrane-ligand association is only seen on EGFR expressed membrane with no ligand-membrane association seend on non-expressed membranes. The ability to directly transfer transmembrane proteins in stabilized, physiological lipid membranes onto porous supports opens new avenues for the development of sensing, separation, and catalysis based on functional membrane proteins.

CHAPTER 7
Conclusions and Future Directions

7.1 Conclusions

Chapters 2 through 6 of this work have outlined the application a porous, large diameter synthetic particle for the investigation of interactions at the biological interface. The porous inorganic material used in this work is synthesized from the precursor tetraethoxylorthosilane while a dual surfactant system (CTAB and P123) is used to control both particle morphology (spherical) and pore diameter. The surfactant pore template is sensitive to the materials synthesis temperature, making possible the tuning of pore diameters in the final material. In addition to tuning material properties during synthesis, materials can be post-synthetically functionalized to impart application specific surface chemistries. A literature survey of mesoporous silica synthesis, applications with proteins, surface chemistries and lipid bilayers can be found in Chapter 2.

Porous silica particles supporting active enzymes within pores are frequently used as a biocatalytic platform. Understanding the interaction and diffusion of proteins within particles and on the surface of supports is of great interest. In Chapter 3, the synthesis and application of pore size tunable, large diameter particles was demonstrated in the protection of fluorescent proteins as a function of pore diameter, controlled via hydrothermal aging. The fluorescent protein EGFP and the protease Pepsin A were employed to demonstrate pore size dependent diffusion and protection within the tuned pore diameters (5.4 nm – 11.6 nm). For the smallest diameter pores, neither EGFP nor Pepsin A were capable of diffusing into pores and EGFP was thus hydrolyzed from the surface of the particle. Between the pore diameters of 7.3 nm and 11.3 nm EGFP protein diffusion in the pores was seen, with the greatest retention of protein fluorescence, and

thus activity, seen at a pore diameter of 7.3 nm. At 11.6 nm, full accessibility to both

EGFP and Pepsin A was observed and all fluorescence within the pores was removed by

the hydrolysis of EGFP by Pepsin A. There are two major contributions of this result to

the field of protein immobilization of porous supports. When matching the accessibility

of proteins to pore diameters, around 1 nm – 2 nm of space is required to allow proper

diffusion into the pores. Also, a method is developed to remove proteins from the surface

of particles. Pepsin A was shown as a tool to hydrolyze proteins from the surface of

particles and its larger size is well applied to limit its accessibility to pores while proteins

within pores retain their function.

In Chapter 4 the selective surface functionalization of these large diameter,

protein accessible materials was demonstrated. The surface functionalization of

mesoporous silica particles is frequently employed to control surface binding, covalently

attach proteins, increase bio-inertness and control pore accessibility. In a variety of these

applications, selectively modifying the exterior or interior only of the particle is desirable.

In previous accounts, selective external functionalization is demonstrated on particles

with narrow, protein inaccessible pore diameters by physically blocking accessibility to

the pore with the pore template. In this work, a post synthetic method is developed for

functionalization of materials after synthesis and removal of pore template. This method

of functionalization is time dependent, where short exposure times to functional agents

result in exterior only functionalization and longer exposures results in full exterior and

pore wall functionalization. Time dependent functionalization was tested in both pores

blocked and free of pore template resulting in time dependent selective functionalization

regardless of template presence. These results are confirmed via confocal microscopy

imaging, a technique uniquely available to these large diameter particles. In addition to the demonstration of selective functionalization, fully and selectively functionalized particles are probed with the model protein lysozyme to confirm pore accessibility in the presence of functional groups. Previous attempts at surface-only functionalization were in materials inaccessible to biologically functioning proteins, severely limiting their application potential. Herein a method of selective surface functionalization, regardless of pore blocking is, demonstrated in silica materials capable of housing proteins for biological activity.

The synthetic analog of biological membranes, lipid bilayers, have significantly aided the fields of drug discovery, separations and sensing. Lipid bilayer membranes have been incorporated on the surface of mesoporous silica particles for a variety of applications including stealth therapeutic delivery, particle targeting, selective permeation and separations and small molecule discovery. Porous nanoparticles are common supports for lipid membranes although little attention has been given to the impact of the underlying porous support on membrane function. This is partially due to the nano-scale dimensions of the particle, which limits the ability to characterize particle-lipid bilayer interactions. The most common parameter used to characterize lipid membranes is membrane fluidity, which controls membrane permeability and membrane protein function.

In Chapter 5, particles were synthesized with pore size ranges between 3.0 and 9.1 nm in diameter, above and below the thickness of the DPPC lipid membrane (4 nm). Membranes were formed within pores using a unique solvent casting and re-hydrating technique. Imaging using confocal microscopy confirmed bilayers were incapable of

forming within the more narrow 3.0 nm pore diameters, but were accessible to materials with 5.4 nm and 9.1 nm pore diameters. Interestingly, after surface tethering with the lipid like silane CDSMH (approximately 10 percent surface coverage) bilayer accessibility within 5.4 nm materials was also prohibited. The fluidity of bilayer membranes both on the surface of and incorporated within pores was investigated using the confocal microscopy technique FRAP. As pore diameters decreased, bilayer fluidity decreased both within pores and on the surface of the pores, indicating a pore diameter effect on bilayer diffusivity both within pores and in bilayers spanning pores (enveloped particles). Tethering of bilayers had a greater impact on reducing bilayer fluidity as it immobilized portions of the bilayer with covalent tethering. A coupled small pore diameter effect and tethering on 2.9 nm pore diameter CDSMH functionalized materials resulted in a fluidity reduced below the level of detection. In this work, the solvent casting method of lipid deposition is demonstrated as a unique method of bilayer formation within porous materials with large pore diameters as well as bilayer formation on the external surfaces of narrow pore diameter materials. Large particle diameters make possible the use of confocal microscopy visualization and uniquely FRAP measurements of bilayer fluidity on particle surface and within nanopores.

A recurring challenge in the supported synthetic bilayer field is the incorporation of membrane proteins within the bilayer to provide biological activity to the membrane. Purification and reincorporation of membrane proteins frequently results in their denaturing and inactivation prior to incorporation. In order to circumvent this it is most desirable to incorporate membrane proteins in their native physiological membrane system. In Chapter 6, an effective method of expressing desired membrane proteins in

cell membranes, formation and purification of plasma membrane vesicles from the cell membrane and incorporation on mesoporous silica supports is demonstrated. Epidermal growth factor receptors (EGFR) were effectively transfected and expressed in the membrane, incorporated on a particle surface and function was demonstrated through the binding of the epidermal growth factor (EGF) ligand. EGF ligands did not associate with non-EGFR expressed membranes, indicating EGFR binding results were not the result of non-specific binding. This is a powerful demonstration of selective protein expression and supporting on synthetic particles within native biological membranes. Supporting membranes on particles provided a platform for membrane protein investigation as well as the potential for investigating pore-forming protein function as mesoporous provide reservoirs for molecular transport.

7.2 Future Directions

Mesoporous silica nanoparticles have been developed for a variety of cellular applications, most notably for the delivery of therapeutic molecules for disease treatment. Nanoparticle diameters between 50 nm and 200 nm are most ideal for cellular uptake.[76] Mesoporous silica nanoparticles are limited by the narrow pore diameters achievable in nanoparticle systems, limiting intracellular delivery to smaller biomolecules. For the delivery of larger macromolecules such as proteins and RNA, understanding the interaction between macromolecules of interest and nano-pore dimensions is critical to maximize the use of available pore diameters. Chapter 3 of this work investigates the interaction of a multiprotein system with pore size tunable silica particles to understand relationship between pore diameter and biomacromolecule accessibility and protection

within pores. Biomacromolecular diffusion within pore spaces requires pore diameters slightly larger than the dimensions of the diffusing molecule.

Delivery of DNA and RNA for gene therapies in both mammalian and insect applications, specifically for disease prevention and population control in the latter, is complicated by the stability of DNA and RNA in biological systems. Using the understanding of biomacromolecule diffusion in nano-porous systems, porous nanoparticles (150 nm diameter) are being developed for the delivery of nucleic acids to insects in culture for gene regulation. Nanoparticle uptake has been confirmed in cell culture after colocalization of rhodamine b tagged nanoparticles within cells. Similar to the model protease Pepsin A in Chapter 3, ribonuclease are proteins produced by cells that breakdown RNA into smaller components in solution, rendering the RNA inactive. Ribonuclease have dimensions of approximately 4 x 4 x 9 nm [179] making confirmation of RNA diffusion and protection within pores critical for cellular delivery. Future work will focus on understanding the diffusion of RNA within pores of varying diameter for protection from ribonuclease. Additionally, surface functionalization of particles will be used to control affinity of RNA to particle surfaces for controlled delivery within cells, using functionalization techniques developed in Chapter 4. After confirmation of RNA uptake within nano-pores, RNA delivery and gene transfection can be evaluated in DNA or RNA-loaded nanoparticles

In addition to nano and micron particle development, our lab focuses on silica thin film membranes for separations. Mesoporous silica thin films are used for a variety of membrane separation applications in both the gas and liquid phase.[180] Functionalization of thin films with organic moieties alters the permeability of the

membrane providing selective separation potentials.[181] Selective functionalization techniques form Chapter 4 can be transferred from particle platforms to thin films membranes for specific solution interactions. In our lab, hydrophobic functionalization of silica thin film membranes with decyl functional groups has been used to reduce membrane permeability to water while not impacting the flux of alcohols through the membrane.[181] A primary concern during functionalization of membranes is non-specific pore and surface functionalization, which can block pores, reducing transport potential. Controlled exposure times to functional groups, approaches developed in Chapter 4, can be used with membrane systems to ensure single sided membrane functionalization for controlled transport. Future work will focus on controlled placement of functional groups on membrane surfaces for separation of carbohydrates.

Large diameter silica particles have been shown in this work as valuable tools to investigate biomacromolecule and lipid membrane interactions at the nano-porous interface. Lipid bilayer membranes on particles and thin films have been used for a variety of separations often mediated by transporters within the bilayer. Bilayers themselves are excellent membranes as their non-polar lipid cores prohibit transport of polar species from aqueous solutions. The permeability of bilayers to ions and water flux is susceptible to chemical perturbants, such as cholesterol which decreases bilayer permeability by altering lipid order.[182] Bilayer fluidity is directly dependent on environmental temperature and bilayer permeability increases with increased bilayer fluidity.[182] As opposed to porating bilayers with proteins or controlling permeability via bilayer fluidity, small molecule transporters can be used to mediate small molecule transport into and through the non-polar membrane region.[170, 183] A prominent class

of transport molecules is boronic acids, which are used to both identify and transport carbohydrates. [170]

Boronic acids detect different types of carbohydrates in solution as well as transports them through bilayers via non covalent interactions with carbohydrate diols.[170, 184] The majority of methods used to identify and separate carbohydrates are based on covalent interactions, employing enzymes or sugar binding proteins to interact with sugars in solution. [184] On the other hand, boronic acids, interact reversibly with the 1,2 and 1,3 diols of carbohydrates which are highly enantiomerically specific. Fortunately, boronic acid backbones are synthetically versatile to interact specifically with distinct carbohydrates.[184] Selecting a variety of commercially available boronic acids with organic backbones (of the phenyl class to infiltrate the non-polar bilayer core), Westmark et.al. demonstrated their ability to separate a mixture of glucose, fructose and sorbitol across DPPC membranes depending on boronic acid type.[170] Selective sugar transport into lipid vesicles was demonstrated, although limited by the small interior volume of vesicles and large concentration gradients required to drive transport.

Using the large, open pore volumes and high surface areas of mesoporous silica capable of loading large quantities of lipid membrane, we hypothesize that lipid loaded silica particles are efficient boronic acid mediate carbohydrate separation platform. The non-polar lipid loaded core is expected to provide reservoirs for the sugar species transported by the boronic acid. Preliminary investigations in our laboratory indicate a 2.4 fold increase in selective glucose transport into particle supported membranes with boronic acid transporter, as compared membrane uptake without the acid transporter. Tuning of boronic acid concentrations within bilayers is expected to optimize uptake of

carbohydrates from solution while future work aims to transfer supported bilayer technology from particles to thin film platforms for bulk membrane separations.

Chapter 6 demonstrated the effectiveness of porous silica particles as supports for cell derived plasma membranes. In addition to confirming location on particles, membrane receptor activity was confirmed via selective ligand binding. Future work will focus on increasing the variety of membrane receptors expressed and supported on porous particles with a focus on the use of receptors in lipid membranes for the identification of therapeutics from plant derived metabolites. While metabolite and therapeutic receptors and ligands have been identified, incorporation and methods of confirming ligand binding were yet to be discussed. We can now imagine using cell lines capable of transfection and expressing receptors of interest, separating their membranes and wrapping on particles to probe receptor function and transport potential. This method is significantly easier than re-incorporation of purified membrane proteins, allowing research methods to focus on tailored particle interactions with transported species and potential commercial applications.

APPENDIX A

Confidence Intervals of Bilayer Diffusivity Calculations

The following tables present the upper and lower 95% confidence intervals from diffusivity models of FRAP data.

Table A1. Calculated diffusivity values of SBAS-3.0 Cap FRAP measurements along with 95% confidence intervals

Sample	Diffusivity	± C.I.
1	4.30E-05	1.52E-05
2	5.90E-05	9.75E-06
3	1.80E-05	3.85E-06
4	5.00E-05	1.64E-05
5	5.80E-05	1.13E-05
6	1.80E-05	7.10E-06
7	4.40E-05	2.04E-05
8	6.10E-05	1.69E-05
Average	4.39E-05	
Std Dev	1.73E-05	

Table A2. Calculated diffusivity values of SBAS-5.4 Core FRAP measurements along with 95% confidence intervals

Sample	Diffusivity	± C.I.
1	2.47E-04	5.20E-05
2	3.23E-04	5.20E-05
3	3.46E-04	1.09E-04
4	3.96E-04	8.60E-05
5	3.83E-04	9.15E-05
6	3.60E-04	9.55E-05

	7	1.99E-04	5.15E-05
Average		3.22E-04	
Std Dev		7.30E-05	

Table A3. Calculated diffusivity values of SBAS-5.4 Mid-Core FRAP measurements along with 95% confidence intervals

Sample	Diffusivity	± C.I.
1	2.68E-04	7.15E-05
2	3.80E-04	6.40E-05
3	3.05E-04	6.40E-05
4	2.21E-04	4.70E-05
5	3.28E-04	1.01E-04
6	3.58E-04	7.85E-05
7	2.69E-04	7.60E-05
Average	3.04E-04	
Std Dev	5.58E-05	

Table A4. Calculated diffusivity values of SBAS-5.4 Cap FRAP measurements along with 95% confidence intervals

Sample	Diffusivity	± C.I.
1	3.34E-04	8.30E-05
2	2.66E-04	6.25E-05
3	3.63E-04	7.55E-05
4	3.39E-04	7.75E-05
5	4.85E-04	1.20E-04
6	2.95E-04	6.65E-05
7	3.81E-04	1.00E-04

Average	3.52E-04	
Std Dev	7.05E-05	

Table A5. Calculated diffusivity values of SBAS-9.1 Core FRAP measurements along with 95% confidence intervals

Sample	Diffusivity	± C.I.
1	4.39E-04	7.15E-05
2	5.41E-04	7.20E-05
3	4.63E-04	9.30E-05
4	6.39E-04	1.32E-04
5	5.00E-04	7.25E-05
6	5.03E-04	7.10E-05
Average	5.14E-04	
Std Dev	7.06E-05	

Table A6. Calculated diffusivity values of SBAS-9.1 Mid-Core FRAP measurements along with 95% confidence intervals

Sample	Diffusivity	± C.I.
1	4.79E-04	5.75E-05
2	5.02E-04	7.80E-05
3	4.58E-04	6.70E-05
4	4.08E-04	6.20E-05
5	4.61E-04	7.20E-05
6	5.83E-04	8.40E-05
7	7.39E-04	1.20E-04
8	5.27E-04	7.65E-05
Average	5.20E-04	

Std Dev	1.03E-04

Table A7. Calculated diffusivity values of SBAS-9.1 Cap FRAP measurements along with 95% confidence intervals

Sample	Diffusivity	± C.I.
1	7.77E-04	2.12E-04
2	6.51E-04	1.89E-04
3	4.61E-04	1.05E-04
4	8.63E-04	1.75E-04
5	5.21E-04	1.48E-04
6	6.74E-04	1.34E-04
7	8.69E-04	2.59E-04
Average	6.88E-04	
Std Dev	1.59E-04	

Table A8. Calculated diffusivity values of TLB-5.4 Cap FRAP measurements along with 95% confidence intervals

Sample	Diffusivity	± C.I.
1	1.160E-04	4.650E-05
2	8.700E-05	1.300E-05
3	1.340E-04	1.850E-05
4	8.700E-05	2.030E-05
6	7.600E-05	1.685E-05
7	1.000E-04	1.920E-05
8	6.300E-05	1.145E-05
Average	9.471E-05	
Std Dev	2.415E-05	

Table A9. Calculated diffusivity values of TLB-9.0 Core FRAP measurements along with 95% confidence intervals

Sample	Diffusivity	± C.I.
1	4.630E-04	4.700E-05
2	3.720E-04	3.650E-05
3	4.560E-04	1.070E-04
4	3.970E-04	5.450E-05
5	4.040E-04	5.100E-05
6	4.050E-04	5.300E-05
7	5.150E-04	7.100E-05
Average	4.303E-04	
Std Dev	4.957E-05	

Table A10. Calculated diffusivity values of TLB-9.0 Mid-Core FRAP measurements along with 95% confidence intervals

Sample	Diffusivity	± C.I.
1	3.690E-04	3.550E-05
2	4.550E-04	5.050E-05
3	3.400E-04	5.150E-05
4	3.250E-04	4.450E-05
5	4.710E-04	5.450E-05
6	4.930E-04	-6.000E-06
7	4.300E-04	6.500E-05
8	5.960E-04	9.900E-05
Average	4.349E-04	

Std Dev	8.983E-05

Table A11. Calculated diffusivity values of TLB-9.0 Cap FRAP measurements along with 95% confidence intervals

Sample	Diffusivity	± C.I.
1	2.300E-04	5.200E-05
2	4.920E-04	1.100E-04
3	3.890E-04	1.095E-04
4	3.820E-04	6.950E-05
5	4.000E-04	7.400E-05
6	2.580E-04	4.500E-05
Average	3.585E-04	
Std Dev	9.761E-05	

APPENDIX B

Quercetin Adsorption and Stability on Functionalized Silica Nano-Particles

B.1 Abstract

The interaction of flavonoids with silica surfaces is of interest for separation and recovery of these natural products with potential anti-oxidant and anti-inflammatory properties. The benefit of tailored silica materials for natural product separation is based on the ability to readily tune their surface functionality and pore structure. In this work, the adsorption of quercetin, a model plant-derived flavonoid, was measured on silica particles (450 nm diameter) that were non-functionalized, hydrophobically functionalized (16.2 mg decyl groups/g) or titania modified (0.33 to 9.83 mg TiO_2/g). Quercetin interactions with these functionalized silica particles were interpreted from adsorption measurements on non-porous silica particles, which eliminate the potential diffusional and steric constraints of pores. Titania functionalized particles are found to exhibit significantly increased adsorption capacities compared to non-functionalized and decyl functionalized materials, presumably due to chelation of quercetin to the metal oxide, and this capacity increased linearly with surface coverage of titania. The ability to recover the activity of chelated quercetin is demonstrated using a 2,2-diphenyl-1-picrylhydrazyl (DPPH) assay. This investigation provides guidelines for the surface modification of both porous and nonporous silica for the recovery of natural product flavonoids, taking advantage of the polarity or chelating properties of the silica surface.

B.2 Introduction

Quercetin is a common secondary plant metabolite possessing a variety of therapeutic medicinal uses. A known antioxidant, quercetin has been shown to reduce the effects of oxidative stress on a variety of cell lines by scavenging free radical oxygen species. [185, 186] Quercetin has been investigated for disease prevention, for example its roles in modulating signal transduction pathways associated with carcinogenesis as well as Alzheimer's disease. [187, 188] The anti-thrombosis and anti-inflammatory effects of quercetin may aid in the reduction of obesity. [189] Secondary metabolites produced by plants, such as quercetin, are of high value, although traditional methods of metabolite recovery are expensive, detrimental to plant cells and require large quantities of plant cell tissue. [190] A common method of recovery is exudation, or altering of the

cell membrane permeability for release of produced molecules. [191] An alternative proposed method is the use of nanoparticles for recovery of metabolites in plant cell cultures. [192] Understanding the interaction of nanoparticle systems with plant metabolites is a crucial first step in designing nano-particle based metabolite scavenging systems.

Silica nanoparticles are increasingly investigated for the loading of therapeutics and for topical delivery applications. [193, 194] Silica materials are robust, employ well known aqueous-based synthesis protocols and are widely used in the fields of catalysis, chromatography and therapeutics delivery. [16, 17, 31] Versatile synthesis techniques have been developed for silica thin films and particles of controlled pore structure, and pore size. Using modified silanes, hydrophilic silica can be functionalized with a variety of organic moieties to modify surface properties including charge and hydrophobicity. [195, 196]Deposition of reactive metal oxide precursors on the silica surface results in different metal oxide coatings, including titania. [50] Titania coated silica nanocomposites, in particular, have been identified as an alternative to pure titania particles because the ability to control particle properties (porosity, morphology, and particle size) is better established in silica than titania. [197-199]

Quercetin is a hydrophobic, polar polyphenolic flavonoid, with an octanol/water partition coefficient of 1.82.[200] Quercetin shows an unusually low solubility in both octanol and water, which is why high uptake and bioavailability of free quercetin is difficult to achieve.[200] As a model antioxidant, the adsorption of quercetin onto nanoparticles has been investigated, primarily with a focus on the delivery of therapeutics and metal chelation. [49, 196, 201, 202] Previous investigations of quercetin adsorption examined its interactions with silica or silica modified with pharmaceutical binders. The adsorption of quercetin drastically increased on silica modified with the pharmaceutical binder polyvinylpyrolidone (PVP , terminated with carboxylic acids) as compared to unmodified silica (terminated in hydroxyl groups), due to the increase in quercetin hydrogen bonding sites and stabilization within the polymer.[202] With hydrogen bonding playing a direct role in quercetin binding, a clearer comparison of quercetin adsorption between hydrophilic and hydrophobic surfaces, such as unmodified and alkyl chain modified silica, respectively, is needed.

The chelation of quercetin and titania provides a strong interaction for the design of adsorbents for quercetin.   Bulk titania, while possessing powerful optic, catalytic and chelating properties, has an isoelectric point near pH = 6.5 [203], which is expected to lead to particle flocculation near plant physiological pH values (5.5 to 7.5). In contrast, silica has an isolectric point near pH = 2 [204] and would be expected to remain colloidally stable near pH 7. In addition, titania is polymorphic and may undergo phase transformations upon aging in aqueous solution or heating during regeneration, whereas titania dispersed on silica spheres has significantly increased thermal stability and catalytic activity properties.[205, 206] Pure nonporous titania nanoparticles (2.8 ± 1.4 nm) have been investigated for the recovery of quercetin in plant cells. [192] Quercetin chelation to the metal oxide TiO_2 was indicated by a noticeable color shift in the adsorbate. Quercetin, which is light yellow in solution, turns dark orange upon adsorption to a titania surface, corresponding to a readily measurable bathochromic shift.[192]   This coloration shift has been employed in TiO_2 modified silica xerogel materials for the spectroscopic detection of a variety of polyphenolic compounds including catechol, quercetin, rutin, gallic, caffeic and ferulic acids. [207] Quercetin has also been demonstrated to stabilize silica from hydrolysis when investigated on a quercetin-functionalized, titania-capped silica, used for mercury chelation and removal. [201]

This work examines the interaction of the model antioxidant, quercetin, with modified silica surfaces for the design of silica platforms for flavonoid recovery. Non-porous silica particles, synthesized by the Stöber method [208] with average particle diameters of 450 nm, were functionalized by post-synthesis grafting with decyl groups (using n-decyltriethoxysilane silane) or with a reactive titania precursor (titanium (IV) ethoxide). While non-porous particles do not have the high surface area of mesoporous silica, they allow for the investigation of solute-surface interactions in the absence of steric and diffusional limitations of pores, with evenly accessible exterior particle surfaces for functionalization, solute adsorption and activity assays.[209] The titania precursor concentration was varied to achieve lightly-functionalized to near-monolayer coverage of titania on nonporous silica, as verified by a colorimetric titania dissolution assay. The quercetin loading of unmodified, hydrophobically modified, and titania

coated particles was measured via solution depletion experiments. The ability to recover the antioxidant activity of quercetin adsorbed on titania-coated silica particles was demonstrated using a 1,1-diphenyl-2-picryl-hydrazyl reduction assay. The results provide a basis for tuning silica surfaces with titania for the recovery of active antioxidants from solution, and can be extended to mesoporous silica platforms with high surface area for the selective separation and recovery of antioxidant compounds.

B.3 Experimental

B.3.1 Materials

Ethanol (200 proof), de-ionized ultra purified water and ammonium hydroxide (14.8 M, ACS grade) were purchased from Fisher Scientific. Tetraethyl orthosilicate (TEOS) (98%) was purchased from Acros Organics. n-decyltriethoxysilane (D-TEOS) was purchased from Gelest, Morrisville PA. Quercetin (≥95%), Titanium (IV) ethoxide (TEO, technical grade) and anhydrous toluene (99.8%) was purchased from Sigma-Aldrich. 2,2-diphenyl-1-picrylhydrazyl (DPPH, 95%) was purchased from Alfa-Aesar.

B.3.2 Materials Synthesis

Stöber particles were synthesized using a modified Stöber method. [208] Particles were prepared by mixing ethanol (58.22 g), concentrated ammonium hydroxide (9.8 mL), DIUF water (10.8 g) and TEOS (5.26 g). Turbidity was seen after 10 minutes. Particles solutions were stirred for 24 hours and the particles were recovered from solution by centrifugation at 5000 RPM. After centrifugation, particles were dried in an oven at 80°C for 12 hours. After drying, particles were washed 3 times in ethanol (20 mL) followed by repeated vortexing and centrifugation. Particles were re-dried at 80°C for a minimum of 12 hours prior to characterization or functionalization.

B.3.3 Titania Functionalization of Stöber Particles (SP-T)

SP-T particles were synthesized using a modified version of the method of Hanprasopwattana et al. [50]. A stock solution of titanium (IV) ethoxide (TEO) was prepared in an inert atmosphere. In nitrogen purged bag, TEO (1, 20, 100 or 300 µL) was pipetted into dry ethanol (7.15 mL). This solution was sealed prior to use. In a 250 mL round bottom flask, dry ethanol (100 mL) and synthesized SPs (900 mg) were sonicated for 15 minutes. This solution was refluxed (~78°C) for 1.5 hours under vigorous mixing with DIUF water (1.62 mL), ethanol (142.55 mL) and the dilute TEO solution previously

prepared in an inert environment. After refluxing, particles were removed from solution by centrifugation at 5000 RPM for 5 minutes. Particles were washed 3 times in ethanol (20 mL) with repeated vortexing and centrifugation and dried in an oven at 80°C for 24 hours.

B.3.4 Decyl Functionalization of Stöber Particles (SP-D)

SP-D particles were prepared using a modified version of Berlier's method. [196] In anhydrous toluene (30 mL), prepared SPs (1 g) were added and sonicated for 15 minutes. This solution was refluxed (~110°C) under vigorous mixing and D-TEOS (0.8 mL) was added. This solution was refluxed for 8 hours followed by centrifugation to recover the particles. Particles were washed 3 times in ethanol (20 mL) with repeated vortexing and centrifugation followed by drying overnight at 80°C.

B.3.5 Materials Characterization

Particle size distributions before and after functionalization were measured by dynamic light scattering (DLS) using a Delsa Nano C particle analyzer (Beckman Coulter, Pasadena Ca). The particles were suspended via sonication in DIUF prior to DLS measurements. Nitrogen adsorption experiments (Micromeritics Tristar 3000) conducted at 77 K were used to confirm that particles were non-porous. Samples were degassed at 120°C for a minimum of 4 hours under flowing nitrogen gas before analysis. Particles were imaged using a Hitachi S-4300 Scanning Electron Microscope (SEM). SEM samples were prepared by sprinkling the particles onto double sided carbon tape and attaching the tape to a 15 mm aluminum mount. Excess silica materials were blown off of the sample with nitrogen. Samples were prepared 24 hours in advance and left in a desiccator prior to being sputter coated in a gold-palladium alloy before analysis. Particle diameters were measured from SEM images using Image J Software. [210] Particle diameter averages and standard deviations were calculated from the measurement of 14 random particles throughout the SEM images.

B.3.6 Quercetin Adsorption Isotherms

Quercetin adsorption measurements were performed using a solution depletion method and performed in triplicate at room temperature. Quercetin loading onto SP, SP-D and SP-T particles was measured at equilibrium by prewetting 25 mg of particles in a 2 mL centrifuge tube with 1 mL of ethanol under vortex mixing. After 24 hours, particles

were centrifuged for 15 minutes at 17,000×G and the supernatant was discarded. To pre-wet SP and SP-D particles, 1 mL of .0025, .005, .01, .025, or .05 mg/mL of quercetin dissolved in ethanol was added. To pre-wet SP-T particles 1 mL of .0025, .005, .01, .025, .05, .1, .25, .5 or 1 mg/mL quercetin dissolved in ethanol was added. After vortex mixing for 24 hours, particles were centrifuged for 15 minutes at 17,000 x g and a 200 µL sample of the supernatant was analyzed in a clear 98 well plate with clear top. The 98 well plate was read using a BioTek (Winooski, VT) plate reader at 371 nm. Absorbance readings for the initial solution concentrations were measured simultaneously and adsorbed quercetin was calculated from the difference between initial and final solution concentrations. A Shimadzu Prominence LC-20 AB HPLC system installed with a Waters 2410 refractive index detector with a Phenomenex Luna 5um C18 column (25 cm x 4.6 cm) was used to confirm quercetin was stable and non-degraded during adsorption measurements.

B.3.7 Thermo Gravimetric Analysis (TGA)

TGA was used to determine the quantity of grafted decyl groups on the surface of silica nanoparticles. A TA Instruments (New Castle, DE) Q600 was used under nitrogen flow with approximately 3 mg of sample and a ramp rate 10°C / minute from 30° C to 700° C. Particles were first stabilized at 100°C for 10 minutes prior to the ramp to drive off any remaining solvent residue. The percentage difference in mass loss between SP and SP-D particles in the 435° C - 700° C was associated with the decomposition of the decyl functional group.

B.3.8 Titania Quantification

The quantity of titania coated on the surface of Stöber particles was determined by dissolving the titania from the surface of the particles and quantified using the reaction of titania with H_2O_2, which is detectable using UV-Vis. In 2 M H_2SO_4 (20 mL) at 90°C, SP-T particles (50 mg) were mixed vigorously for 20 minutes. The dissolved particle solution was then filtered through a 0.2 µm PTFE syringe filter. To 1 mL of filtrate, H_2O_2 (1 µL) was added and the solution turned yellow. Absorbance of the titania- H_2O_2 complex was measured at 407 nm. A calibration curve was developed by adding SP particles (50 mg) to refluxing 2 M H_2SO_4 (20 mL) with 4% titanium(IV) ethoxide (500 µL) in anhydrous ethanol and letting the solution mix vigorously for 20 minutes. After

mixing, the sample was filtered and analyzed in the same manner as the SP-T particles. The filtrate was diluted to a variety of different concentrations with 2 M H_2SO_4 to develop a calibration curve. Particles were named based on their titania grafting densities i.e. SP-T functionalized at 9.8 mg TiO_2 / g silica was named SP-T-9.8.

B.3.9 Quercetin Activity Assay

The antioxidant activity of quercetin adsorbed on SP-T particles was measured relative to the activity of the same amount of quercetin dissolved in ethanol solutions (free quercetin). The quantity of quercetin adsorbed on the particles was determined using the quercetin adsorption procedure described previously. Free quercetin solutions with concentrations of 0, 0.1, 1.0, 5.0, 10.0, and 250.0 µg/mL quercetin in ethanol were prepared. SP-T-9.8 particles (50 mg) were loaded with quercetin, using the solution depletion method above, to approximately 0.5 mg quercetin / gram particle. After centrifugation, the supernatant was removed and the particle / quercetin complex was diluted to a quercetin concentration in solution matching the free quercetin concentration solutions prepared. The antioxidant activity of quercetin adsorbed on SP-T particles was determined from the reduction of the 2,2-diphenyl-1-picrylhydrazyl (DPPH) radical ion in the presence of antioxidants, as measured by the corresponding reduction in DPPH absorbance at 517 nm. The antioxidant activity is reported as the radical scavenging activity (RSA)[211] and is measured using the absorbance of DPPH before and after exposure to quercetin or quercetin / particle complex. RSA is calculated by dividing the decrease in DPPH absorbance after exposure to quercetin or quercetin adsorbed on particles by the initial DPPH absorbance. To determine the RSA, one mL of a 70 µm DPPH in ethanol solution was mixed with .05 mL of either free quercetin or quercetin on SP-T particle suspension in ethanol for 5 minutes. After 5 minutes the absorbance of DPPH was measured. For quercetin complexed to titania particles, the solution was rapidly filtered through a 0.2 µm filter prior to analysis of DPPH absorbance.

B.4 Results and Discussion

Non-porous silica particles were synthesized using the modified Stöber method. [208] Stöber particles were chosen as adsorbents because of their non-porous, spherical morphology and ease of functionalization and characterization. The unmodified (SP), decyl-modified (SP-D) and titania-modifid (SP-T) silica particles are smooth, spherical

and homogenous (SEM images in **Figure B.1**), and indicate no major change in particle morphology after surface functionalization. Dynamic light scattering (DLS) measurements confirm mono-modal particle size distributions with diameters of 452 ± 52.6 nm, 464.5 ± 27.2 nm and 516.7 ± 24.9 nm for SP, SP-D and SP-T-9.8 materials, respectively. Mono-modal distributions are consistent with the absence of secondary particle formation during surface functionalization with n-decyltriethoxysilane (D-TEOS) or titanium (IV) ethoxide (TEO). Nitrogen adsorption on particles follows Type II adsorption isotherms, with no evidence of capillary condensation, confirming the synthesis of non-porous particles **(Figure B.2)**.
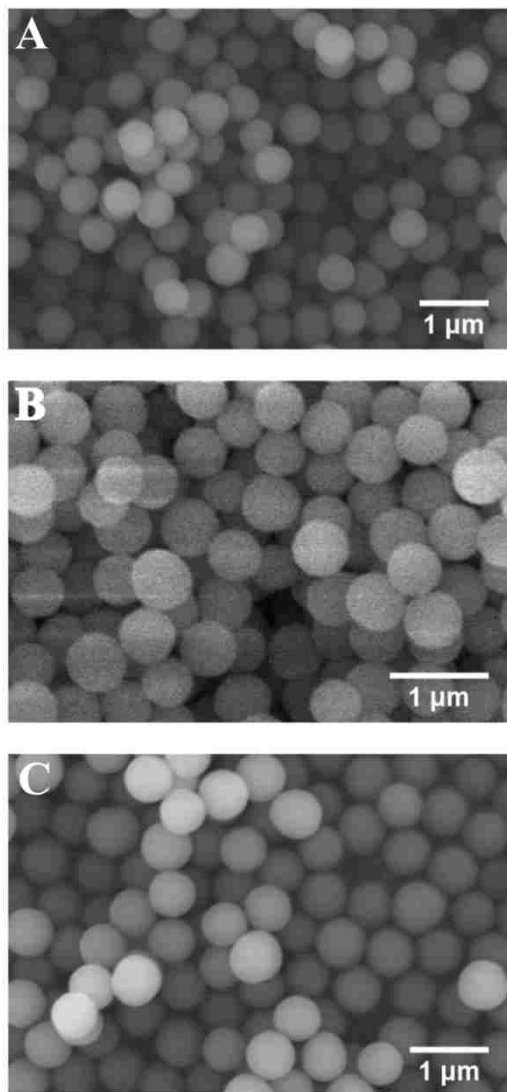
Figure B.1 SEM images of A) Stöber particles B) decyl functionalized particles and C) titania coated particles (SP-T-9.8).
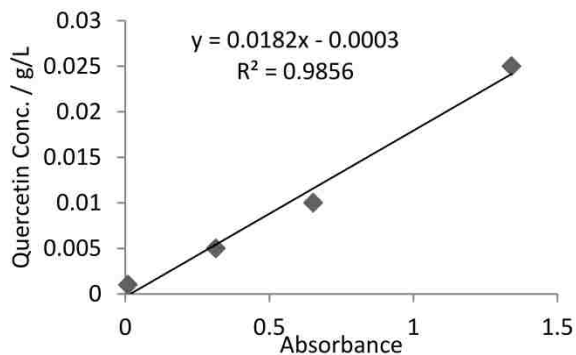
Figure B.2 2,2-diphenyl-1-picrylhydrazyl (DPPH) quercetin assay calibration curve as a function of absorbanceat 517 nm.

Post synthetic grafting of non-polar D-TEOS on nonfunctionalized particles was used impart hydrophobicity for adsorption of quercetin, which is considered to be hydrophobic $(\log(K_{ow}) = 1.82)$.[200] Thermogravimetric analysis of SP-D particles reveals a characteristic mass loss due to the decomposition of decyl functional groups above 435°C relative to non-functionalized (SP) particles **(Figure B.3)**.[81, 196] The increased mass loss of 1.62% corresponds to a grafting of 16.2 mg decyl groups / gram silica.
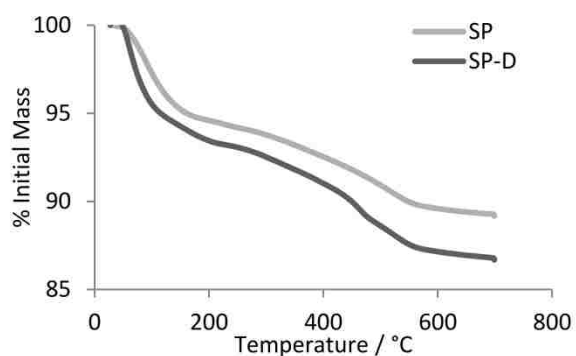
Figure B.3 Results of thermogravimetric (TGA) analysis of SP and SP-D particles.

The quantity of titania grafted to the surface of non-porous particles was determined following titania dissolution and complexation with H_2O_2, where the complex absorbs light at 407 nm (calibration curve, **Figure B.4**).[212] The amount of grafted titania on the particles increased linearly with the amount of titania precursor used during grafting **(Figure B.5)**. From this analysis, the amount of titania on the particle surface is determined to be 0.33, 1.17, 2.61 and 9.83 mg of TiO_2 per gram silica. Guo et.al. determined that monolayer coverage of titania corresponds to approximately 1.9 mg TiO_2 / m^2 surface area.[205] The average diameter of non-functionalized particles (450 nm) and the approximate density of silica (2.2 g/cm^3) were used to convert the measured values of TiO_2 grafted to the particles (in mg TiO_2/g silica) to surface coverage (in mg TiO_2/m^2 silica).Titania coating densities for synthesized particles are 0.05, 0.19, 0.43 and 1.6 mg TiO_2/m^2, which ranges from a light to near monolayer titania coverage (2.6% - 84% of a monolayer) on the nonporous particles. The use of non-porous, spherical silica particles ensured that all surfaces were uniform and equally accessible to functional groups during functionalization as well as dissolution analysis.
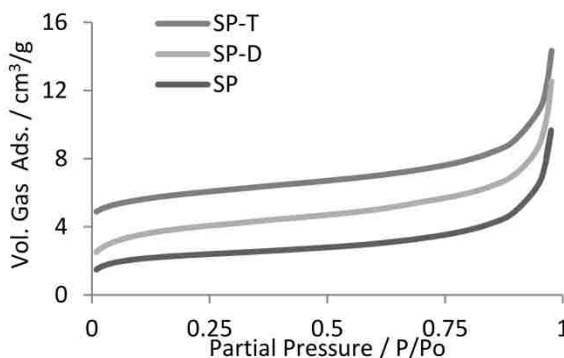
Figure B.4 Nitrogen adsorption isotherms of SP, SP-D and SP-T materials. SP-D and SP-T isotherms are shifted upwards 2 and 4 cm^3/g, respectively, for clarity.
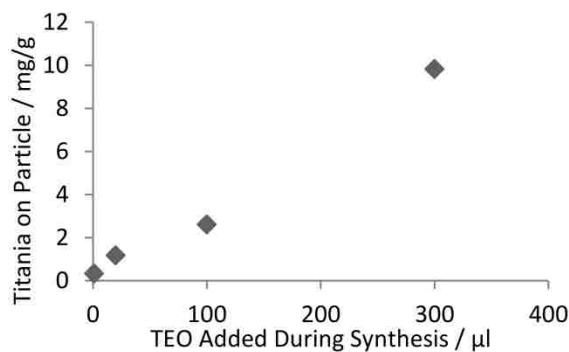
Figure B.5 Grafting densitites of titania on metal oxide functionalized Stöber particles as a function of metal oxide precursor addition.

Adsorption isotherms of quercetin onto SP, SP-D and SP-T particles were measured by the solution-depletion method using quercetin concentrations between 0.0 mg/mL and 0.05 mg/mL in ethanol for SP and SP-D particles and 0.0 to 1.0 mg/mL for SP-T particles. Quercetin stability in ethanol solutions was evaluated via HPLC. The elution of quercetin solutions during use was compared to freshly prepared quercetin in ethanol solutions to ensure the molecule was not degraded. No small molecular weight fragments were seen in prepared or used solutions, indicating intact molecules. Adsorption isotherms for all materials mimicked a Type II adsorption isotherm, with evident multilayer quercetin adsorption at concentrations above 0.015, 0.0045 and 0.09 mg/mL quercetin for SP, SP-D and SP-T particles, respectively. The portion of the adsorption isotherms corresponding to monolayer (i.e., Langmuir adsorption) adsorption is shown in Figure 4 (for bare silica and decyl-functionalized silica) and Figure 5 (for titania-modified silica). The adsorption of quercetin on unmodified Stöber particles can be described by a Langmuir adsorption isotherm (**Figure B.6**), with an adsorption capacity of approximately 0.3 mg quercetin / g silica. Although quercetin is generally recognized as a hydrophobic molecule, and is sparingly soluble in water, quercetin has multiple hydroxyl groups and hydrogen bonding dominates the interaction of quercetin with silica surfaces. [202]
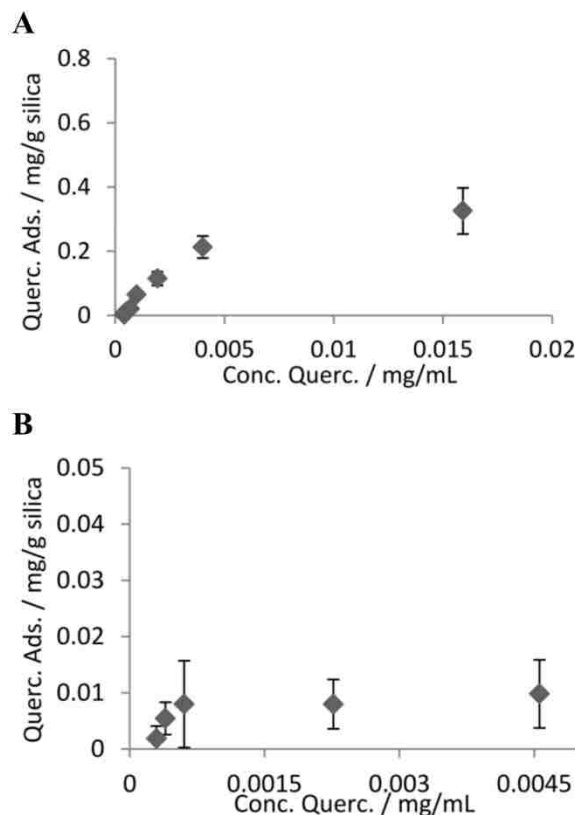
Figure B.6 Adsorption isotherm of quercetin from ethanol solutions onto A) non-functionalized Stöber Particles (SP) and B) decyl functionalized Stöber particles (SP-D) at room temperature. Error in measurement reproducibility is less than 10%.

The adsorption of quercetin on SP-D (**Figure B.6B**) particles follows a similar Langmuir adsorption isotherm to SP particles with a monolayer adsorption capacity of approximately 0.01 mg quercetin / gram SP-D. Adsorption capacities above 0.01 mg/g are not presented as they follow type II adsorption kinetics, indicating multilayer quercetin adsorption on particles. Investigations by Berlier et.al. into the stabilization of quercetin on silica and alkane modified silica particles via IR surface measurements indicate van der Waals type interactions between quercetin and non-polar octyl chains are much weaker than the hydrogen bonding based interactions between quercetin and

unmodified silica. [196] Relative to adsorption on SP materials (**Figure B.6A**), SP-D materials (**Figure B.6B**) possess significantly reduced adsorption capacities potentially due to the reduced bonding strength between non-polar decyl groups and quercetin in solution.

Quercetin adsorption on titania coated silica particles is a strong function of titania grafting density (**Figure B.7**). Titania grafting densities between 0.3 mg TiO$_2$/g particle – 9.8 mg TiO$_2$/g particle result in quercetin capacities of 0.52, 0.65, 0.88, and 1.66 mg quercetin / g silica, respectively, corresponding to a linear increase in capacity with grafting density (**Figure B.8**). This relationship between quercetin capacity and grafting density results in tunable adsorption of quercetin on materials for the design of tailored adsorption properties. The interaction of quercetin with titania is based on a chelation of the compound to the metal oxide, which is characterized by a shift in the color of quercetin from light yellow to an orange / brown chelated product. [192, 213]This transition was seen in these adsorption studies as a function of both increasing titania grafting density and quercetin concentration.
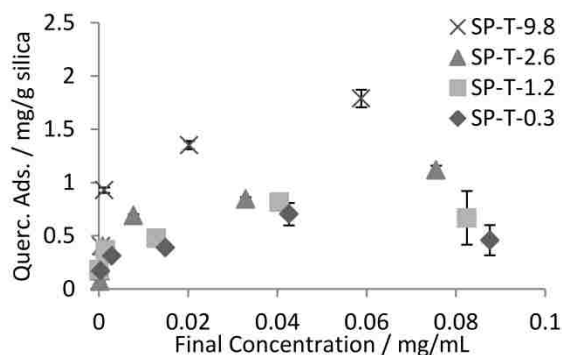
Figure B.7 Adsorption isotherms of quercetin in ethanol on titania coated Stober particles (SP-T) as a function of titania grafting density.
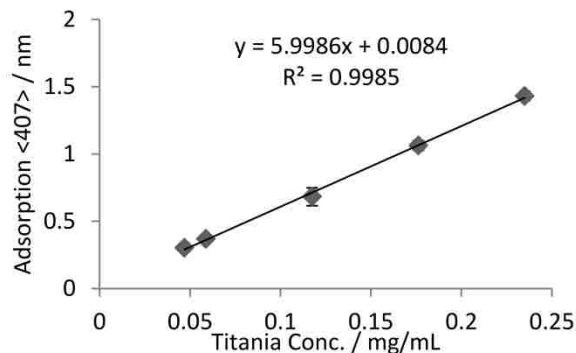
Figure B.8 TiO_2 dissolution assay
calibration curve.

The antioxidant activity of titania-bound, adsorbed quercetin and free quercetin was compared using the DPPH assay of antioxidant activity. [214] In its radical form DPPH adsorbs light at 515 nm, which is reduced in intensity as DPPH is chemically reduced by quercetin.[214, 215] The DPPH assay was chosen due to its greater accuracy in alcohol, amenable to the quercetin adsorption from ethanol system used in this study.. The nonporous nature of titania coated silica particles simplifies the interpretation of this time-based measurement by eliminating assay reactant and product diffusion times in pores. Quercetin complexed to SP-T-9.8 retains antioxidant capacity nearly equivalent to the same concentration of quercetin freely dissolved in ethanol, with minimal reduction in antioxidant capacity due to chelation with titania **(Figure B.9)**. Standard t-tests between free quercetin and particle adsorbed quercetin activities indicate statistically different activities ($P \leq 0.05$) for 0.0, 1.0 and 10 µg/mL. The ability to recover bioactive molecules is critical in designing nanoparticles for the separation of metabolites from cultures using strong specific interactions such as chelation.

133
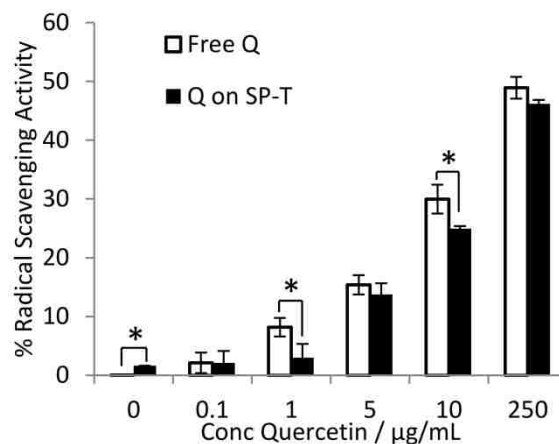
Figure B.9 Radical scavenging activity of free quercetin (Free Q) and quercetin complexed to titania particles (Q on SP-T). Statistically different ($P \leq 0.05$) values based on unpaired t-tests are indicated with (*).

B.5 Conclusions

Functionalized silica nanoparticles are promising materials platforms for the adsorption and recovery of polyphenol compounds. Non-polar decyl functional groups showed minimal affinity for quercetin (0.01 mg quercetin / g particles), while hydrogen bonding interactions between quercetin and unmodified silica substantially increased nanoparticle loading capacity (0.3 mg quercetin/g particles). Chelation to the metal oxide titania not only showed the greatest capacity for titania adsorption (1.66 mg quercetin /g particles), but also provided tunable loading capacities as a function of titania grafting densities. Titania coated on silica particles is expected to be significantly more stable than bulk titania, and advances in the synthesis of mesoporous silica (different morphologies, particle and pore diameter control, surface functionality) make titania coated silica materials a more versatile materials platform than pure TiO_2 materials. Additionally, quercetin chelated to titania retains the same antioxidant activity as the equivalent amount of quercetin free in solution. Retention of antioxidant capacity is critical for the use of these materials in separations and recovery of polyphenolic bioactive compounds.

REFERENCES

[1] C.R. Silva, C. Airoldi, Acid and Base Catalysts in the Hybrid Silica Sol–Gel Process, J. Colloid Interface Sci., 195 (1997) 381-387.

[2] J.R. Lakowicz, Principles of Fluorescence Spectroscopy, Third Edition, Journal of Biomedical Optics, 13 (2008) 029901-029901.

[3] D. Zhao, J. Feng, Q. Huo, N. Melosh, G.H. Fredrickson, B.F. Chmelka, G.D. Stucky, Triblock Copolymer Syntheses of Mesoporous Silica with Periodic 50 to 300 Angstrom Pores, Science (New York, N.Y.), 279 (1998) 548-552.

[4] D. Zhao, J. Sun, Q. Li, G.D. Stucky, Morphological Control of Highly Ordered Mesoporous Silica SBA-15, Chemistry of Materials, 12 (2000) 275-279.

[5] A. Katiyar, L. Ji, P. Smirniotis, N.G. Pinto, Protein adsorption on the mesoporous molecular sieve silicate SBA-15: effects of pH and pore size, J. Chromatogr. A, 1069 (2005) 119-126.

[6] Z.K. Sun, Y.H. Deng, J. Wei, D. Gu, B. Tu, D.Y. Zhao, Hierarchically Ordered Macro-/Mesoporous Silica Monolith: Tuning Macropore Entrance Size for Size-Selective Adsorption of Proteins, Chem. Mater., 23 (2011) 2176-2184.

[7] A. Katiyar, N.G. Pinto, Visualization of Size-Selective Protein Separations on Spherical Mesoporous Silicates, Small (Weinheim an der Bergstrasse, Germany), 2 (2006) 644-648.

[8] F. de Juan, E. Ruiz-Hitzky, Selective Functionalization of Mesoporous Silica, Adv. Mater., 12 (2000) 430-432.

[9] J.D. Lunn, D.F. Shantz, Novel polypeptide/thiol-SBA-15 hybrid materials synthesized via surface selective grafting, Chem. Commun., 46 (2010) 2926-2928.

[10] K. Benson, E.A. Prasetyanto, H.J. Galla, N.S. Kehr, Self-assembled monolayers of bifunctional periodic mesoporous organosilicas for cell adhesion and cellular patterning, Soft Matter, 8 (2012) 10845-10852.

[11] M.S. Kim, J.B. Jeon, J.Y. Chang, Selectively functionalized mesoporous silica particles with the PEGylated outer surface and the doxorubicin-grafted inner surface: Improvement of loading content and solubility, Microporous Mesoporous Mater., 172 (2013) 118-124.

[12] Q. Wei, Z.X. Zhong, Z.R. Nie, J.L. Li, F. Wang, Q.Y. Li, Catalytically active gold nanoparticles confined in periodic mesoporous organosilica (PMOs) by a modified external passivation route, Microporous Mesoporous Mater., 117 (2009) 98-103.

[13] M.E.L. C.T. Kresge, W.J. Roth, J.C. Vartuli & J.S. Beck, Ordered mesoporous molecular sieves synthesized by a liquid-crystal template mechanism, Nature, 359 (1992) 3.

[14] K. Ariga, Y. Okahata, Permeability controllable membranes. 11. Polymerized monolayers of single-, double-, and triple-chain silane amphiphiles and permeation control through the monolayer-immobilized porous glass plate in an aqueous solution, J. Am. Chem. Soc., 111 (1989) 5618-5622.

[15] P.C.A. Alberius, K.L. Frindell, R.C. Hayward, E.J. Kramer, G.D. Stucky, B.F. Chmelka, General Predictive Syntheses of Cubic, Hexagonal, and Lamellar Silica and Titania Mesostructured Thin Films, Chem. Mater., 14 (2002) 3284-3294.

[16] P. Kumar, V.V. Guliants, Periodic mesoporous organic–inorganic hybrid materials: Applications in membrane separations and adsorption, Microporous Mesoporous Mater., 132 (2010) 1-14.

[17] R. Martín-Aranda, J. Čejka, Recent Advances in Catalysis Over Mesoporous Molecular Sieves, Top. Catal., 53 (2010) 141-153.

[18] L.L. Hench, J.K. West, The sol-gel process, Chem. Rev., 90 (1990) 33-72.

[19] F.D.O.a.E.R. Pohl, Kinetics of the hydrolysis and condensation of organofunctional alkoxysilanes: a review, J. Adhes. Sci. Technol., 6 (1992).

[20] C.J.B.a.G.W. Scherer, Sol-Gel Science: The Physics and Chemistry of Sol-Gel Processing, Academic Press Limited, San Diego, CA, 1990.

[21] Q. Huo, D.I. Margolese, G.D. Stucky, Surfactant Control of Phases in the Synthesis of Mesoporous Silica-Based Materials, Chem. Mater., 8 (1996) 1147-1160.

[22] J.L. Blin, B.L. Su, Tailoring Pore Size of Ordered Mesoporous Silicas Using One or Two Organic Auxiliaries as Expanders, Langmuir, 18 (2002) 5303-5308.

[23] J.S. Beck, J.C. Vartuli, W.J. Roth, M.E. Leonowicz, C.T. Kresge, K.D. Schmitt, C.T.W. Chu, D.H. Olson, E.W. Sheppard, A new family of mesoporous molecular sieves prepared with liquid crystal templates, J. Am. Chem. Soc., 114 (1992) 10834-10843.

[24] A. Corma, Q. Kan, M.T. Navarro, J. Pérez-Pariente, F. Rey, Synthesis of MCM-41 with Different Pore Diameters without Addition of Auxiliary Organics, Chem. Mater., 9 (1997) 2123-2126.

[25] M. Mesa, L. Sierra, B. López, A. Ramirez, J.-L. Guth, Preparation of micron-sized spherical particles of mesoporous silica from a triblock copolymer surfactant, usable as a stationary phase for liquid chromatography, Solid State Sci, 5 (2003) 1303-1308.

[26] D.Y. Zhao, Q.S. Huo, J.L. Feng, B.F. Chmelka, G.D. Stucky, Nonionic triblock and star diblock copolymer and oligomeric surfactant syntheses of highly ordered, hydrothermally stable, mesoporous silica structures, J. Am. Chem. Soc., 120 (1998) 6024-6036.

[27] D.M. Schlipf, S.E. Rankin, B.L. Knutson, Pore-Size Dependent Protein Adsorption and Protection from Proteolytic Hydrolysis in Tailored Mesoporous Silica Particles, ACS Appl. Mater. Interfaces, 5 (2013) 10111-10117.

[28] Z.-L. Hua, J.-L. Shi, L. Wang, W.-H. Zhang, Preparation of mesoporous silica films on a glass slide: surfactant template removal by solvent extraction, J. Non-Cryst. Solids, 292 (2001) 177-183.

[29] F. Bérubé, S. Kaliaguine, Calcination and thermal degradation mechanisms of triblock copolymer template in SBA-15 materials, Microporous Mesoporous Mater., 115 (2008) 469-479.

[30] R.A. Sheldon, Enzyme Immobilization: The Quest for Optimum Performance, Adv. Synth. Catal., 349 (2007) 1289-1307.

[31] Z. Li, J.C. Barnes, A. Bosoy, J.F. Stoddart, J.I. Zink, Mesoporous silica nanoparticles in biomedical applications, Chem. Soc. Rev., 41 (2012) 2590-2605.

[32] S. Hudson, J. Cooney, E. Magner, Proteins in Mesoporous Silicates, Angew. Chem. Int. Ed., 47 (2008) 8582-8594.

[33] C.-H. Lee, T.-S. Lin, C.-Y. Mou, Mesoporous materials for encapsulating enzymes, Nano Today, (2009).

[34] S. Sotiropoulou, V. Vamvakaki, N.A. Chaniotakis, Stabilization of enzymes in nanoporous materials for biosensor applications, Biosens. Bioelectron., 20 (2005) 1674-1679.

[35] J. Kim, J.W. Grate, P. Wang, Nanostructures for enzyme stabilization, Chem. Eng. Sci., 61 (2006) 1017-1026.

[36] M. Hartmann, Ordered Mesoporous Materials for Bioadsorption and Biocatalysis, Chem. Mater., 17 (2005) 4577-4593.

[37] M. Hartmann, D. Jung, Biocatalysis with enzymes immobilized on mesoporous hosts: the status quo and future trends, J. Mater. Chem., 20 (2010) 844-857.

[38] M. Hartmann, X. Kostrov, Immobilization of enzymes on porous silicas - benefits and challenges, Chem. Soc. Rev., 42 (2013) 6277-6289.

[39] J. Dordick, A. Freeman, Biocatalysis as a discovery tool: from nanoscale to high-throughput and beyond, Curr. Opin. Biotechnol., 17 (2006) 559-561.

[40] S. Lu, Z. An, J. Li, J. He, pH-Triggered Adsorption–Desorption of Enzyme in Mesoporous Host to Act on Macrosubstrate, The Journal of Physical Chemistry B, 115 (2011) 13695-13700.

[41] H.H.P. Yiu, P.A. Wright, N.P. Botting, Enzyme immobilisation using SBA-15 mesoporous molecular sieves with functionalised surfaces, J. Mol. Catal. B: Enzym., 15 (2001) 81-92.

[42] J.D. Brennan, Biofriendly sol-gel processing for the entrapment of soluble and membrane-bound proteins: toward novel solid-phase assays for high-throughput screening, Acc. Chem. Res., 40 (2007) 827-835.

[43] Y. Wang, F. Caruso, Mesoporous Silica Spheres as Supports for Enzyme Immobilization and Encapsulation, Chem. Mater., 17 (2005) 953-961.

[44] A.S.S. Ibrahim, A.A. Al-Salamah, A.M. El-Toni, M.A. El-Tayeb, Y.B. Elbadawi, Cyclodextrin glucanotransferase immobilization onto functionalized magnetic double mesoporous core–shell silica nanospheres, Electron. J. Biotechnol., 17 (2014) 55-64.

[45] E. Magner, Immobilisation of enzymes on mesoporous silicate materials, Chem. Soc. Rev., 42 (2013) 6213-6222.

[46] H. Jaladi, A. Katiyar, S.W. Thiel, V.V. Guliants, N.G. Pinto, Effect of pore diffusional resistance on biocatalytic activity of Burkholderia cepacia lipase immobilized on SBA-15 hosts, Chem. Eng. Sci., 64 (2009) 1474-1479.

[47] Y. Ma, P. Rajendran, C. Blum, Y. Cesa, N. Gartmann, D. Brühwiler, V. Subramaniam, Microspectroscopic analysis of green fluorescent proteins infiltrated into mesoporous silica nanochannels, J. Colloid Interface Sci., 356 (2011) 123-130.

[48] S. Lu, Z. Song, J. He, Diffusion-Controlled Protein Adsorption in Mesoporous Silica, J. Phys. Chem. B, 115 (2011) 7744-7750.

[49] T.V. Fedyanina, V.N. Barvinchenko, N.A. Lipkovskaya, V.K. Pogorelyi, The effect of complexation with biopolymers on the adsorption of quercetin on silica, Colloid J., 70 (2008) 215-220.

[50] A. Hanprasopwattana, S. Srinivasan, A.G. Sault, A.K. Datye, Titania Coatings on Monodisperse Silica Spheres (Characterization Using 2-Propanol Dehydration and TEM), Langmuir, 12 (1996) 3173-3179.

[51] F. Chen, H. Hong, S. Shi, S. Goel, H.F. Valdovinos, R. Hernandez, C.P. Theuer, T.E. Barnhart, W. Cai, Engineering of Hollow Mesoporous Silica Nanoparticles for Remarkably Enhanced Tumor Active Targeting Efficacy, Sci. Rep., 4 (2014).

[52] R. Takeuchi, A. Shoji, M. Sugawara, A solid phase-based nanopore sensing system for biomolecules using lipid-loaded mesoporous silica MCM-41 and a fluorescent dye, Sensors Actuators B: Chem., 181 (2013) 29-37.

[53] R. Kumar, I. Roy, T.Y. Ohulchanskyy, L.N. Goswami, A.C. Bonoiu, E.J. Bergey, K.M. Tramposch, A. Maitra, P.N. Prasad, Covalently Dye-Linked, Surface-Controlled, and Bioconjugated Organically Modified Silica Nanoparticles as Targeted Probes for Optical Imaging, ACS nano, 2 (2008) 449-456.

[54] B.W. Chen, W. Qi, X.L. Li, C.H. Lei, J. Liu, Heated Proteins are Still Active in a Functionalized Nanoporous Support, Small (Weinheim an der Bergstrasse, Germany), 9 (2013) 2228-2232.

[55] V. Puddu, C.C. Perry, Interactions at the Silica-Peptide Interface: The Influence of Particle Size and Surface Functionality, Langmuir, 30 (2014) 227-233.

[56] S.C. Shen, W.K. Ng, L. Chia, Y.C. Dong, R.B.H. Tan, Sonochemical synthesis of (3-aminopropyl)triethoxysilane-modified monodispersed silica nanoparticles for protein immobilization, Mater. Res. Bull., 46 (2011) 1665-1669.

[57] P.A. Russo, M. Carrott, P.A.M. Mourao, P.J.M. Carrott, Tailoring the surface chemistry of mesocellular foams for protein adsorption, Colloid Surf. A-Physicochem. Eng. Asp., 386 (2011) 25-35.

[58] A. Nieto, M. Colilla, F. Balas, M. Vallet-Regi, Surface Electrochemistry of Mesoporous Silicas as a Key Factor in the Design of Tailored Delivery Devices, Langmuir, 26 (2010) 5038-5049.

[59] A.J. Di Pasqua, K.K. Sharma, Y.L. Shi, B.B. Toms, W. Ouellette, J.C. Dabrowiak, T. Asefa, Cytotoxicity of mesoporous silica nanomaterials, J. Inorg. Biochem., 102 (2008) 1416-1423.

[60] A. Lankoff, M. Arabski, A. Wegierek-Ciuk, M. Kruszewski, H. Lisowska, A. Banasik-Nowak, K. Rozga-Wijas, M. Wojewodzka, S. Slomkowski, Effect of surface modification of silica nanoparticles on toxicity and cellular uptake by human peripheral blood lymphocytes in vitro, Nanotoxicology, 7 (2013) 235-250.

[61] F.Q. Tang, L.L. Li, D. Chen, Mesoporous Silica Nanoparticles: Synthesis, Biocompatibility and Drug Delivery, Adv. Mater., 24 (2012) 1504-1534.

[62] J. Kecht, A. Schlossbauer, T. Bein, Selective Functionalization of the Outer and Inner Surfaces in Mesoporous Silica Nanoparticles, Chem. Mater., 20 (2008) 7207-7214.

[63] M.S. Kim, J.Y. Chang, Preparation of multifunctional mesoporous silica particles: the use of an amphiphilic silica precursor with latent amine functionality in selective functionalization of the inner surface, J. Mater. Chem., 21 (2011) 8766-8771.

[64] M. Qhobosheane, S. Santra, P. Zhang, W. Tan, Biochemically functionalized silica nanoparticles, The Analyst, 126 (2001) 1274-1278.

[65] D. Bruhwiler, Postsynthetic functionalization of mesoporous silica, Nanoscale, 2 (2010) 887-892.

[66] K. Cheng, C.C. Landry, Diffusion-Based Deprotection in Mesoporous Materials: A Strategy for Differential Functionalization of Porous Silica Particles, J. Am. Chem. Soc., 129 (2007) 9674-9685.

[67] V. Cauda, A. Schlossbauer, J. Kecht, A. Zurner, T. Bein, Multiple Core-Shell Functionalized Colloidal Mesoporous Silica Nanoparticles, J. Am. Chem. Soc., 131 (2009) 11361-11370.

[68] M. Bouchoucha, R. C.-Gaudreault, M.-A. Fortin, F. Kleitz, Mesoporous Silica Nanoparticles: Selective Surface Functionalization for Optimal Relaxometric and Drug Loading Performances, Adv. Funct. Mater., (2014) n/a-n/a.

[69] K. Cheng, C.C. Landry, Diffusion-based deprotection in mesoporous materials: A strategy for differential functionalization of porous silica particles, J. Am. Chem. Soc., 129 (2007) 9674-9685.

[70] N. Gartmann, D. Brühwiler, Controlling and Imaging the Functional-Group Distribution on Mesoporous Silica, Angew. Chem. Int. Ed., 48 (2009) 6354-6356.

[71] K. Hara, S. Akahane, J.W. Wiench, B.R. Burgin, N. Ishito, V.S.Y. Lin, A. Fukuoka, M. Pruski, Selective and Efficient Silylation of Mesoporous Silica: A Quantitative Assessment of Synthetic Strategies by Solid-State NMR, J. Phys. Chem. C, 116 (2012) 7083-7090.

[72] R.A. Roggers, V.S.Y. Lin, B.G. Trewyn, Chemically Reducible Lipid Bilayer Coated Mesoporous Silica Nanoparticles Demonstrating Controlled Release and HeLa and Normal Mouse Liver Cell Biocompatibility and Cellular Internalization, Mol. Pharm., 9 (2012) 2770-2777.

[73] J. Jackman, W. Knoll, N.-J. Cho, Biotechnology Applications of Tethered Lipid Bilayer Membranes, Materials, 5 (2012) 2637-2657.

[74] M. Khan, N. Dosoky, J. Williams, Engineering Lipid Bilayer Membranes for Protein Studies, International Journal of Molecular Sciences, 14 (2013) 21561-21597.

[75] M.A.R.B. Castanho, M.X. Fernandes, Lipid membrane-induced optimization for ligand–receptor docking: recent tools and insights for the "membrane catalysis" model, Eur. Biophys. J., 35 (2006) 92-103.

[76] C.E. Ashley, E.C. Carnes, G.K. Phillips, D. Padilla, P.N. Durfee, P.A. Brown, T.N. Hanna, J. Liu, B. Phillips, M.B. Carter, N.J. Carroll, X. Jiang, D.R. Dunphy, C.L. Willman, D.N. Petsev, D.G. Evans, A.N. Parikh, B. Chackerian, W. Wharton, D.S. Peabody, C.J. Brinker, The targeted delivery of multicomponent cargos to cancer cells by nanoporous particle-supported lipid bilayers, Nat Mater, 10 (2011) 389-397.

[77] C.E. Ashley, E.C. Carnes, K.E. Epler, D.P. Padilla, G.K. Phillips, R.E. Castillo, D.C. Wilkinson, B.S. Wilkinson, C.A. Burgard, R.M. Kalinich, J.L. Townson, B. Chackerian, C.L. Willman, D.S. Peabody, W. Wharton, C.J. Brinker, Delivery of Small Interfering

RNA by Peptide-Targeted Mesoporous Silica Nanoparticle-Supported Lipid Bilayers, ACS nano, 6 (2012) 2174-2188.

[78] G. Nordlund, J.B. Sing Ng, L. Bergstrom, P. Brzezinski, A membrane-reconstituted multisubunit functional proton pump on mesoporous silica particles, ACS nano, 3 (2009) 2639-2646.

[79] V. Oliynyk, C. Mille, J.B. Ng, C. von Ballmoos, R.W. Corkery, L. Bergstrom, Selective and ATP-driven transport of ions across supported membranes into nanoporous carriers using gramicidin A and ATP synthase, Phys. Chem. Chem. Phys., 15 (2013) 2733-2740.

[80] S. Chemburu, K. Fenton, G.P. Lopez, R. Zeineldin, Biomimetic Silica Microspheres in Biosensing, Molecules, 15 (2010) 1932-1957.

[81] A.R. Piper-Feldkamp, M. Wegner, P. Brzezinski, S.M. Reed, Mixtures of Supported and Hybrid Lipid Membranes on Heterogeneously Modified Silica Nanoparticles, The Journal of Physical Chemistry B, 117 (2013) 2113-2122.

[82] L.-S. Wang, L.-C. Wu, S.-Y. Lu, L.-L. Chang, I.T. Teng, C.-M. Yang, J.-a.A. Ho, Biofunctionalized Phospholipid-Capped Mesoporous Silica Nanoshuttles for Targeted Drug Delivery: Improved Water Suspensibility and Decreased Nonspecific Protein Binding, ACS nano, 4 (2010) 4371-4379.

[83] F. Heinrich, T. Ng, D.J. Vanderah, P. Shekhar, M. Mihailescu, H. Nanda, M. Lösche, A New Lipid Anchor for Sparsely Tethered Bilayer Lipid Membranes†, Langmuir, 25 (2009) 4219-4229.

[84] M.K. Sharma, M.L. Gilchrist, Templated assembly of biomembranes on silica microspheres using bacteriorhodopsin conjugates as structural anchors, Langmuir, 23 (2007) 7101-7112.

[85] L. Zhong, R. Tu, M.L. Gilchrist, Tether-Supported Biomembranes with α-Helical Peptide-Based Anchoring Constructs, Langmuir, 29 (2012) 299-307.

[86] A.H. Pande, S. Qin, S.A. Tatulian, Membrane Fluidity Is a Key Modulator of Membrane Binding, Insertion, and Activity of 5-Lipoxygenase, Biophys. J., 88 (2005) 4084-4094.

[87] M.B. Lande, J.M. Donovan, M.L. Zeidel, The relationship between membrane fluidity and permeabilities to water, solutes, ammonia, and protons, The Journal of General Physiology, 106 (1995) 67-84.

[88] C. Scomparin, S. Lecuyer, M. Ferreira, T. Charitat, B. Tinland, Diffusion in supported lipid bilayers: Influence of substrate and preparation technique on the internal dynamics, Eur. Phys. J. E, 28 (2009) 211-220.

[89] F. Roder, S. Waichman, D. Paterok, R. Schubert, C. Richter, B. Liedberg, J. Piehler, Reconstitution of Membrane Proteins into Polymer-Supported Membranes for Probing Diffusion and Interactions by Single Molecule Techniques, Anal. Chem., 83 (2011) 6792-6799.

[90] G. Gopalakrishnan, I. Rouiller, D.R. Colman, R.B. Lennox, Supported Bilayers Formed from Different Phospholipids on Spherical Silica Substrates, Langmuir, 25 (2009) 5455-5458.

[91] T. Buranda, J. Huang, G.V. Ramarao, L.K. Ista, R.S. Larson, T.L. Ward, L.A. Sklar, G.P. Lopez, Biomimetic Molecular Assemblies on Glass and Mesoporous Silica Microbeads for Biotechnology†, Langmuir, 19 (2003) 1654-1663.

[92] R.W. Davis, A. Flores, T.A. Barrick, J.M. Cox, S.M. Brozik, G.P. Lopez, J.A. Brozik, Nanoporous Microbead Supported Bilayers: Stability, Physical Characterization, and Incorporation of Functional Transmembrane Proteins, Langmuir, 23 (2007) 3864-3872.

[93] L. Guo, J.Y. Har, J. Sankaran, Y. Hong, B. Kannan, T. Wohland, Molecular diffusion measurement in lipid bilayers over wide concentration ranges: a comparative study, Chemphyschem : a European journal of chemical physics and physical chemistry, 9 (2008) 721-728.

[94] A.A. Spector, M.A. Yorek, Membrane lipid composition and cellular function, J. Lipid Res., 26 (1985) 1015-1035.

[95] M.A. Deverall, E. Gindl, E.K. Sinner, H. Besir, J. Ruehe, M.J. Saxton, C.A. Naumann, Membrane Lateral Mobility Obstructed by Polymer-Tethered Lipids Studied at the Single Molecule Level, Biophys. J., 88 (2005) 1875-1886.

[96] M. Claesson, R. Frost, S. Svedhem, M. Andersson, Pore Spanning Lipid Bilayers on Mesoporous Silica Having Varying Pore Size, Langmuir, 27 (2011) 8974-8982.

[97] D. Mowrey, Q. Chen, Y. Liang, J. Liang, Y. Xu, P. Tang, Signal Transduction Pathways in the Pentameric Ligand-Gated Ion Channels, PLoS ONE, 8 (2013) e64326.

[98] J.-L. Rigaud, B. Pitard, D. Levy, Reconstitution of membrane proteins into liposomes: application to energy-transducing membrane proteins, Biochim. Biophys. Acta, 1231 (1995) 223-246.

[99] Y. Li, M. Ge, L. Ciani, G. Kuriakose, E.J. Westover, M. Dura, D.F. Covey, J.H. Freed, F.R. Maxfield, J. Lytton, I. Tabas, Enrichment of endoplasmic reticulum with cholesterol inhibits sarcoplasmic-endoplasmic reticulum calcium ATPase-2b activity in parallel with increased order of membrane lipids: implications for depletion of endoplasmic reticulum calcium stores and apoptosis in cholesterol-loaded macrophages, J. Biol. Chem., 279 (2004) 37030-37039.

[100] X. Liu, F. Fagotto, A method to separate nuclear, cytosolic, and membrane-associated signaling molecules in cultured cells, Science signaling, 4 (2011) pl2.

[101] A. Ljunglöf, J. Thömmes, Visualising intraparticle protein transport in porous adsorbents by confocal microscopy, J. Chromatogr. A, 813 (1998) 387-395.

[102] C.W. Suh, M.Y. Kim, J.B. Choo, J.K. Kim, H.K. Kim, E.K. Lee, Analysis of protein adsorption characteristics to nano-pore silica particles by using confocal laser scanning microscopy, J. Biotechnol., 112 (2004) 267-277.

[103] M. Sauer, J. Hofkens, J. Enderlein, Basic Principles of Fluorescence Spectroscopy, Handbook of Fluorescence Spectroscopy and Imaging, Wiley-VCH Verlag GmbH & Co. KGaA2011, pp. 1-30.

[104] J.R. Lakowicz, Principles of Fluorescence Spectroscopy, 3 ed., Springer Science, New York, NY, 2006.

[105] B.R. Masters, The Development of Fluorescence Microscopy, eLS, John Wiley & Sons, Ltd2001.

[106] M. Abramowitz, K.R. Spring, H.E. Keller, M.W. Davidson, Basic principles of microscope objectives, BioTechniques, 33 (2002) 772-781.

[107] V. Prasad, D. Semwogerere, E.R. Weeks, Confocal microscopy of colloids, J. Phys.: Condens. Matter, 19 (2007) 113102.

[108] A.J. Diaz, F. Albertorio, S. Daniel, P.S. Cremer, Double cushions preserve transmembrane protein mobility in supported bilayer systems, Langmuir, 24 (2008) 6820-6826.

[109] E.E. Ross, M.J. Wirth, Silica Colloidal Crystals as Three-Dimensional Scaffolds for Supported Lipid Films, Langmuir, 24 (2008) 1629-1634.

[110] D. Axelrod, D.E. Koppel, J. Schlessinger, E. Elson, W.W. Webb, Mobility measurement by analysis of fluorescence photobleaching recovery kinetics, Biophys. J., 16 (1976) 1055-1069.

[111] M. Kang, A. Kenworthy, Complex Applications of Simple FRAP on Membranes, in: R. Faller, M.L. Longo, S.H. Risbud, T. Jue (Eds.) Biomembrane Frontiers, Humana Press2009, pp. 187-221.

[112] L. Wang, J. Lei, J. Zhang, Building of multifluorescent mesoporous silica nanoparticles, Chem. Commun., (2009) 2195-2197.

[113] T. Förster, O. Sinanoglu, Modern quantum chemistry, Academic Press, New York, 3 (1965).

[114] H.C. Ishikawa-Ankerhold, R. Ankerhold, G.P. Drummen, Advanced fluorescence microscopy techniques--FRAP, FLIP, FLAP, FRET and FLIM, Molecules, 17 (2012) 4047-4132.

[115] A. Katiyar, S. Yadav, P.G. Smirniotis, N.G. Pinto, Synthesis of ordered large pore SBA-15 spherical particles for adsorption of biomolecules, J. Chromatogr. A, 1122 (2006) 13-20.

[116] J. Ambati, A.M. Lopez, D. Cochran, P. Wattamwar, K. Bean, T.D. Dziubla, S.E. Rankin, Engineered silica nanocarriers as a high-payload delivery vehicle for antioxidant enzymes, Acta Biomater., 8 (2012) 2096-2103.

[117] H.-P. Lin, C.-P. Kao, C.-Y. Mou, S.-B. Liu, Counterion Effect in Acid Synthesis of Mesoporous Silica Materials, J. Phys. Chem. B, 104 (2000) 7885-7894.

[118] H. Yang, G. Vovk, N. Coombs, I. Sokolov, G. A. Ozin, Synthesis of mesoporous silica spheres under quiescent aqueous acidic conditions, J. Mater. Chem., 8 (1998) 743-750.

[119] J. He, Z. Liu, C. Hai, Adsorption heterogeneity of lysozyme over functionalized mesoporous silica: Effect of interfacial noncovalent interactions, AlChE J., 54 (2008) 2495-2506.

[120] P.P. Yang, S.L. Gai, J. Lin, Functionalized mesoporous silica materials for controlled drug delivery, Chem. Soc. Rev., 41 (2012) 3679-3698.

[121] S. Lu, Z. An, J. Li, J. He, pH-Triggered Adsorption–Desorption of Enzyme in Mesoporous Host to Act on Macrosubstrate, J. Phys. Chem. B, 115 (2011) 13695-13700.

[122] A. Malik, R. Rudolph, B. Söhling, Use of enhanced green fluorescent protein to determine pepsin at high sensitivity, Anal. Biochem., 340 (2005) 252-258.

[123] A.R. Sielecki, A.A. Fedorov, A. Boodhoo, N.S. Andreeva, M.N.G. James, Molecular and crystal structures of monoclinic porcine pepsin refined at 1.8A˚resolution, J. Mol. Biol., 214 (1990) 143-170.

[124] H.G. Manyar, E. Gianotti, Y. Sakamoto, O. Terasaki, S. Coluccia, S. Tumbiolo, Active Biocatalysts Based on Pepsin Immobilized in Mesoporous SBA-15, J. Phys. Chem. C, 112 (2008) 18110-18116.

[125] M.R. Bhambhani, P.A. Cutting, K.S.W. Sing, D.H. Turk, Analysis of nitrogen adsorption isotherms on porous and nonporous silicas by the BET and αs methods, J. Colloid Interface Sci., 38 (1972) 109-117.

[126] S. Brunauer, P.H. Emmett, E. Teller, Adsorption of Gases in Multimolecular Layers, J. Am. Chem. Soc., 60 (1938) 309-319.

[127] E.P. Barrett, L.G. Joyner, P.P. Halenda, The Determination of Pore Volume and Area Distributions in Porous Substances. I. Computations from Nitrogen Isotherms, J. Am. Chem. Soc., 73 (1951) 373-380.

[128] M. Ormo, A.B. Cubitt, K. Kallio, L.A. Gross, R.Y. Tsien, S.J. Remington, Crystal structure of the Aequorea victoria green fluorescent protein, Science (New York, N.Y.), 273 (1996) 1392-1395.

[129] F. Yang, L.G. Moss, G.N. Phillips, The molecular structure of green fluorescent protein, Nat. Biotechnol., 14 (1996) 1246-1251.

[130] W.W. Ward, S.H. Bokman, Reversible denaturation of Aequorea green-fluorescent protein: physical separation and characterization of the renatured protein, Biochemistry, 21 (1982) 4535-4540.

[131] D.K. Eggers, J.S. Valentine, Molecular confinement influences protein structure and enhances thermal protein stability, Protein Sci., 10 (2001) 250-261.

[132] B. Campanini, S. Bologna, F. Cannone, G. Chirico, A. Mozzarelli, S. Bettati, Unfolding of Green Fluorescent Protein mut2 in wet nanoporous silica gels, Protein Sci., 14 (2005) 1125-1133.

[133] D.I. Fried, F.J. Brieler, M. Froba, Designing Inorganic Porous Materials for Enzyme Adsorption and Applications in Biocatalysis, ChemCatChem, 5 (2013) 862-884.

[134] F. Jia, B. Narasimhan, S. Mallapragada, Materials-Based Strategies for Multi-Enzyme Immobilization and Co-Localization: A Review, Biotechnol. Bioeng., 111 (2014) 209-222.

[135] M. Malmsten, Inorganic nanomaterials as delivery systems for proteins, peptides, DNA, and siRNA, Curr. Opin. Colloid Interface Sci., 18 (2013) 468-480.

[136] J.M. Rosenholm, C. Sahlgren, M. Linden, Multifunctional Mesoporous Silica Nanoparticles for Combined Therapeutic, Diagnostic and Targeted Action in Cancer Treatment, Curr. Drug Targets, 12 (2011) 1166-1186.

[137] Z. Zhou, M. Hartmann, Progress in enzyme immobilization in ordered mesoporous materials and related applications, Chem. Soc. Rev., 42 (2013) 3894-3912.

[138] P. Hudson Sarah, S. White, D. Goradia, H. Essa, B. Liu, L. Qiao, Y. Liu, C. Cooney Jakki, B.K. Hodnett, E. Magner, Proteins in Mesoporous Silicates, Biomolecular Catalysis, American Chemical Society2008, pp. 49-60.

[139] T. Shimomura, T. Itoh, T. Sumiya, F. Mizukami, M. Ono, Electrochemical biosensor for the detection of formaldehyde based on enzyme immobilization in mesoporous silica materials, Sensors Actuators B: Chem., 135 (2008) 268-275.

[140] C. Lei, M.M. Valenta, K.P. Saripalli, E.J. Ackerman, Biosensing Paraoxon in Simulated Environmental Samples by Immobilized Organophosphorus Hydrolase in Functionalized Mesoporous Silica, J. Environ. Qual., 36 (2007) 233-238.

[141] Z. Dai, X. Xu, L. Wu, H. Ju, Detection of Trace Phenol Based on Mesoporous Silica Derived Tyrosinase-Peroxidase Biosensor, Electroanalysis, 17 (2005) 1571-1577.

[142] Y. Ma, L. Qi, J. Ma, Y. Wu, O. Liu, H. Cheng, Large-pore mesoporous silica spheres: synthesis and application in HPLC, Colloids Surf. Physicochem. Eng. Aspects, 229 (2003) 1-8.

[143] J. Kim, R.J. Desch, S.W. Thiel, V.V. Guliants, N.G. Pinto, Energetics of biomolecule adsorption on mesostructured cellular foam silica, Microporous Mesoporous Mater., 170 (2013) 95-104.

[144] Y. Kuthati, P.J. Sung, C.F. Weng, C.Y. Mou, C.H. Lee, Functionalization of Mesoporous Silica Nanoparticles for Targeting, Biocompatibility, Combined Cancer Therapies and Theragnosis, J. Nanosci. Nanotechnol., 13 (2013) 2399-2430.

[145] H. Salmio, D. Brühwiler, Distribution of Amino Groups on a Mesoporous Silica Surface after Submonolayer Deposition of Aminopropylsilanes from an Anhydrous Liquid Phase, J. Phys. Chem. C, 111 (2006) 923-929.

[146] N. Gartmann, D. Brühwiler, Correlation of Nitrogen Sorption and Confocal Laser Scanning Microscopy for the Analysis of Amino Group Distributions on Mesoporous Silica, Materials, 4 (2011) 1096-1103.

[147] A.-H. Lu, W.-C. Li, A. Kiefer, W. Schmidt, E. Bill, G. Fink, F. Schüth, Fabrication of Magnetically Separable Mesostructured Silica with an Open Pore System, J. Am. Chem. Soc., 126 (2004) 8616-8617.

[148] H. Ritter, M. Nieminen, M. Karppinen, D. Brühwiler, A comparative study of the functionalization of mesoporous silica MCM-41 by deposition of 3-aminopropyltrimethoxysilane from toluene and from the vapor phase, Microporous Mesoporous Mater., 121 (2009) 79-83.

[149] Protein Desalting Spin Columns #89849, InstructionsThermo Scientific, 2013.

[150] B. Arkles, J.R. Steinmetz, J. Zazyczny, P. Mehta, Factors contributing to the stability of alkoxysilanes in aqueous solution, J. Adhes. Sci. Technol., 6 (1992) 193-206.

[151] H. Ritter, D. Brühwiler, Accessibility of Amino Groups in Postsynthetically Modified Mesoporous Silica, J. Phys. Chem. C, 113 (2009) 10667-10674.

[152] T. Yokoi, H. Yoshitake, T. Tatsumi, Synthesis of amino-functionalized MCM-41 via direct co-condensation and post-synthesis grafting methods using mono-, di- and tri-amino-organoalkoxysilanes, J. Mater. Chem., 14 (2004) 951-957.

[153] M. Etienne, A. Walcarius, Analytical investigation of the chemical reactivity and stability of aminopropyl-grafted silica in aqueous medium, Talanta, 59 (2003) 1173-1188.

[154] K.C. Vrancken, K. Possemiers, P. Van Der Voort, E.F. Vansant, Surface modification of silica gels with aminoorganosilanes, Colloids Surf. Physicochem. Eng. Aspects, 98 (1995) 235-241.

[155] V. Antochshuk, M. Jaroniec, Functionalized Mesoporous Materials Obtained via Interfacial Reactions in Self-Assembled Silica−Surfactant Systems, Chem. Mater., 12 (2000) 2496-2501.

[156] Z. Zhai, Y. Wang, Y. Chen, G. Luo, Fast adsorption and separation of bovine serum albumin and lysozyme using micrometer-sized macromesoporous silica spheres, J. Sep. Sci., 31 (2008) 3527-3536.

[157] H. Shirahama, J. Lyklema, W. Norde, Comparative protein adsorption in model systems, J. Colloid Interface Sci., 139 (1990) 177-187.

[158] J.F. Díaz, K.J. Balkus Jr, Enzyme immobilization in MCM-41 molecular sieve, J. Mol. Catal. B: Enzym., 2 (1996) 115-126.

[159] S. Wang, R.G. Larson, Coarse-grained molecular dynamics simulation of tethered lipid assemblies, Soft Matter, 9 (2013) 480-486.

[160] M.L. Wagner, L.K. Tamm, Tethered Polymer-Supported Planar Lipid Bilayers for Reconstitution of Integral Membrane Proteins: Silane-Polyethyleneglycol-Lipid as a Cushion and Covalent Linker, Biophys. J., 79 (2000) 1400-1414.

[161] K.R. Poudel, D.J. Keller, J.A. Brozik, The effect of a phase transition on single molecule tracks of Annexin V in cushioned DMPC assemblies, Soft Matter, 8 (2012) 11285-11293.

[162] M. Claesson, A. Ahmadi, H.M. Fathali, M. Andersson, Improved QCM-D signal-to-noise ratio using mesoporous silica and titania, Sensors Actuators B: Chem., 166–167 (2012) 526-534.

[163] S. Kaufmann, M. Tanaka, Cell adhesion onto highly curved surfaces: one-step immobilization of human erythrocyte membranes on silica beads, Chemphyschem : a European journal of chemical physics and physical chemistry, 4 (2003) 699-704.

[164] E.E. Ross, S.-W. Mok, S.R. Bugni, Assembly of Lipid Bilayers on Silica and Modified Silica Colloids by Reconstitution of Dried Lipid Films, Langmuir, 27 (2011) 8634-8644.

[165] T.V. Ratto, M.L. Longo, Obstructed Diffusion in Phase-Separated Supported Lipid Bilayers: A Combined Atomic Force Microscopy and Fluorescence Recovery after Photobleaching Approach, Biophys. J., 83 (2002) 3380-3392.

[166] N. Kučerka, M.-P. Nieh, J. Katsaras, Fluid phase lipid areas and bilayer thicknesses of commonly used phosphatidylcholines as a function of temperature, Biochim. Biophys. Acta, 1808 (2011) 2761-2771.

[167] G.D. Bothun, B.L. Knutson, H.J. Strobel, S.E. Nokes, Liposome Fluidization and Melting Point Depression by Pressurized CO_2 Determined by Fluorescence Anisotropy, Langmuir, 21 (2004) 530-536.

[168] P.F. Fahey, W.W. Webb, Lateral diffusion in phospholipid bilayer membranes and multilamellar liquid crystals, Biochemistry, 17 (1978) 3046-3053.

[169] A.S. Campbell, Y. Yu, S. Granick, A.A. Gewirth, PCB Association with Model Phospholipid Bilayers, Environ. Sci. Technol., 42 (2008) 7496-7501.

[170] P.R. Westmark, S.J. Gardiner, B.D. Smith, Selective Monosaccharide Transport through Lipid Bilayers Using Boronic Acid Carriers, J. Am. Chem. Soc., 118 (1996) 11093-11100.

[171] S. Kaufmann, I.M. Weiss, M. Tanaka, Quantitative in vitro biopolymerization to chitin in native chitosomal membranes supported by silica microparticles, J. Am. Chem. Soc., 129 (2007) 10807-10813.

[172] M. Tutus, S. Kaufmann, I.M. Weiss, M. Tanaka, Functional Coating of Porous Silica Microparticles with Native Biomembranes towards Portable Flow-Through Biochemical Microreactors, Adv. Funct. Mater., 22 (2012) 4873-4878.

[173] T. Kim, J. Eberwine, Mammalian cell transfection: the present and the future, Anal. Bioanal. Chem., 397 (2010) 3173-3178.

[174] S. Roizard, C. Danelon, G. Hassaïne, J. Piguet, K. Schulze, R. Hovius, R. Tampé, H. Vogel, Activation of G-Protein-Coupled Receptors in Cell-Derived Plasma Membranes Supported on Porous Beads, J. Am. Chem. Soc., 133 (2011) 16868-16874.

[175] R.M. Dowben, P.M. Lynch, H.L. Nadler, D.Y. Hsia, Polyribosomes from L cells, Exp. Cell Res., 58 (1969) 167-169.

[176] F.H. Moonschi, A.K. Effinger, X. Zhang, W.E. Martin, A.M. Fox, D.K. Heidary, J.E. DeRouchey, C.I. Richards, Cell-Derived Vesicles for Single-Molecule Imaging of Membrane Proteins, Angew. Chem. Int. Ed., (2014) n/a-n/a.

[177] P. Klein, D. Mattoon, M.A. Lemmon, J. Schlessinger, A structure-based model for ligand binding and dimerization of EGF receptors, Proceedings of the National Academy of Sciences of the United States of America, 101 (2004) 929-934.

[178] I. Le Trong, S. Freitag, L.A. Klumb, V. Chu, P.S. Stayton, R.E. Stenkamp, Structural studies of hydrogen bonds in the high-affinity streptavidin-biotin complex: mutations of amino acids interacting with the ureido oxygen of biotin, Acta crystallographica. Section D, Biological crystallography, 59 (2003) 1567-1573.

[179] M. Genz, V. Köhler, M. Krauss, D. Singer, R. Hoffmann, T.R. Ward, N. Sträter, An Artificial Imine Reductase based on the Ribonuclease S Scaffold, ChemCatChem, 6 (2014) 736-740.

[180] M.E. Davis, Ordered porous materials for emerging applications, Nature, 417 (2002) 813-821.

[181] M.K. Wooten, Nanofiltration membranes from oriented mesoporous silica thin films, University of Kentucky, Lexington, KY, 2014.

[182] D.W. Deamer, J. Bramhall, Permeability of lipid bilayers to water and ionic solutes, Chem. Phys. Lipids, 40 (1986) 167-188.

[183] V. Sidorov, F.W. Kotch, J.L. Kuebler, Y.-F. Lam, J.T. Davis, Chloride Transport Across Lipid Bilayers and Transmembrane Potential Induction by an Oligophenoxyacetamide, J. Am. Chem. Soc., 125 (2003) 2840-2841.

[184] X. Wu, Z. Li, X.X. Chen, J.S. Fossey, T.D. James, Y.B. Jiang, Selective sensing of saccharides using simple boronic acids and their aggregates, Chem. Soc. Rev., 42 (2013) 8032-8048.

[185] T.-J. Chen, J.-Y. Jeng, C.-W. Lin, C.-Y. Wu, Y.-C. Chen, Quercetin inhibition of ROS-dependent and -independent apoptosis in rat glioma C6 cells, Toxicology, 223 (2006) 113-126.

[186] M. Alía, S. Ramos, R. Mateos, A.B. Granado-Serrano, L. Bravo, L. Goya, Quercetin protects human hepatoma HepG2 against oxidative stress induced by tert-butyl hydroperoxide, Toxicol. Appl. Pharmacol., 212 (2006) 110-118.

[187] A. Murakami, H. Ashida, J. Terao, Multitargeted cancer prevention by quercetin, Cancer Lett., 269 (2008) 315-325.

[188] S. Dhawan, R. Kapil, B. Singh, Formulation development and systematic optimization of solid lipid nanoparticles of quercetin for improved brain delivery, J. Pharm. Pharmacol., 63 (2011) 342-351.

[189] S.C. Bischoff, Quercetin: potentials in the prevention and therapy of disease, Current Opinion in Clinical Nutrition & Metabolic Care, 11 (2008) 733-740 710.1097/MCO.1090b1013e32831394b32831398.

[190] K.-M. Oksman-Caldentey, D. Inzé, Plant cell factories in the post-genomic era: new ways to produce designer secondary metabolites, Trends Plant Sci., 9 (2004) 433-440.

[191] Z. Cai, A. Kastell, D. Knorr, I. Smetanska, Exudation: an expanding technique for continuous production and release of secondary metabolites from plant cell suspension and hairy root cultures, Plant Cell Rep., 31 (2012) 461-477.

[192] J. Kurepa, R. Nakabayashi, T. Paunesku, M. Suzuki, K. Saito, G.E. Woloschak, J.A. Smalle, Direct isolation of flavonoids from plants using ultra-small anatase TiO2 nanoparticles, The Plant Journal, 77 (2014) 443-453.

[193] I.I. Slowing, B.G. Trewyn, S. Giri, V.S.Y. Lin, Mesoporous Silica Nanoparticles for Drug Delivery and Biosensing Applications, Adv. Funct. Mater., 17 (2007) 1225-1236.

[194] L. Gastaldi, E. Ugazio, S. Sapino, P. Iliade, I. Miletto, G. Berlier, Mesoporous silica as a carrier for topical application: the Trolox case study, PCCP, 14 (2012) 11318-11326.

[195] P. Majewski, T. Albrecht, S. Weber, COOH-functionalisation of silica particles, Appl. Surf. Sci., 257 (2011) 9282-9286.

[196] G. Berlier, L. Gastaldi, E. Ugazio, I. Miletto, P. Iliade, S. Sapino, Stabilization of quercetin flavonoid in MCM-41 mesoporous silica: positive effect of surface functionalization, J. Colloid Interface Sci., 393 (2013) 109-118.

[197] J.-H. Wu, X.-S. Li, Y. Zhao, Q. Gao, L. Guo, Y.-Q. Feng, Titania coated magnetic mesoporous hollow silica microspheres: fabrication and application to selective enrichment of phosphopeptides, Chem. Commun., 46 (2010) 9031-9033.

[198] S. Kamaruddin, D. Stephan, The preparation of silica–titania core–shell particles and their impact as an alternative material to pure nano-titania photocatalysts, Catal. Today, 161 (2011) 53-58.

[199] C. Wang, Y. Ao, P. Wang, J. Hou, J. Qian, A facile method for the preparation of titania-coated magnetic porous silica and its photocatalytic activity under UV or visible light, Colloids Surf. Physicochem. Eng. Aspects, 360 (2010) 184-189.

[200] J.A. Rothwell, A.J. Day, M.R.A. Morgan, Experimental Determination of Octanol−Water Partition Coefficients of Quercetin and Related Flavonoids, J. Agric. Food. Chem., 53 (2005) 4355-4360.

[201] K. Abou-El-Sherbini, D. Schiel, R. Stosch, P. Weidler, W. Höll, Stabilization of quercetin-functionalized silica gel against hydrolysis by blocking silanol groups with TiO2 or ZrO2 and its application for the removal of Hg(II), J. Sol-Gel Sci. Technol., 57 (2011) 57-67.

[202] O.A. Kazakova, V.M. Gun'ko, N.A. Lipkovskaya, E.F. Voronin, V.K. Pogorelyi, Interaction of Quercetin with Highly Dispersed Silica in Aqueous Suspensions, Colloid J., 64 (2002) 412-418.

[203] M.P. Finnegan, H. Zhang, J.F. Banfield, Phase Stability and Transformation in Titania Nanoparticles in Aqueous Solutions Dominated by Surface Energy, The Journal of Physical Chemistry C, 111 (2007) 1962-1968.

[204] R.K. Iler, The Chemistry of Silica: Solubility, Polymerization, Colloid and Surface Properties and Biochemistry of Silica, Wiley, New York, 1979.

[205] X.-C. Guo, P. Dong, Multistep Coating of Thick Titania Layers on Monodisperse Silica Nanospheres, Langmuir, 15 (1999) 5535-5540.

[206] S. Srinivasan, A.K. Datye, M. Hampden-Smith, I.E. Wachs, G. Deo, J.M. Jehng, A.M. Turek, C.H.F. Peden, The formation of titanium oxide monolayer coatings on silica surfaces, J. Catal., 131 (1991) 260-275.

[207] E.I. Morosanova, Silica and silica–titania sol–gel materials: Synthesis and analytical application, Talanta, 102 (2012) 114-122.

[208] W. Stöber, A. Fink, E. Bohn, Controlled growth of monodisperse silica spheres in the micron size range, J. Colloid Interface Sci., 26 (1968) 62-69.

[209] Y. Fu, F. Ye, W.G. Sanders, M.M. Collinson, D.A. Higgins, Single Molecule Spectroscopy Studies of Diffusion in Mesoporous Silica Thin Films, The Journal of Physical Chemistry B, 110 (2006) 9164-9170.

[210] W.S. Rasband, ImageJ, National Institute of Health, Bethesda, Maryland, USA, 1997-2012.

[211] M.E. Carlotti, S. Sapino, E. Ugazio, G. Caron, On the complexation of quercetin with methyl-β-cyclodextrin: photostability and antioxidant studies, J Incl Phenom Macrocycl Chem, 70 (2011) 81-90.

[212] A.M. Busuioc, V. Meynen, E. Beyers, M. Mertens, P. Cool, N. Bilba, E.F. Vansant, Structural features and photocatalytic behaviour of titania deposited within the pores of SBA-15, Applied Catalysis A: General, 312 (2006) 153-164.

[213] E.I. Morosanova, M.V. Belyakov, Y.A. Zolotov, Silicon-titanium xerogels: Synthesis and application to the determination of ascorbic acid and polyphenoles, J. Anal. Chem., 67 (2012) 14-20.

[214] W. Brand-Williams, M.E. Cuvelier, C. Berset, Use of a free radical method to evaluate antioxidant activity, LWT - Food Science and Technology, 28 (1995) 25-30.

[215] B. Yang, A. Kotani, K. Arai, F. Kusu, Estimation of the antioxidant activities of flavonoids from their oxidation potentials, Anal. Sci., 17 (2001) 599-604.

Vita

Location of Birth: Independence, Ky

Educational Background:

Bachelor of Science in Chemistry, May 2010

Georgetown College

Georgetown, Ky

Work Experience

- **Zoom Essence**, Research Assistant, Hebron, Ky Summer 2010
- **Kao Brands Company**, Research Assistant, Cincinnati, OH Summer 2009
- **Center for Applied Energy Research**, Research Assistant, University of Kentucky, Lexington, Ky Summer 2008

Publications

D.M. Schlipf, S.R. Rankin and B.L. Knutson, **Pore size dependent protein adsorption and protection from proteolytic hydrolysis in tailored mesoporous silica particles** *ACS Applied Materials and Interfaces,* **2013** 5 (20) 10111-10117

D.M. Schlipf, S.R. Rankin and B.L. Knutson, **Selective surface functionalization of large pored silica materials capable of protein loading** *(Submitted, Microporous and Mesoporous Materials)*

D.M. Schlipf, C.A. Jones, M.E. Armbruster, E.S. Rushing, K.M. Wooten, S.R. Rankin and B.L. Knutson, **Quercetin adsorption and stability on functionalized silica nano-particles** *(In press, Journal of Colloids and Surface Science A)*

D.M. Schlipf, S.R. Rankin and B.L. Knutson **Effects of nanopore size and surface functionality on the interactions of lipid bilayers with mesoporous silica** *(In preparation)*

D.M. Schlipf, A.K. Effingers, F.H. Moonschi, C.I. Richards, S.E. Rankin, B.L. Knutson**, Mesoporous silica micro-particles as whole cell plasma membrane supports** *(In preparation)*

Selected Presentations

Poster

Pore size dependent protein capture and protection from proteolytic hydrolysis, Society for Biomaterials Meeting, September 2012, Lexington, KY

Controlling the pore structure of silica platforms for the isolation of bioactive molecules Kentucky Innovation and Entrepreneurship Conference (KIEC), August 2014, Louisville, KY

Oral

Demonstration of size selective protein capture and protection from proteolytic hydrolysis American Institute of Chemical Engineering – Annual Conference, October 2012, Pittsburgh, PA

Selective functionalization of large pore mesoporous silica materials capable of protein capture American Chemical Society – Colloids and Surface Sciences, June 2013, Riverside, CA

Visualization of protein capture within selectively functionalized mesoporous silica Kentucky Nano Symposium, August 2013, Louisville, KY

Effects of nano-pore size on the interactions of lipid bilayers with mesoporous silica American Institute of Chemical Engineering – Annual Conference, November 2014, Atlanta, GA